

POLITECNICO DI TORINO

Master's Degree Program in Environmental Engineering  
Specialization: Climate Change

Master's thesis

**Modeling the thickness of glaciers with geophysical data constraints:  
an extensive application to the Val Ferret (Aosta Valley, NW Italy)**



Supervisor:  
Prof. Chiara Colombero

Author:  
Giacomo Dalmaso

Co-Supervisor:  
Ing. Valeria Strallo

Academic Year: 2024/2025



# ABSTRACT

The retreat of Alpine glaciers is a clear indicator of climate change, with significant implications for hydrology, geomorphology, and local ecosystems. This study focuses on the glaciers of Val Ferret, located on the Italian side of the Mont Blanc massif, applying the GLATE (Glacier Thickness Estimation) model to estimate ice thickness distribution. The model is constrained using Ground Penetrating Radar (GPR) data, improving the accuracy of thickness estimations compared to traditional empirical approaches.

The GLATE model was applied to several glaciers in Val Ferret, including Pré de Bar, Grapillon, Planpincieux, Whymper Serac, Col del Gigante, and Toula glaciers. Results indicate significant spatial variability in ice thickness, with greater depths in accumulation zones and severe thinning in ablation areas, confirming the accelerated retreat of these glaciers. The integration of GPR field data allowed for model refinement, reducing uncertainty and enhancing the reliability of thickness estimations.

A key aspect of the study is the evaluation of GPR data quality and spatial coverage, which play a fundamental role in achieving reliable model outputs. The analysis highlights that gaps or inaccuracies in GPR measurements can propagate errors in thickness estimations, especially in complex glacier geometries. The results emphasize that a denser and well-distributed GPR dataset significantly improves model calibration, reducing uncertainty in interpolations and ensuring better consistency between measured and estimated ice thickness. This underscores the necessity of comprehensive field surveys to enhance the robustness of numerical glacier models.

While the study primarily focuses on glacier thickness estimation, it also briefly discusses the potential consequences of glacier retreat, such as impacts on hydrology and geomorphological stability. However, a deeper analysis of these aspects is suggested for future research.

The findings underline the importance of continuous glacier monitoring, particularly through the integration of numerical modeling, geophysical surveys, and satellite observations. Future improvements to the model should focus on dynamic simulations and expanded field measurements to enhance predictions of glacier evolution in Val Ferret and similar Alpine regions.

# SUMMARY

<b>1</b>	<b>INTRODUCTION.....</b>	<b>1</b>
1.1	GENERAL CONTEXT OF THE STUDY .....	1
1.2	IMPORTANCE OF VAL FERRET GLACIERS' STUDY .....	2
1.3	OBJECTIVES OF THE RESEARCH .....	3
<b>2</b>	<b>STATE OF THE ART.....</b>	<b>4</b>
2.1	LITERATURE REVIEW ON GLACIER MODELS.....	4
2.1.1	Dynamic Models .....	4
2.1.2	Static Models .....	5
2.2	GLACIER DYNAMICS AND CLIMATE CHANGE .....	5
2.2.1	Introduction .....	5
2.2.2	Internal Features of a Glacier.....	9
2.2.3	Dynamic Response to Climate Change .....	12
2.2.4	Regional and Global Effects .....	14
2.3	MODELS PREVIOUSLY APPLIED TO THE ALPS .....	14
2.3.1	The Study by Farinotti et al. (2009).....	14
2.3.2	The Study by Huss and Farinotti (2012).....	15
2.3.3	The Study by McNabb et al. (2019).....	15
<b>3</b>	<b>CHARACTERISTICS OF THE VAL FERRET AND ITS GLACIERS .....</b>	<b>16</b>
3.1	GEOGRAPHY AND MORPHOLOGY OF THE VAL FERRET.....	16
3.2	DESCRIPTION OF THE MAIN GLACIERS OF THE VALLEY .....	18
3.2.1	Pré de Bar Glacier.....	18
3.2.2	Grapillon Glacier .....	19
3.2.3	Planpincieux Glacier .....	20
3.2.4	Grandes Jorasses Glacier (Whymper Serac).....	20
3.2.5	Col del Gigante Glacier .....	21
3.2.6	Toula Glacier (Helbronner) .....	21
3.2.7	Other Val Ferret Glaciers .....	22
3.3	CURRENT MONITORING OF THE GLACIERS IN VAL FERRET .....	22
<b>4</b>	<b>METHODOLOGY .....</b>	<b>24</b>
4.1	DESCRIPTION OF THE MODEL USED .....	24
4.2	OPERATING PRINCIPLES OF GROUND PENETRATING RADAR.....	24
4.2.1	Introduction .....	24
4.2.2	Instrumentation .....	25
4.2.3	Important parameters.....	26
4.3	DATA COLLECTION.....	29
4.3.1	Operating Principles and Radargram Creation.....	29
4.3.2	Influence of Glacier Internal Characteristics .....	31
4.3.3	Logistic Difficulties and Solutions .....	32
4.4	DATA PROCESSING .....	32
4.4.1	Steps in Data Processing .....	32
4.4.2	Processing and problems with Val Ferret glaciers .....	36
<b>5</b>	<b>APPLICATION OF THE GLATE MODEL.....</b>	<b>47</b>
5.1	MODEL DESCRIPTION .....	47
5.1.1	GPR data constraint .....	47

5.1.2	Glaciological constraint .....	47
5.1.3	Definitive model and weighting coefficients .....	49
<b>5.2</b>	<b>APPLICATION OF THE MODEL TO VAL FERRET GLACIERS .....</b>	<b>50</b>
<b>5.3</b>	<b>POTENTIAL LIMITATIONS AND ASSUMPTIONS OF THE MODEL.....</b>	<b>51</b>
<b>6</b>	<b><i>RESULTS</i>.....</b>	<b>53</b>
<b>6.1</b>	<b>PRESENTATION OF SIMULATION RESULTS .....</b>	<b>53</b>
6.1.1	Prè de Bar and Grapillon.....	54
6.1.2	Planpincieux glacier and Whymper serac .....	56
6.1.3	Col del Gigante and Toula glaciers .....	59
<b>6.2</b>	<b>COMPARISON BETWEEN DIFFERENT SMOOTHING FACTORS AND RESOLUTIONS.....</b>	<b>61</b>
<b>6.3</b>	<b>COMPARISON WITH GPR DATA OF GOOD OR POOR QUALITY .....</b>	<b>64</b>
<b>6.4</b>	<b>COMPARISON BETWEEN DIFFERENT EXTENSIONS OF GPR DATA.....</b>	<b>65</b>
<b>6.5</b>	<b>TEMPERATURE ANALYSIS.....</b>	<b>68</b>
6.5.1	Parameter selection .....	68
6.5.2	Gap filling .....	69
6.5.3	Signal processing: Trend enhancement by removal of the periodic component .....	71
6.5.4	Trend estimation .....	73
<b>7</b>	<b><i>CONCLUSIONS</i>.....</b>	<b>74</b>
<b>7.1</b>	<b>SUMMARY AND CRITICAL DISCUSSION OF THE RESULTS .....</b>	<b>74</b>
<b>7.2</b>	<b>POTENTIAL IMPACTS OF GLACIAL CHANGES ON THE VAL FERRET .....</b>	<b>75</b>
<b>7.3</b>	<b>COMPARISON WITH SIMILAR STUDIES IN OTHER ALPINE OR GLOBAL AREAS</b>	<b>76</b>
<b>7.4</b>	<b>LIMITATIONS OF THE RESEARCH AND FUTURE PERSPECTIVES FOR MODEL IMPROVEMENT.....</b>	<b>76</b>
<b>8</b>	<b><i>APPENDIX</i> .....</b>	<b>77</b>
<b>8.1</b>	<b>APPENDIX A .....</b>	<b>77</b>
<b>8.2</b>	<b>APPENDIX B .....</b>	<b>82</b>
<b>8.3</b>	<b>APPENDIX C .....</b>	<b>91</b>
<b>8.4</b>	<b>APPENDIX D .....</b>	<b>92</b>
<b>9</b>	<b><i>LIST OF FIGURES AND TABLES</i> .....</b>	<b>96</b>
<b>10</b>	<b><i>BIBLIOGRAPHY</i>.....</b>	<b>99</b>

# 1 INTRODUCTION

## 1.1 GENERAL CONTEXT OF THE STUDY

One of the most obvious and worrying consequences of ongoing climate change is the retreat of glaciers, which is a physical sign of changes taking place in ecosystems around the world. Globally, glaciers are melting at a rate unprecedented in recent decades, directly affecting mountain regions, water systems, biodiversity, and human populations that rely on these ecosystems for survival. This phenomenon has attracted a lot of interest in scientific and political discussions because of its widespread consequences and obvious link to human-caused climate change. According to the Intergovernmental Panel on Climate Change (IPCC), two of the main contributors to the global sea level increase are mountain glaciers and ice caps. Driven by fast-melting glaciers, this mechanism is complemented by other processes, like the thermal expansion brought on by ocean warming. Sea-level rise poses a significant threat to the millions of people living in low-lying coastal areas, as it exposes them to flooding, coastal erosion, and aquifer salinization. The necessity of coordinated action to reduce the effects and adapt to changing environmental circumstances is crucial, as these consequences not only have an immediate impact on the local population but also on coastal ecosystems and the regional economy [1], [2].

In high regions like the Alps, glaciers are vital for the water supply. In the winter, they function as natural reservoirs, retaining water in ice form and then progressively releasing it in the summer months to ensure a continuous supply for rivers and enable a variety of human activities. Hydropower generates electricity from rivers fed by glaciers, while agriculture uses meltwater for irrigation. On the other hand, the quickly declining volume and surface area of the Alpine glaciers is weakening their regulating function and compromising the social and natural stability of these places [3].

The situation in the Italian Alps is especially alarming: new studies reveal that, with a notable acceleration in recent years, Alpine glaciers have lost more than half of their volume in past decades [4]. These changes not only compromise the availability of water resources but also upset the fragile equilibrium of mountain ecosystems. Melting of ice influences water quality, changes habitat for plants and animals, and alters nutrient cycles. Moreover, the reduction in glacier cover exposes underlying terrain to faster erosion processes, which generates cascading effects on the geomorphological system of the area.

Modern glaciology has developed fundamental methods for analyzing and forecasting glacier dynamics. Numerical models are one of the most successful approaches for simulating glaciers' future behavior in response to climate change. These models predict glacier extension, residual ice volume, and melting rates, giving important information for sustainable natural resource management. However, the quality of the data utilized for constraining the models significantly determines the accuracy of these simulations. Among the most significant data are measurements of ice thickness, as they directly reveal the three-dimensional distribution of glacier mass.

Ground Penetrating Radar (GPR) and other modern technologies have fundamentally modified glacier data-collecting methods. This approach allows us to precisely estimate the depth of ice while tracking the internal stratigraphy of glaciers with great accuracy. When included in numerical models, these data significantly improve the calibration and validation of results by reducing uncertainty in estimations and so improving their dependability. GPR is thus now an indispensable tool in modern glaciology since it provides a more complete understanding of the internal dynamics of glaciers.

Apart from its scientific value, understanding glacier dynamics is also helpful for controlling natural disasters. Dangerous phenomena, including landslides, glacial outburst floods, and serac collapses induced by glacier retreat, increasingly threaten mountain regions. The increasing frequency of serac

collapses and the formation of unstable glacial lakes in the Western Italian Alps pose a significant threat to infrastructure, paths, and territories. Rising tourism combined with more awareness of such hazards emphasizes the need for management and mitigating techniques to save the environment as well as humans [5].

In addition to advancing knowledge of science, the outcomes of glaciological research provide tools for designing environmentally friendly projects, ensuring the security of the mountain surroundings, and thereby preserving natural resources for the next generations.

## 1.2 IMPORTANCE OF VAL FERRET GLACIERS' STUDY

On the Italian side of the Mont Blanc range, Val Ferret offers an ideal location for studies on Alpine glacial dynamics. Though not among the biggest in the Alps, these small to medium-sized glaciers in this valley are vital in preserving the local hydrological balance and guaranteeing geomorphological stability in the region.

Val Ferret's glacial basin is unique in that it features many glaciological events of both scientific and practical interest. Many incidents in recent years have shown the vulnerability of the area: calving of glacier masses, serac collapses, and flooding events connected to faster ice melting. These sometimes-irregular events have significantly impacted the local infrastructure, as well as the safety of the valley's residents and visitors.

Apart from their scientific relevance, analysis of the glaciers in Val Ferret has strategic relevance for land management. Attracting thousands of tourists annually for hiking, mountaineering, and other outdoor sports, the valley is among the most well-known tourist destinations in the Western Alps. But along with the rising visitor number comes more exposure to hazards, especially related to road accessibility and personal safety. Glacier calving and serac collapses seriously threaten the roads and paths crossing the valley, potentially disrupting access to mountain lodges, views, and other tourist facilities [6].

Moreover, the value of the glaciers in Val Ferret goes beyond their impact on safety and tourism: they are a vital part of the hydrological cycle of the valley. As natural water reservoirs, glaciers gradually release water during the summer season. With cascading effects on vegetation, aquatic ecosystems, and the communities dependent on local water supplies for agriculture, drinking water, and hydropower generation, their rapid retreat not only limits water availability but also may change the time and patterns of release [7].

The special mix of accessibility and field data availability distinguishes Val Ferret. Ground-penetrating radar (GPR) surveys conducted on several glaciers in the valley provide valuable information that enhances our understanding of local dynamics [8]. When combined with computer models, such information helps estimate ice thickness and enables the study of the spatial distribution of glacial mass with an uncommon degree of detail.

Furthermore, Val Ferret's research holds greater significance as it can provide valuable information for other alpine regions with similar characteristics. This study's acquired knowledge not only enhances our understanding of local glacial dynamics, but also aids in the development of reproducible methods applicable to other alpine and glacial environments.

This mix of elements makes Val Ferret a region of special importance for glaciological study. Examining the glaciers of the valley not only clarifies glacial dynamics in an alpine environment but also offers necessary information for sustainable management of the area, therefore safeguarding human safety as well as natural resources [9]. This research makes a significant contribution by combining the scientific study of glacier dynamics with practical applications for risk control and water resource preservation.

## 1.3 OBJECTIVES OF THE RESEARCH

With a focus on the spatial distribution of ice thickness, the present work aims to apply and further improve the GLATE (Glacier Thickness Estimation) numerical model to simulate the thickness of glaciers in Val Ferret. With a final objective of extending the simulations to cover the whole glacial basin, this study combines Ground Penetrating Radar (GPR) data acquired from a particular area of the glaciers in the valley. The work aims to overcome some of the limitations of conventional methods of glacial analysis by merging advanced numerical modeling with high-resolution field data.

- **GLATE Model Calibration**

The first objective is to calibrate the GLATE model with GPR data. This phase is absolutely essential for improving the predictive accuracy of the model, as it helps optimize important parameters that affect the projected ice thickness and volume. Calibration guarantees that the model considers the particular properties of the glaciers in Val Ferret, such as their shape, ice dynamics, and local climatic circumstances. A well-calibrated model can greatly improve the dependability of simulations by producing results that are not only more precise but also more realistic for real-world situations.

- **Ice Thickness Distribution Simulation**

Once calibrated, we will use the GLATE model to provide a comprehensive map of ice thickness over the whole Val Ferret glacier basin. This simulation intends to identify significant patterns in the spatial distribution of ice, stressing places that are more susceptible to melting and those with more accumulation. These maps are not only useful for description; they also provide important means of comprehension for the intricate relationships among topography, glacial processes, and climate variables. These realizations can direct research projects as well as useful actions meant to reduce the effects of glacier retreat.

- **Comparison with Conventional Theoretical Models**

The contrast between the conclusions generated from the GLATE model, dependent on GPR data, and those derived from conventional theoretical models is an essential component of the research. The latter often rely on simpler assumptions such as homogeneous ice thickness or static border conditions, which can lead to significant discrepancies when applied to challenging alpine settings. With these variations, the research aims to assess the additional benefit of including high-resolution radar data in numerical modeling. This comparison not only highlights the advantages and disadvantages of each approach, but also underscores the necessity of incorporating field data into glaciological research.

- **Contribution to risk management**

Alpine areas face many hazards from the retreat of glaciers, including landslides, glacial floods, and serac collapse. Local communities, infrastructure, and ecosystems may all suffer greatly from these events. The work intends to provide useful tools for monitoring and controlling these hazards by means of detailed models of ice thickness and spatial variability. Finding regions with unstable seracs or thinning ice, for instance, can guide treatments to lower dangers. Furthermore, the study helps the area to become more resilient by arming stakeholders and politicians with the knowledge required to foresee and handle the difficulties related to glacier retreat.

- **Development of glaciological knowledge**

Apart from its practical uses, the study aims to significantly advance knowledge of alpine glacial dynamics by means of scientific contribution. Both inside the Alps and internationally, the techniques employed in this study can act as a model for such studies in other glacier environments. The study closes important knowledge gaps by merging modern numerical modeling with high-resolution field data and therefore providing a more complete and detailed picture of glacier activity. This development not only improves the scientific literature but also provides the foundation for the next investigations meant to clarify the complexity of glacier-climate interactions.

By means of the accomplishment of these goals, the research addresses various urgent issues in modern glaciology. The retreat of glaciers is a worldwide problem with significant implications for sea-level rise, water supplies, and natural hazards, not only local occurrences. The approaches and revelations of this study should guide more general discussions on resilience and climate adaptation. For areas depending on glaciers for drinking water, agriculture, and electricity, for example, knowledge of the regional variability of ice thickness can help to enhance forecasts of meltwater availability.

Furthermore, the integration of field data with numerical models represents a significant change in the field of glacial studies. Through proving the feasibility and benefits of this strategy, the study promotes the acceptance of similar approaches in other areas experiencing glacial retreat. A more sustainable coexistence between human civilizations and the delicate alpine surroundings they live on depends on such developments.

## **2 STATE OF THE ART**

### **2.1 LITERATURE REVIEW ON GLACIER MODELS**

The study of glacier thickness is a central topic in glaciology; it is fundamental for understanding glacier dynamics, projecting the effects of climate change, and managing water resources derived from glaciers. Various glacier models, each with specific methodological approaches and fields of application, have developed over the years to estimate ice thickness. This section provides a review of the main types of glacier models, divided into dynamic and static models, with a focus on their applications and limitations, particularly in the context of alpine glaciers, such as those in the Val Ferret region.

#### **2.1.1 Dynamic Models**

Dynamic models aim to simulate the temporal evolution of ice, taking into account the physical factors affecting glacier flow. These models especially help predict how glaciers might respond to climate change.

The models based on the Navier-Stokes equations, which characterize ice flow as a non-Newtonian viscous fluid [10], offer high accuracy, including internal deformation and basal motion, but require significant computational resources. They are often applied to ice sheets or complex glaciers, as demonstrated by Schoof (2007) [11].

Assuming small slopes and uniform thicknesses, the Shallow Ice Approximation (SIA), another class of dynamic models, reduces the Navier-Stokes equations [12]. Although they demonstrate significant restrictions in the presence of complicated glacier geometries, these models are computationally efficient and extensively applied for large-scale research. Likewise, the Shallow Shelf Approximation (SSA) is better suited for temperate or marine glaciers since it emphasizes basal ice motion [13].

Lastly, linked mass-balance-dynamic models combine topography and climatic variations to replicate ice development. Using this approach, Huss et al. (2008) [14] investigated alpine glaciers, showing how local topographic variables greatly affect the rate of glacier retreat.

Real-time data assimilation techniques, a recent development in dynamic models, enable the updating of simulations using current field observations. This method has been used to investigate Greenland's ice movement, therefore highlighting its consequences for sea-level rise.

Particularly in the Alps, regional-scale dynamic models have been built for smaller valley glaciers to examine their interaction with hydrological basins. These projects intend to offer a combined view of glacier systems and their effects on water supplies.

### 2.1.2 Static Models

Static models estimate ice thickness under stationary conditions without simulating dynamic flow; they are often used for preliminary studies or when available data is limited.

Based on slope gradient, one of the simplest stationary models evaluates thickness as a function of the glacier surface slope [15]. Despite their ease of use, these models' accuracy in geomorphologically diverse environments suffers from their neglect of intricate physical processes.

Empirical models represent another static approach, using statistical relationships between variables such as glacier length, area, and slope. Though there are significant local-scale restrictions, Bahr et al. (1997) [16] showed that these models can offer good estimations of ice thickness for large glacier ensembles.

Inverse models, which compute ice thickness based on surface velocity and force balance along the glacier [17], provide a more complex method. These models produce reliable findings, but they depend on high-quality data—surface velocity and bedrock topography—which are sometimes difficult to get in far-off alpine locations.

Among the most precise instruments for estimating glacier thickness are geophysical models based on GPR (Ground Penetrating Radar) data. Successfully applied to many alpine glaciers, including those in the Aosta valley, these models map the glacier bed surface using field data.

Recent developments in stationary models focus on combining data from satellite missions such as TerraSAR-X and Copernicus Sentinel, which offer comprehensive topography and surface velocity. Even in distant areas, these developments have greatly raised the accuracy and resolution of estimates of ice thickness.

Moreover, static models are using machine learning methods more and more to forecast ice thickness by linking observable data with topographic, meteorological, and geomorphological variables.

To estimate the glacier thickness in understudied areas, Farinotti et al. (2017) [18] created a hybrid model combining static approaches with geophysical measurements.

Minimal Glacier Models (MGMs), also known as first-order models, are simplified dynamic models designed to capture the essential behavior of glaciers over time. These models use equations that represent the balance between ice flow and mass balance in a computationally efficient manner. While not as detailed as Full-Stokes or Shallow Ice Models, MGMs offer a practical solution for large-scale or long-term glacier studies, particularly when data availability is limited [19].

Usually, MGMs mix aspects of dynamic and stationary models. To project glacier activity, they use simplified relationships, including empirical balance principles or volume-area scaling. Despite their simplicity, they primarily reflect temporal evolution, making them dynamic in nature. Their computational efficiency makes them perfect for investigating climate change scenarios and estimating glacier reaction to global warming.

## 2.2 GLACIER DYNAMICS AND CLIMATE CHANGE

### 2.2.1 Introduction

Glacial dynamics represent a fundamental field of study for understanding climate change and its long-term implications on the Earth's system. Covering a large area of the Earth, the cryosphere—which consists of glaciers, polar ice caps, and permafrost—plays a vital part in the worldwide cycles of carbon, water, and energy. The cryosphere is not only a passive storage system; it is a dynamic system that significantly affects the global temperature by means of feedback mechanisms and intricate interactions with the atmosphere and oceans. For example, the high albedo of ice—that is,

its capacity to reflect solar radiation—helps to preserve low world temperatures, so the cryosphere is a fundamental part of the energy balance of the Earth.

Particularly important components of this system are glaciers, which react extremely sensitively to changes in the temperature. Affected by processes of accumulation (snow precipitation) and ablation (melting, sublimation, and calving of icebergs), their activity is tightly related to the mass balance. These fluctuations provide an ongoing glacial advance and retreat process that can greatly change local and worldwide ecosystems. Moreover, glaciers retain almost 70% of the freshwater on Earth, an important resource for billions of people globally, especially in high areas like the Andes, the Himalayas, and the Alps. Their melting presents a two-edged problem: while in the long run gradual retreat may cause the depletion or removal of vital water supplies, in the summer months it enhances water availability.

Glacial movement also serves as a natural archive of past climate data. Through significant information on atmospheric composition and temperatures from far-off epochs, air bubbles frozen in polar and mountain glaciers help reconstruct climatic oscillations governing the globe. Studies of paleoenvironments on ice cores in Greenland and Antarctica have revealed important information on ancient climatic events, including glacial and interglacial cycles and the effect of volcanic eruptions on the world temperature.

This chapter will investigate the key mechanisms controlling glacier formation and ablation, thereby examining their mass balance and geometry throughout time. We are also going to study how glaciers respond to climate change, stressing internal and basal flow processes controlling ice mobility and their interaction with the substrate. Ultimately, by means of contributions to sea level rise and its socioeconomic consequences, we will examine the repercussions of glacier retreat both regionally, with consequences for water security and natural hazards, and globally.

## Glacier Mass Balance

One of the main instruments for assessing the evolution of a glacier and understanding its dynamics with respect to climate change is its mass balance. Defined as the difference between accumulation and ablation processes, it provides a quantitative measure of a glacier's mass variation over a given period. For the glacier, the mass balance thus serves as a form of energy balance that determines whether it is in a phase of growth, equilibrium, or retreat. The mass balance can be mathematically expressed as:

$$B = C - A \quad (1)$$

where B is the overall mass balance, C is accumulation, and A is ablation. We can further subdivide these two parameters into subprocesses. For instance, accumulation comprises several contributions in addition to snowfall directly falling onto the glacier:

- Snowfall directly on the glacier surface: it is the primary source of accumulation, influenced by local temperature and air circulation patterns.
- Snow transported by wind: Especially in mountainous or arctic areas, the wind can transfer a significant amount of snow from one location to another, thereby dispersing accumulation.
- Avalanches: In steep terrain, avalanches carry large amounts of snow to the lower sections of glacial basins, thereby building up these zones.

On the other hand, ablation is the process that determines the loss of glacial mass. It can occur through several mechanisms:

- Surface melting: Caused mainly by solar radiation, sensible heat (heat exchange with the atmosphere), and, in some regions, warm rainfall. Melting is particularly intense during summer months and at lower elevations.
- Sublimation: This process, involving the direct transition of ice into water vapor without passing through a liquid state, is significant in arid or windy climates where relative humidity is low.

- Iceberg calving: This phenomenon primarily affects glaciers that terminate in the sea or large lakes, where pieces of ice break off to form icebergs.

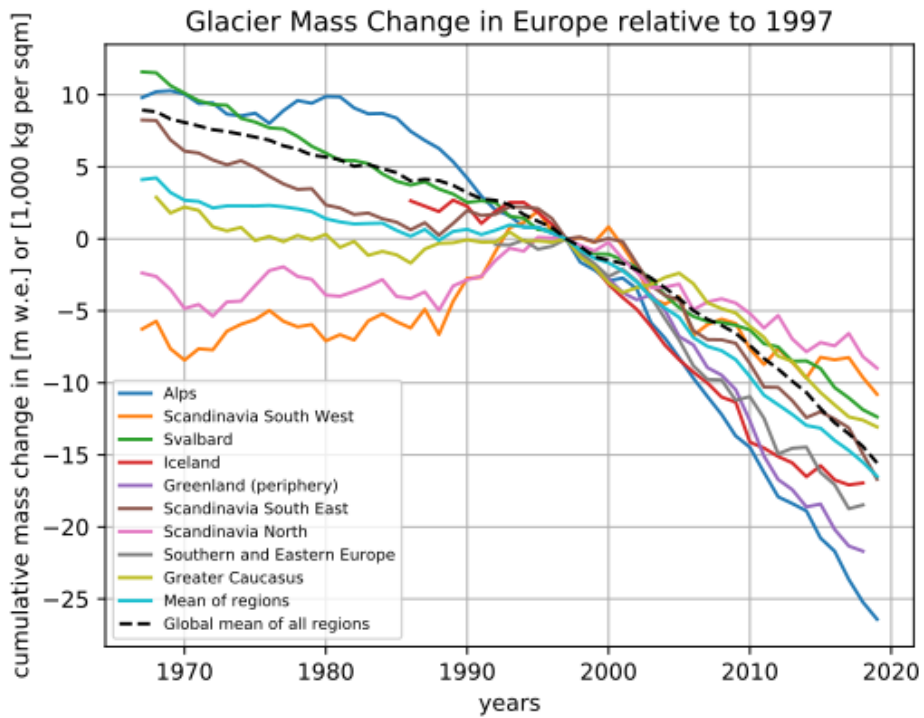


Fig. 1 - Cumulative glacier mass changes in Europe from 1967-2018 for glaciers with long-term records in nine different regions. Data source: WGMS (2017, updated). Credit: WGMS /Copernicus Climate Change Service (C3S)

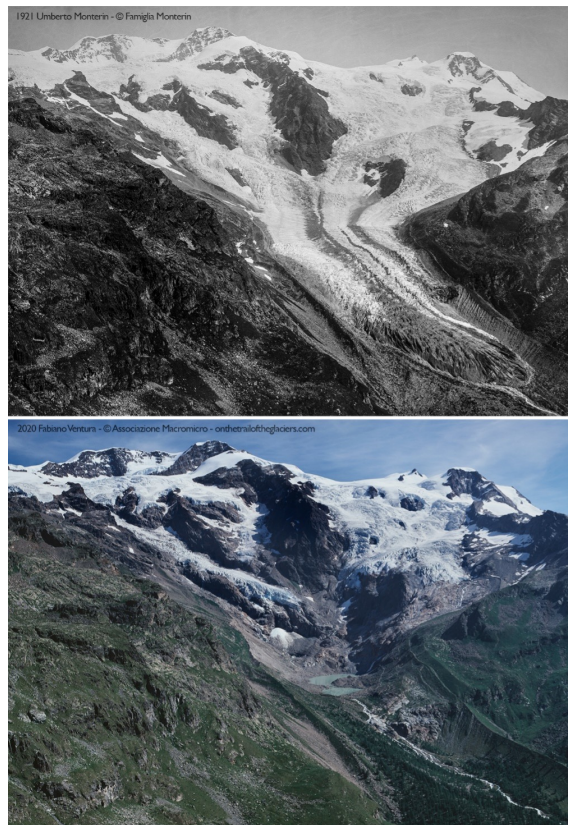


Fig. 2 - Comparison of Lys Glacier in 1921 and 2020. Source: Umberto Monterin (credit: Famiglia Monterin), Fabiano Ventura (Associazione Macromicro)

## Mass Balance measuring techniques

Measuring mass balance is essential to understanding glacier health and their response to climate change. This measurement can be carried out through a combination of direct and indirect approaches:

- Direct techniques: these approaches monitor variations in the height of ice or snow over time by installing measuring stakes on the glacier. Snow and ice core samples could potentially be part of direct measurements to determine density and hence mass variations. Although these methods are quite precise, they are time- and resource-intensive and require direct access to study locations, which are sometimes difficult to reach.
- Remote techniques: Technological advancements have enabled the development of faster and more effective methods to monitor mass balance on a large scale. Among these, the use of satellites, such as those from the GRACE (Gravity Recovery and Climate Experiment) and ICESat (Ice, Cloud, and Land Elevation Satellite) missions, stands out. These devices indirectly assess mass changes by sensing fluctuations in Earth's gravity and glacier surface elevation. Also, drones are increasingly used for smaller-scale, high-resolution data collecting.

## Factors influencing Mass Balance

The mass balance of glaciers is influenced by several factors, including:

- Local climatic conditions: Temperature, precipitation, and wind play a crucial role in determining the rate of accumulation and ablation
- Glacier geometry: Larger and thicker glaciers tend to have greater thermal inertia, responding more slowly to climatic changes compared to smaller glaciers.
- Altitude: Generally speaking, ablation is more severe at lower altitudes; accumulation dominates at higher altitudes. Global warming is progressively lowering accumulation zones by causing an upward shift in the equilibrium line altitude (ELA).
- Interactions with the substrate: Contact with a warm or water-saturated bedrock may accelerate glacier movement and impact ablation processes in temperate glaciers.

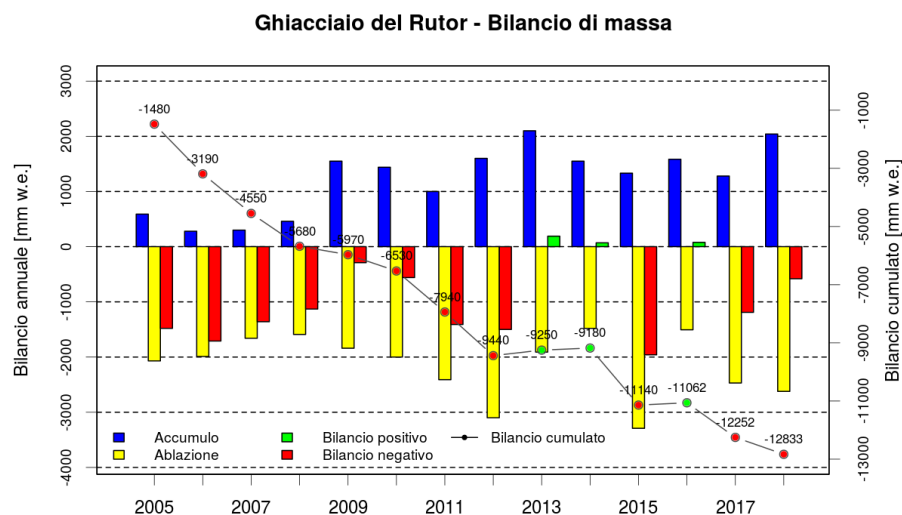


Fig. 3 - Mass balance of Rutor glacier from 2005 to 2018. Source: Arpa VdA (RSA 2018)

## Global Implications of Mass Balance

Direct effects of changes in glacial mass balance are local as well as worldwide. Locally, these changes impact the availability of water for towns that rely on glaciers for domestic, commercial, and industrial purposes. Globally, the loss of glacial mass significantly accelerates sea level rise. With major implications for coastal and island people, recent studies suggest that mountain glaciers contribute around one-third of the overall sea level rise [20].

Therefore, forecasting the future growth of glaciers and formulating strategies for mitigating and adapting to climate change rely on continuous monitoring of the glacial mass balance.

### 2.2.2 Internal Features of a Glacier

Glaciers are complex systems characterized by a variety of internal structures resulting from physical and dynamic processes that regulate ice movement and evolution. These internal characteristics not only influence the dynamics of the glacier but also play a crucial role in its ability to store, transport, and release water. Crevasses, englacial moraines, water fractures, cavities, and water pockets are among the most important forms of structure.

#### Crevasses

Tensile forces within the ice cause surface fissures known as crevasses when they exceed its stress resistance. They mostly grow in the accumulation zone and the upper section of the ablation zone, where differential ice flow takes place—that is, in locations where ice accelerates or bends over topographic obstacles.



Fig. 4 - Crevasses in Washington Glacier, Alaska. Source: L. Petersen, Crevasses, 2021

Crevasses vary in depth, width, and orientation:

**Depth:** Although they can reach tens of meters, ice behaves plastically at this depth; therefore, they rarely exceed 30–40 meters.

**Width:** The width could range from a few centimeters to several meters.

**Orientation:** Their orientation depends on the stress regime; transversal crevasses develop in extensional zones while longitudinal crevasses occur in compressive zones.

Crevasses allow surface water to penetrate deep into the glacier, therefore acting as sources of vulnerability. This infiltration can change the temperature regime of the glacier and support subglacial drainage systems [13], [21].

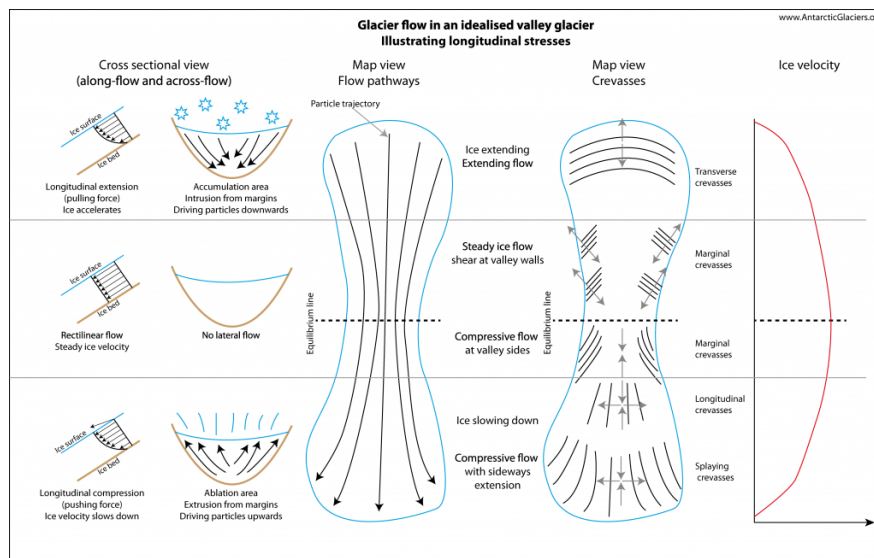


Fig. 5 - Crevasse formation on valley glacier. Source: B. Davies, Structural glaciology, 2023

## Englacial Moraines

Englacial moraines are sediments and rock debris buried within the glacier mass. These materials originate primarily from landslides, basal erosion, or incorporation of lateral and frontal moraines. The distribution of these materials occurs in three main locations:

**Superficial:** Usually carried by crevasses or landslides, debris accumulates on the glacier surface.

**Internal:** The debris buried in the ice body is derived from surface moraines or basal erosion.

**Basal:** Intense ice-bedrock interaction causes materials to be pulled at the glacier base. Englacial moraines may alter the mechanical behavior of the glacier or the physical characteristics of ice, therefore enhancing solar heat absorption (for surface debris).

## Water Fractures

Water fractures develop when liquid water enters pre-existing crevasses or fissures, flowing deeper into the glacier. During summer melt, when surface meltwater runs across the glacier surface and gains access to the subglacial system, this process is very common.

Water fractures significantly influence the dynamics of glaciers:

**Water transport:** They enable the swift movement of surface water to the glacier base, thereby influencing subglacial flow.

**Fracture growth:** Water pressure within fractures can propagate them to the glacier base.

**Thermal effects:** Liquid water, with its heat transport capacity, can locally alter the ice temperature [21], [22].

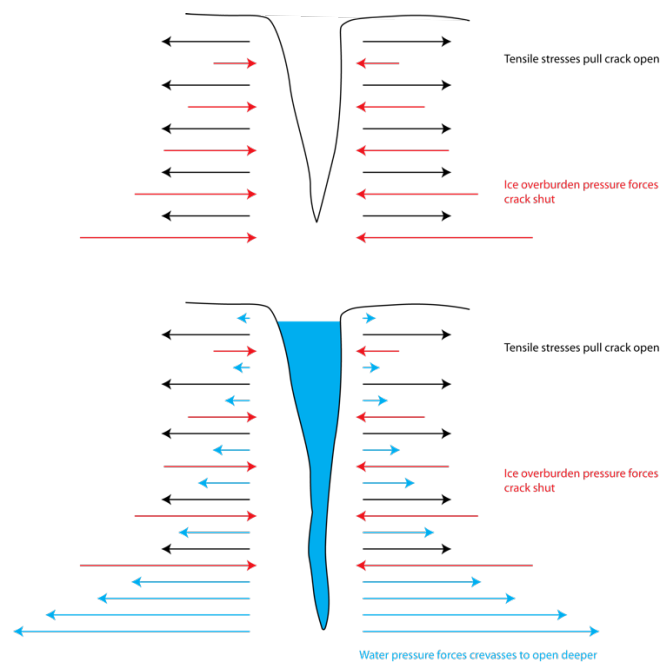


Fig. 6 - Controls on crevasse depth in valley glaciers. Source: B. Davies, Structural glaciology, 2023

## Cavities

Usually resulting from glacial erosion or ice detachment from the underlying substrate, glacial cavities are voids either inside or under the glacier. These cavities range from tiny, isolated gaps to vast areas supporting subglacial lakes in scale.

Cavities are essential for:

**Subglacial flow:** These channels serve as temporary pathways for the drainage of water.

**Ice deformation:** These factors influence the movement of glaciers, creating zones of faster sliding.

**Water storage:** In certain conditions, cavities can host water pockets, retaining liquid water within the glacier [13], [23].

## Water Pockets

Water pockets are liquid water reservoirs within the ice, often formed due to local pressure or temperature variations. These pockets can be isolated or connected to a larger drainage system. Usually, they arise where water pressure is higher than the underlying ice pressure, therefore avoiding freezing.

Water pockets have several meanings:

**Glacial drainage:** They can release large quantities of water during sudden outbursts, known as jökulhlaups.

**Local deformation:** The presence of liquid water alters the mechanical properties of ice, making it more prone to deformation.

**Radar effects:** Due to the high electrical conductivity of water, pockets can reflect or attenuate electromagnetic waves, complicating ice thickness detection, as well as water fractures [23],[24].

Key components for comprehending ice dynamics and the physical mechanisms driving a glacier's behavior are its internal features, including crevasses, englacial moraines, water fractures, cavities, and water pockets. We will later explore how these characteristics directly influence surveying methods like Ground Penetrating Radar (GPR), necessitating their proper consideration in glaciological research and practical applications.

### 2.2.3 Dynamic Response to Climate Change

Glaciers respond in a complex and nonlinear way to climatic variations, acting as dynamic systems where accumulation and ablation processes continuously interact with changes in temperature, precipitation, and solar radiation. Considering global warming, where even small temperature fluctuations can cause major changes in glacier dynamics, this vulnerability is especially clear. The Equilibrium Line Altitude (ELA), the height at which accumulation and ablation processes are balanced, shows one of the clearest consequences of such changes: an upward shift.

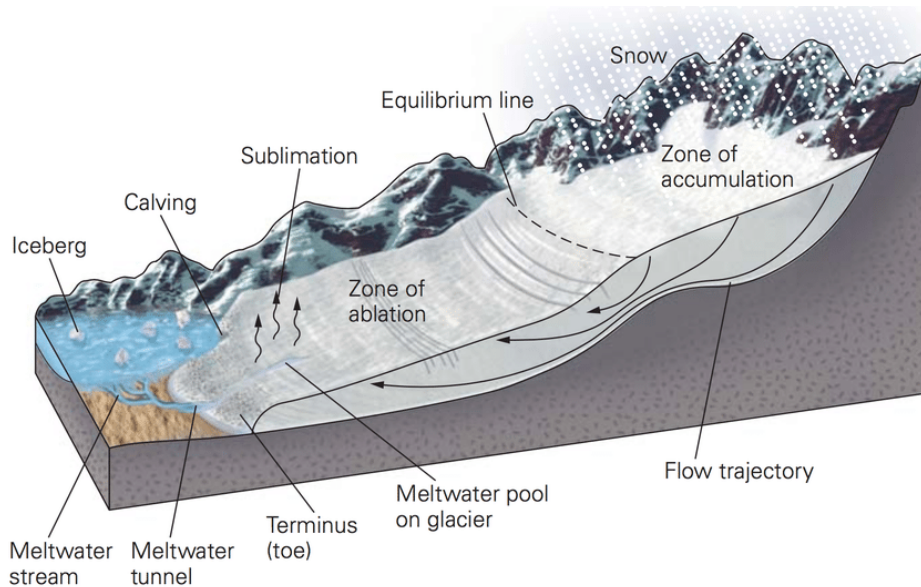


Fig. 7 - The equilibrium line separates the zone of accumulation from the zone of ablation. Source: S. Bate, A reconstruction of ELA of little ice glacier in Linnédalen, 2018

#### The Shift of the ELA and its implications on Glacier Mass Balance

The upward change in the Equilibrium Line Altitude (ELA) has a direct effect on the balance of glacial mass because it reduces the surface area of the accumulation zone and increases the ablation zone by the same amount. Historical studies of climatic and glaciological data have well documented this phenomenon in high areas such as the Andes, the Himalayas, and the Alps. Researchers have calculated that for every 1°C increase in global temperature, the ELA rises by 50 to 200 meters, resulting in significant glacier mass loss [25].

Rising global temperatures also influence ablation processes simultaneously. At lower elevations, when sensible heat, solar radiation, and warm rain accelerate the process, surface melting gets more intense. In arid areas or low relative humidity, such as Tibet or the Atacama Desert, sublimation becomes a predominant phenomenon. The combination of melting and sublimation results in faster glacier mass loss, directly impacting the long-term stability of glaciers.

#### Glacier Flow Dynamics and Glen's Law

Beyond mass balance, a glacier's dynamic response to climate change manifests through its flow velocity. Flow velocity refers to the rate at which ice moves along a glacier's slope, influenced by gravity, internal stress, and basal conditions. This process is mathematically described by Glen's law:

$$\varepsilon = A\tau^n \quad (2)$$

where:

- $\dot{\epsilon}$  is the strain rate, representing the change in ice shape under stress;
- $A$  is a parameter dependent on temperature, increasing exponentially with warming, making the ice more deformable;
- $\tau$  is the shear stress, determined by gravity, the glacier slope, and ice thickness;
- $n$  is an empirical exponent, generally equal to 3, reflecting the nonlinearity of the relationship between stress and deformation.

Glen's law highlights the crucial role of temperature in glacial dynamics. Temperate glaciers, characterized by ice near the melting point, exhibit significantly higher flow velocities compared to polar glaciers, where temperatures are much lower. This behavior is particularly evident in glaciers in Greenland and Alaska, where climate warming has accelerated glacial movement, with flow speeds exceeding 10 meters per day in some areas [26].

### Substrate Interactions and Basal Sliding

In addition to internal ice deformation, basal sliding—that is, the sliding of ice over its underlying bedrock—affects glacier movement. Liquid water created by high pressure or geothermal heat at the glacier base helps accelerate this process. As a lubricant, water lowers friction and lets the ice flow faster. Basal sliding may account for up to 90% of the overall flow velocity in temperate glaciers [27], so these systems are especially susceptible to variations in the temperature.

Basal water can also become trapped in subglacial cavities or channels, leading to episodic variations in flow velocity known as glacial surges. These phenomena, observed in glaciers in Alaska and the Himalayas, can result in rapid glacier front advances followed by stasis or retreat.

### Climatic Effects and Dynamic Feedback

Glacier flow velocity may boost the consequences of climate change by means of feedback systems. Greater ablation in terminal zones, where the ice thins and becomes more vulnerable to melting, could result from a rise in flow velocity. Ocean interactions amplify the impact of mass loss in glaciers that end in the sea, such as those on the Antarctic Peninsula.

Prediction of glacier behavior depends on an awareness of glacier flow dynamics and their relationship with climate. Advanced numerical models that use Glen's law and basal sliding dynamics can help to recreate complicated situations involving climate, hydrology, and landforms. Planning mitigating and adaptation strategies to handle the increasingly evident consequences of climate change depends on these technologies.

### Climatic Feedback of Glaciers

Glaciers play a significant role in climatic feedback systems, influencing both local and global climates. Key feedback mechanisms include:

- **Albedo feedback:** Ice melting reduces the reflectivity of the Earth's surface, increasing the absorption of solar radiation and consequently raising temperatures. This effect is self-reinforcing, accelerating ice melting.
- **Hydrological feedback:** Melting glaciers changes seasonal water flows, hence enhancing summer water availability but leading long-term declines as glaciers retreat.
- **Sea-level feedback:** Glacier mass loss directly causes sea-level rise; consequences of this process are enhanced by ocean thermal expansion.

Greenland provides a clear illustration of albedo feedback since exposed ice regions have grown in recent years, raising local temperatures and hastening melting [28].

## 2.2.4 Regional and Global Effects

At a regional level, glacier retreat significantly impacts local ecosystems, water resources, and community safety. The formation of new proglacial lakes—water basins that occur in regions left unoccupied by retreating ice—is one of the most noticeable outcomes. Fragile moraines, unconsolidated glacial debris deposits, often dam these lakes, causing sudden collapse and catastrophic events known as Glacial Lake Outburst Floods (GLOFs). Such phenomena are particularly common in the mountainous regions of the Himalayas, the Andes, and the Alps, where global warming is accelerating glacier retreat.

GLOFs may have disastrous effects. For instance, the Dig Tsho proglacial lake's collapse in 1985 in the Himalayan area destroyed agricultural land, villages, and infrastructure in eastern Nepal. Rising global temperatures are predicted to increase the probability of such catastrophes, impacting nearby mountain valley populations. Beyond the danger of floods, glacier retreat changes seasonal water flow. Glaciers' natural reservoirs in mountain basins store winter's water and release it gradually in the summer. But as shown in the Ganges, Indus, and Mekong basins, declining glaciers lead this balance to change: in the short term, melting may boost water flows; in the long run, it results in lower water availability during periods of drought [29].

Particularly in the arid areas of Peru, Bolivia, and Chile, the faster melting of Andean glaciers is compromising water supplies for millions of people in Latin America. With effects on agriculture and hydroelectric generation, the retreat of the largest tropical glacier in the world, the Quelccaya Glacier in Peru, endangers the water supplies of nearby towns.

Globally, glacier retreat strongly influences sea-level rise and the decrease of freshwater reserves. Terrestrial glaciers, excluding the Antarctic and Greenland ice sheets, have lost an average of 270 billion tons of ice per year in recent decades. Based on IPCC estimations, this glacier mass loss accounts for one of the primary causes of sea-level rise—about 3.3 millimeters per year. Sea-level rise poses particularly serious threats to coastal and island populations, such as increased floods, erosion, and saltwater intrusion into aquifers [1].

## 2.3 MODELS PREVIOUSLY APPLIED TO THE ALPS

The modeling of Alpine glaciers has played a fundamental role in studying glacier dynamics, providing indispensable tools for understanding the distribution of glacial mass and its interaction with hydrological systems. The innovative techniques have especially concentrated on studying glacier thickness, thereby improving knowledge of freshwater supplies in mountainous areas. Studies by Farinotti et al. (2009), Huss and Farinotti (2012), and McNabb et al. (2019), which established solid and detailed modeling of Alpine glaciers, rank among the most important contributions.

### 2.3.1 The Study by Farinotti et al. (2009)

One of the first methodical attempts to measure the thickness of Alpine glaciers by means of an integrated methodology combining mass balance data with glacier flow dynamics is the 2009 Farinotti et al. [30] study. The proposed approach integrates numerical models capable of reconstructing the spatial distribution of glacier thickness with field observations, encompassing geodetic and glaciological surveys.

One important result of this work was the publication of accurate maps of glacier thickness throughout several Alpine areas. Farinotti et al. emphasized that local precipitation patterns, temperature gradients, and bed topography caused marked geographical heterogeneity. This work underlines the need to precisely represent the distribution of glacier mass using high-resolution regional models, a necessary feature for evaluating Alpine water reserves.

Independent data comparisons validated the results of the study, demonstrating the great dependability of the model. These results are especially related to water resource management since they gave a strong foundation for estimating how glacier retreat would affect hydrological basins.

### 2.3.2 The Study by Huss and Farinotti (2012)

Expanding on the previous study, Huss and Farinotti (2012) added a more comprehensive and worldwide approach to calculating glacier thickness, with a special focus toward the Alpine area. Their work used a distributed numerical model to combine topography and high-resolution climatic data, therefore allowing a more accurate representation of glacier movements [31].

With the intention of generating a dataset relevant for several scientific and management uses, one of the most innovative features of this work was the investigation of glacier thickness distribution on regional and worldwide levels. The authors emphasized that high-altitude regions, favored by colder climatic conditions and abundant precipitation, hold the highest ice reserves in the Alps. Understanding glacier thickness is not only necessary for estimating glacier volume but also for more precisely modeling their contribution to seasonal water flows, especially during the summer months; Huss and Farinotti also underlined that this work further enhanced the model's resilience by introducing simulations accounting for beginning data and climatic inputs and therefore addressing uncertainty. The data gave important new perspectives on the possible long-term effects of glacier retreat.

### 2.3.3 The Study by McNabb et al. (2019)

Thanks to the merging of high-resolution radar data and numerical inversion techniques, McNabb et al. (2019) [32] produced a further development in glacier thickness modeling. This method let us obtain comprehensive maps of glacier thickness with unprecedented spatial resolution, including several mountain ranges, such as the Alpine arc.

Supported by extensive verification using Ground Penetrating Radar (GPR) data and aerial surveys, the project distinguished itself by the precision of the estimates acquired. The scientists showed that the geomorphological arrangement of Alpine glaciers greatly affects the distribution of glacial mass; some places exhibit more resistance to climatic fluctuations (McNabb et al., 2019).

The results of the investigation affected not only knowledge of glacier dynamics but also risk management in mountainous areas. Evaluation of the possible contribution of ice to fast melt processes and hydrogeological dangers depends on thorough awareness of glacier thickness distribution.

The studies presented offer a significant basis for the present research since they underline the need for precise glacier thickness modeling for comprehending the features and distribution of glacial mass in the Alps. This work applies the GLATE model, which builds on past knowledge and complements previously reported methods.

GLATE especially benefits from the incorporation of GPR data acquired in the field since it enables a more comprehensive display of glacier bed geometry. However, this suggests an integration that satisfies specific criteria related to the glaciers of Val Ferret, such as the necessity of combining field observations with numerical simulations, rather than surpassing previous models.

This method aims to provide clarity on the distribution of glacial mass, thereby broadening the scope of existing regional studies. Although GLATE aims to produce results congruent with and complementary to current regional analyses, underlining the need for cooperation between several research approaches, it shares some common limitations, such as dependability on the quality of input data.

# 3 CHARACTERISTICS OF THE VAL FERRET AND ITS GLACIERS

## 3.1 GEOGRAPHY AND MORPHOLOGY OF THE VAL FERRET

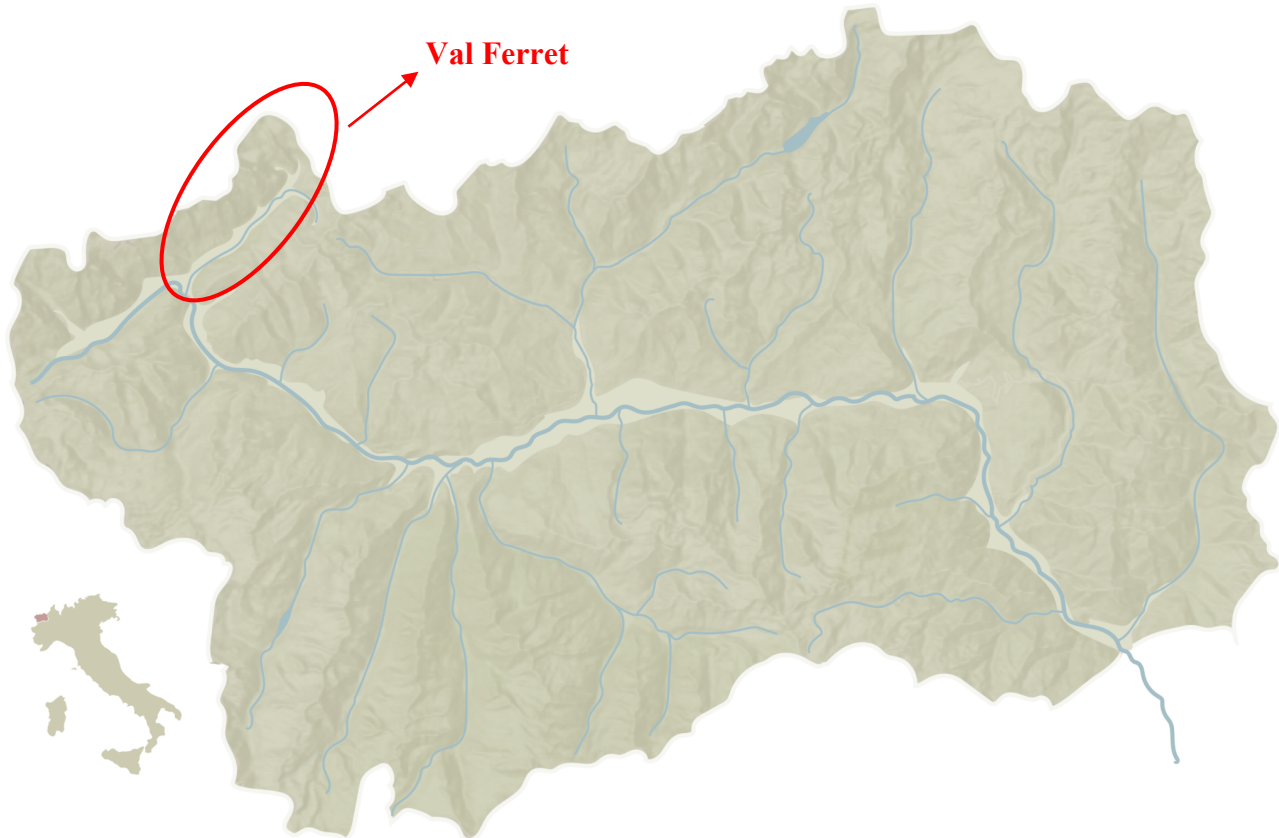


*Fig. 8 - Geographical location of the study area.*

### Introduction to Val Ferret

On the Italian side of the Mont Blanc range, Val Ferret is among the most iconic alpine valleys. Situated in the Aosta Valley, it shows a scene of amazing natural beauty along a northeast-southwest axis for almost twenty kilometers. Mont Blanc, the highest peak in Europe at 4,810 meters, dominates the range of striking mountains that surrounds the valley, several of which rise more than 3,000 meters. Val Ferret is a special site for glaciological, geomorphological, and environmental studies [33] because of its combination of high altitudes, active glaciers, and varied vegetation. Beyond its natural and scenic beauty, Val Ferret is also a well-known hiking and alpine tourism destination with numerous trails across immaculate surroundings and linking historic mountain refuges. However, its geological and geomorphological framework holds significant importance for scientific studies.

### Geomorphology of Val Ferret: Formation of the Valley

Val Ferret's present configuration is the outcome of a complicated interaction between glacial and geological processes that evolved over millions of years. Throughout glacial periods, ice sheets subjected the area to erosive activity, sculpting the valley into a distinct U-shaped profile with a very

flat valley floor and steep lateral slopes. Further underlined by the existence of lateral and terminal moraines, glacial cirques, and surfaces polished by ice [24], this profile is a classic example of glacial modeling.

### Geological Structures and Lithology

Geologically, Val Ferret forms a component of the Mont Blanc massif's metamorphic and plutonic units. Derived from the deep change of sedimentary and magmatic rocks during the Alpine orogeny, predominant rocks are gneiss, micaschist, and quartzite. Granite intrusions enrich these lithological units, giving the landscape a rough and commanding look, especially shown in the jagged ridges and peaks all around the valley.

Striations and *roche moutonnées*, which testify to the movement of ancient glaciers, show clear indicators of glacial activity on the stony surfaces. Higher-altitude glacial cirques indicate the starting locations of past glacier flows that sculpted the current terrain [34].

### Val Ferret's Hydrography: The Dora di Ferret River's contribution

The Dora di Ferret stream, which runs along the valley floor and collects water from glaciers and high-altitude streams, dominates Val Ferret's hydrological system. The stream, mostly fed by meltwater, exhibits a significant seasonal discharge pattern, with high flows in summer and low flows in winter. Typical glacial valleys, where melting ice provides the main water source [35], follow this trend.

The river plays a crucial role in both the ecology of the valley and human activity. Particularly in the surrounding areas, it is a vital supply for agriculture and helps generate hydroelectric power. But glacial retreat is gradually changing the water balance, which has long-term consequences regarding water availability.

### Glacial Lakes and Geomorphological Risks

Apart from the mainstream, Val Ferret includes several little glacial lakes created in depressions left behind by glaciers. Usually hidden back behind moraines, these lakes are not only a remarkable sight but also a possible geomorphological hazard. The development of proglacial lakes might result in moraine dam breaches, hence generating downstream flooding.

### Temperature and Vegetation: Climatic Variation with Altitude

From 1,500 meters at the valley bottom to over 4,000 meters at the nearby summits, Val Ferret shows notable climate gradients driven by altitude. While higher altitudes exhibit a nivale climate with plenty of snowfall and temperatures remaining below freezing for much of the year, at lower elevations, the climate is subalpine, marked by cold winters and cool summers. Although continuous climate change is accelerating their retreat, this environment helps glaciers to exist and be preserved [1].

### Valley's Biodiversity

The vegetation reflects this climate variety, from larch and spruce forests at lower altitudes to alpine meadows and lichens at mid-elevations and barren, rocky parts at higher altitudes. Rich in biodiversity, these habitats support many of which are peculiar to the Alps and species suited for hostile conditions.

Val Ferret is an extraordinary natural laboratory for studying alpine dynamics. Unique landscapes, great climatic and environmental variety, and active glaciers together offer the perfect setting for multidisciplinary scientific study. Knowing the topography and geology of this valley not only helps to better understand alpine systems but also provides necessary instruments for handling issues with natural resource management and climate change.

### 3.2 DESCRIPTION OF THE MAIN GLACIERS OF THE VALLEY

Val Ferret is home to some of the most representative and studied glaciers on the Italian side of the Mont Blanc massif. Apart from shaping the terrain, these glaciers offer important understanding of glacial dynamics and climate change. The major glaciers are described here together with their particular features, important problems, and function in the geomorphological setting of the valley. Additional important glaciers are also discussed to offer a more complete knowledge of the glacial complexity of Val Ferret.

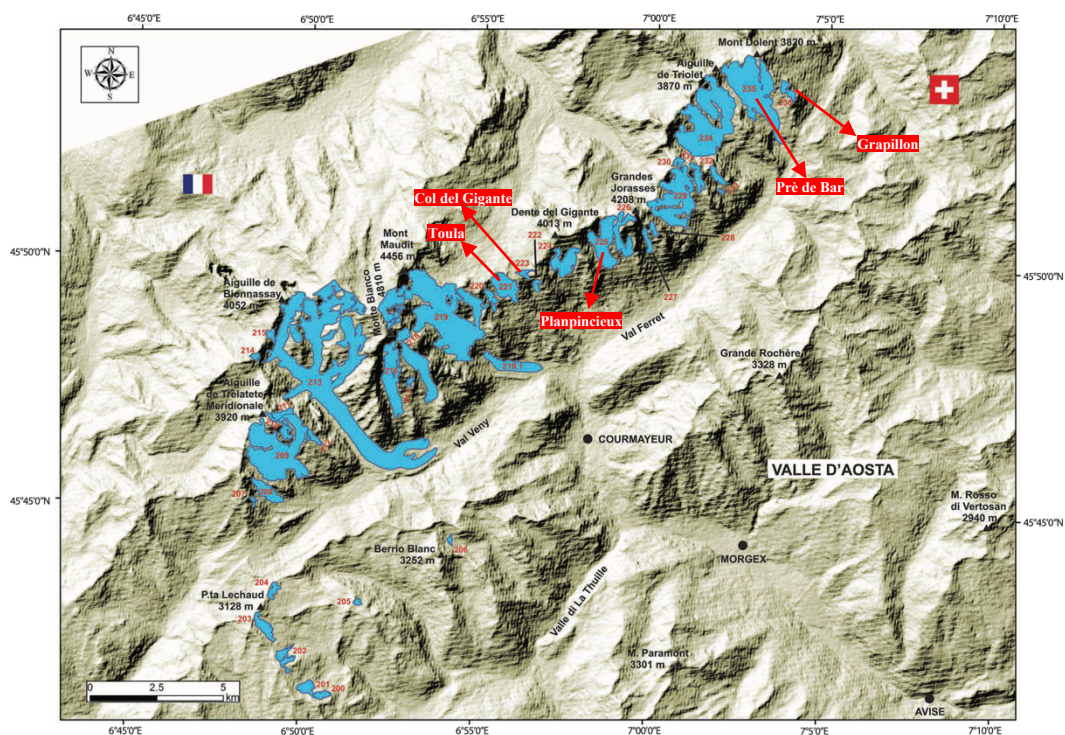


Fig. 9 - Overview of Val Ferret glaciers (the processed ones are in red), Source: 4-valle-daosta.pdf

#### 3.2.1 Pré de Bar Glacier

The Pré de Bar Glacier, one of the most iconic and characteristic glaciers of the valley, is located in northern Val Ferret. Showcasing classic glacial morphology, it originates on the Italian slope of Mont Dolent and extends toward the valley floor. The glacier spans altitudes between 2200 and 3500 meters [35]. Its narrow and well-defined tongue is marked by crevasses, indicating ongoing dynamic flow, while the accumulation zone is situated in the higher elevations of Mont Dolent, an area dominated by nival conditions for most of the year.

The glacier has undergone significant retreat over the past few decades, with its area decreasing by approximately 30% since the 20th century [38]. This retreat has become especially apparent during warmer seasons, exposing unstable surfaces that increase the risk of landslides and debris flows.



*Fig. 10 – Prè de Bar glacier in 1897 (Druetti photo)*



*Fig. 11 - Prè de Bar glacier in 1993 (A. Cerutti photo)*

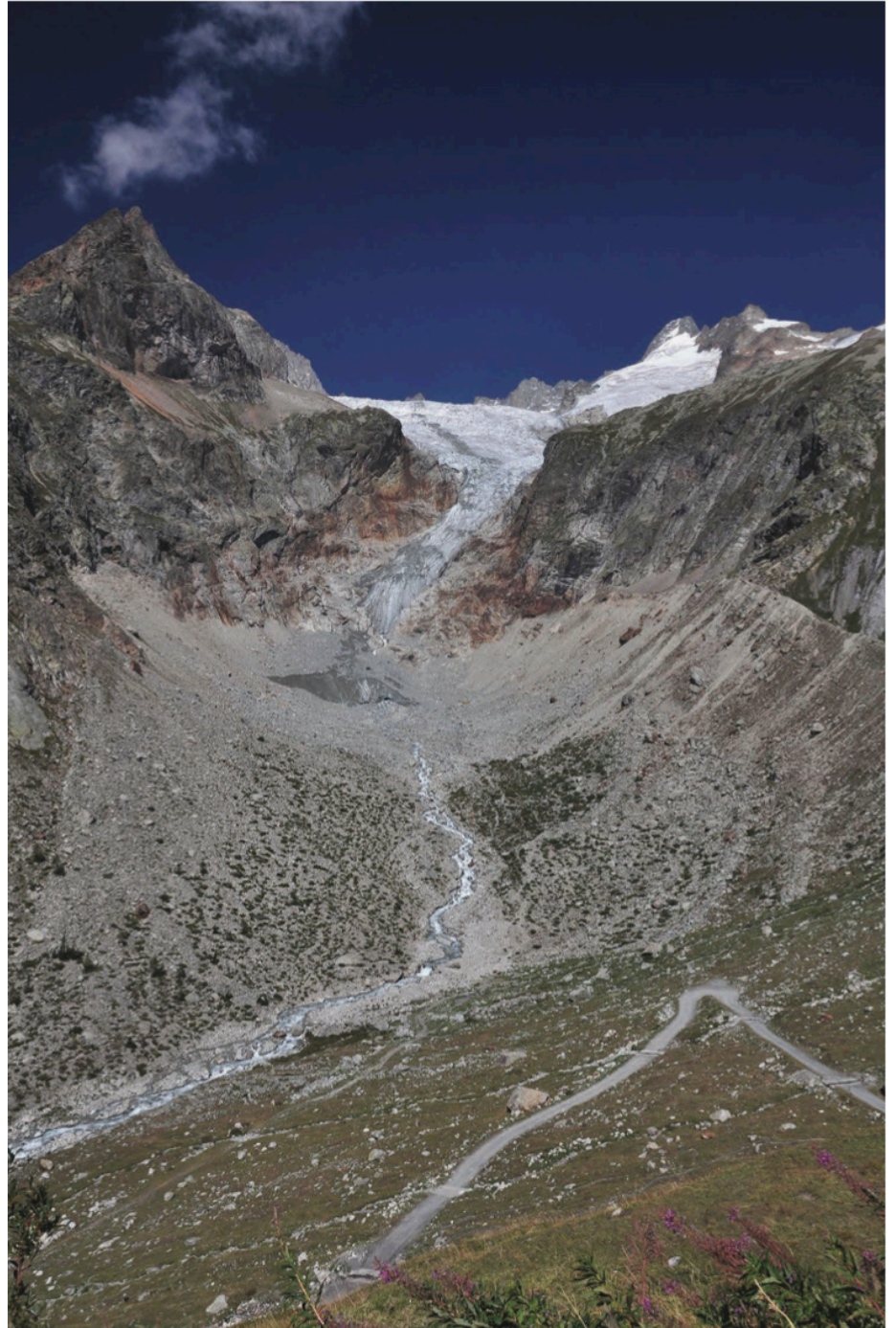


*Fig. 12 – Prè de Bar glacier in 2012 (L. Mercalli photo)*

### 3.2.2 Grapillon Glacier

One of the most dynamic and extensively studied glacier masses in Val Ferret, the Grapillon Glacier is located adjacent to the Prè de Bar Glacier. Despite its relatively small size, it displays significant flow activity, sustained by a substantial accumulation zone at higher altitudes. Its steep and fractured tongue, characterized by prominent seracs, defines its dynamic morphology.

The glacier is particularly affected by seasonal climate variations and experiences rapid ablation during hotter summers. Changes in its ice mass have a direct impact on local water flows, playing a crucial role in regulating the hydrological cycle of the Dora di Ferret stream.

### 3.2.3 Planpincieux Glacier

Because of the hazards related to its instability, the Planpincieux Glacier—which lies on the Grandes Jorasses—is among the most under-observed glaciers in Val Ferret.

The Planpincieux Glacier is a temperate glacier with an internal temperature consistently around zero, allowing liquid water to exist both at its base and within its structure, significantly influencing its dynamics. These characteristics make it historically prone to ice collapses.

The glacier's accumulation area consists of two cirques, amphitheater-shaped cavities with steep walls carved into the mountain's side. The most prominent cirque lies at the base of the Grandes Jorasses, at an altitude of 3500 meters. Ice from these cirques converges into a basin area that feeds two lower lobes, with their fronts located at around 2600 meters. The ice flow is primarily channeled into the right lobe, a dynamically active region with an average slope of 32° and a heavily crevassed morphology.

Its suspended tongue overlooks the valley floor, making it a visually striking but potentially hazardous glacier. The glacier spans altitudes ranging from approximately 2650 to 4020 meters [36]. The front of the right lobe features a vertical ice wall 20 to 30 meters high, descending into the steep Montitaz channel, where numerous ice collapses occur, particularly during the summer.

The glacier's seracs are notorious for their regular instability, with detachment events posing significant risks to the valley floor and nearby infrastructure. Recent studies [37] indicate that warming temperatures accelerate the glacier's movement, increasing the likelihood of catastrophic events.

The dynamic behavior of the Planpincieux Glacier can be summarized in two distinct phases:

- A quiescent phase, typical of winter or particularly cold periods, characterized by low displacement speed of the glacier mass and the absence of accelerations.
- An active phase, observed during specific moments in the summer–autumn period, marked by high glacier mass dynamism, significant accelerations, and compartmentalization into sectors. During this phase, a highly visible basal water flow is usually observed [38].

### 3.2.4 Grandes Jorasses Glacier (Whymper Serac)

One of the most striking glacial forms in the Alps, the Whymper Serac, makes the Grandes Jorasses Glacier famous.

The Whymper serac is situated at an altitude of 4,050 meters and is classified as a cold glacier. In a cold glacier, the entire mass remains below the melting point, meaning there is no liquid water present.

The movement of the serac is primarily influenced by the effect of gravity. It grows cyclically, accumulating part of the snow that falls during winter and increasing in volume until it reaches a point of imbalance. This process leads to the detachment of ice blocks from the main body, potentially causing collapses of varying magnitudes. Seasonal temperature changes have also an impact on the stability of the serac; in recent years, there has been an increase in large-scale detachment episodes, partially linked to these thermal fluctuations.

A key issue affecting the region is the rising frequency of landslides and rockfalls in the adjacent deglaciated areas, which alters the geomorphological balance of the valley. This phenomenon adds to the complex dynamics and risks associated with the serac [38].

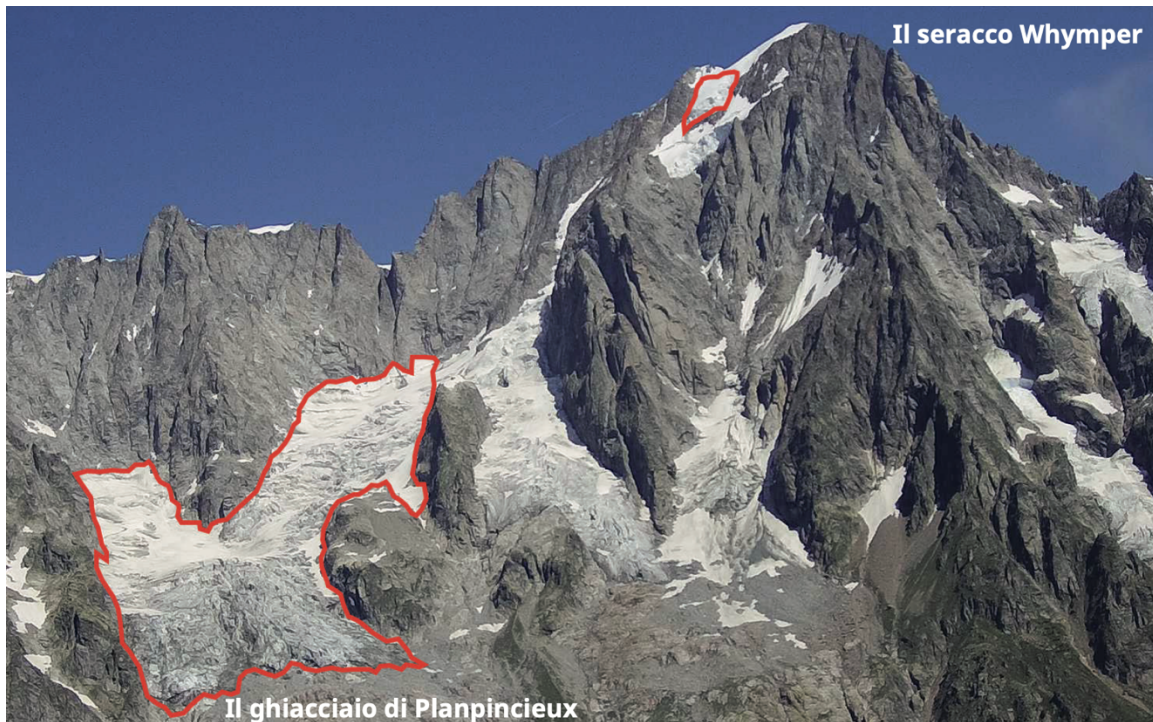


Fig. 13 - Planpincieux glacier and Whymper serac, Source: [fondazionemontagnasicura.org](http://fondazionemontagnasicura.org)

### 3.2.5 Col del Gigante Glacier

Near the Punta Helbronner station, at one of the highest points in Val Ferret, lies the Col del Gigante Glacier. Rising above 3000 meters, the glacier features a large accumulation zone directly fed by the Mont Blanc massif. It plays a significant role in the valley's water system.

The glacier's gradual melting has led to the formation of new proglacial lakes, which pose potential geomorphological hazards. Additionally, the thinning ice is altering the structure of the underlying permafrost, contributing to further changes in the landscape.

### 3.2.6 Toula Glacier (Helbronner)

Also near Punta Helbronner, the Toula Glacier is one of Val Ferret's most renowned glaciers due to its strategic location and significance for tourism. The glacier features a southeast-pointing tongue [40] and a large accumulation zone. As one of the most frequently visited glaciers in the area, it is easily accessible from the Skyway Monte Bianco.

However, rising anthropogenic pressure, combined with the effects of climate change, is accelerating the glacier's structural breakdown. Additionally, the presence of seracs poses significant risks to mountaineering activities due to frequent detachment incidents.



*Fig. 14 - Skyway station, between Toula and Col del Gigante glaciers. Source: <https://www.montebianco.com/it/funivie/punta-helbronner-the-sky>*

### 3.2.7 Other Val Ferret Glaciers

Apart from the above-mentioned glaciers, which will be the focus of the study, Val Ferret hosts other important glacial systems, including the Triolet Glacier and the Brenva Glacier. Though not discussed in this paper, these glaciers complete the geomorphological framework of the valley and offer insightful analysis. The Triolet Glacier, known for its unstable seracs and hydrological function, exemplifies the dynamic nature of alpine glaciers. The Brenva Glacier, with its extensive glacial tongue, has been the site of extreme geomorphological events, such as debris flows and icefall detachment [36].

## 3.3 CURRENT MONITORING OF THE GLACIERS IN VAL FERRET

Global warming is causing major changes in the glaciers of Val Ferret, as in many other Alpine glacier regions. Rising average temperatures and declining snowfall have accelerated melting events, leading to a reduction in the general glacier mass. In this context, knowledge of the dynamics of glaciers depends on their monitoring, which also helps prevent risky situations and guide possible mitigating actions. The following are the principal monitoring systems currently in use for the glaciers of Val Ferret, with special reference to the systems installed for the glaciers of Planpincieux, Grandes Jorasses, Prè de Bar, Grapillon, Col del Gigante, and Toula.

### Total Station (Grandes Jorasses)

Monitoring the serac of Whymper depends fundamentally on this station. This technology sends a laser signal to reflecting prisms placed straight on the ice surface to track the motion of the serac. Regular interval assessments of movement velocity and potential acceleration yield highly precise information that may point to approaching instability conditions.

### Photographic System (Planpincieux and Grandes Jorasses)

Comprising a sequence of high-resolution cameras positioned in strategic points, the photographic system constantly monitors glacier surfaces. These cameras provide quantitative research employing photogrammetric techniques as well as qualitative analysis—that is, tracking visual changes in the ice. Processed photos are used to quantify displacements, volume changes, and changes in glacier form.

### GBInSAR Radar (Planpincieux and Grandes Jorasses)

Ground-Based Interferometric Synthetic Aperture Radars (GBInSAR) are installed on both the Planpincieux and Grandes Jorasses glaciers. These instruments monitor glacier displacements by measuring the phase difference between microwaves emitted and received in two successive acquisitions. This method allows for micrometric precision in detecting surface movements, even in adverse weather conditions.

### Doppler Radar and Traffic Light System (Planpincieux)

Doppler radar senses potential ice collapses in real time. This system is particularly crucial for public safety as it activates the traffic signal system that runs alongside the municipal route to Planpincieux. Should a catastrophic occurrence arise, the traffic light automatically turns red, therefore preventing access and alerting the relevant authorities [38].

### Monitoring System on Pre-Bar Glacier

Monitoring work on the Prè de Bar Glacier includes regular mapping of the glacier surface using drones. Drones provide high-resolution images for the construction of digital terrain models (DTM), which enable the evaluation of changes in the glacier's mass balance. Additionally, GPS sensors installed in key points of the glacier detect surface displacements and deformations.

### Monitoring System on Grapillon Glacier

The Grapillon Glacier is mainly monitored using thermal and pluviometric sensors installed near its base. Essential for the hydrological balance and knowledge of surface melting processes, this equipment gathers data on ice temperature and precipitation.

### Monitoring System on Col del Gigante Glacier

An integrated system combines ground-penetrating radar (GPR) and meteorological stations atop the Col del Gigante Glacier. While the weather stations provide data on temperature, wind, and solar radiation, valuable for predicting glacier evolution, the GPR examines the underlying structure of the ice, spotting fractures or cavities.

### Monitoring System on Toula Glacier

Piezometric sensors installed in the subglacial outflow zones of the Toula Glacier monitor its movement. These sensors track changes in water pressure, therefore revealing information on subglacial hydrological activity. Furthermore, drones are employed to gather photographs, updating digital surface models and investigating possible instability events.

## 4 METHODOLOGY

### 4.1 DESCRIPTION OF THE MODEL USED

Advanced knowledge of the ice thickness distribution within glaciers is of fundamental importance in the context of climate change monitoring in alpine areas. Ice thicknesses can be modeled using glacier surface features, but the resulting models can be prone to considerable uncertainties. Alternatively, it is possible to measure ice thicknesses, for example, with Ground Penetrating Radar (GPR). Such measurements are typically restricted to a few profiles, with which it is not possible to obtain spatially unaliased subsurface images.

For this reason, the analysis conducted in this thesis is based on the use of the GLATE (Glacier Thickness Estimation) model, which was developed to estimate glacier thickness distribution by combining modeled results with measurements. Ground Penetrating Radar (GPR) data constrained the estimates derived from the model to reduce uncertainties in the final results.

In order to optimally combine modeling results and measured ice thicknesses, GLATE uses an inversion procedure to obtain overall thickness distributions. It offers the flexibility to integrate any existing modeling algorithm and to add further constraints.

### 4.2 OPERATING PRINCIPLES OF GROUND PENETRATING RADAR

#### 4.2.1 Introduction

Ground Penetrating Radar (GPR) is a versatile and widely applied geophysical technique used for exploring subsurface structures, including the internal composition and dynamics of glaciers. This non-invasive method depends on the propagation of electromagnetic waves, which are transmitted into the subsurface and then reflected back to the surface when encountering material boundaries with differing electromagnetic properties. Variations in permittivity and conductivity define these boundaries and help determine the strength and nature of reflected signals. The core of GPR technology involves two main components: a transmitting antenna and a receiving antenna. Short high-frequency electromagnetic wave pulses from the transmitting antenna reach the glacier. As these waves travel through the ice, they encounter interfaces such as bedrock, air pockets, water inclusions, or layers of debris. Part of the wave energy reflects back to the receiving antenna at every interface; the rest keeps moving farther down into the ground. GPR systems can precisely determine the depth of these interfaces by timing the difference between the transmitted and received signals.

GPR is particularly effective in glaciological studies due to its ability to penetrate ice (which has low conductivity) with minimal signal attenuation. This allows researchers to obtain detailed profiles of ice thickness, detect internal stratigraphy, and locate inclusions such as water or debris. These abilities are crucial for mapping ice thickness, reconstructing past climatic conditions using internal stratigraphy, locating subglacial features such as bedrock topography and subglacial lakes, and tracking glacier dynamics by spotting thickness or potential instability zones. In glaciology, GPR's high-resolution data makes it an essential instrument. Unlike other techniques, GPR can cover large areas quickly and provide continuous profiles of subsurface structures. Its non-invasive nature ensures that the glacier remains undisturbed during surveys, making it suitable for use in sensitive environments. Additionally, the portability and adaptability of GPR equipment allow researchers to deploy it in remote and challenging terrains.

Though GPR is a useful instrument, its efficacy relies on multiple factors. The existence of impurities in the ice, such as sediments or high water content, which raise attenuation, may affect signal penetration. Interpreting GPR data requires careful analysis and often the integration of complementary data sources, such as borehole measurements or remote sensing imagery, to validate the results. Despite these difficulties, GPR is still very useful in providing thorough insights on ice thickness, internal layering, and subglacial characteristics, thereby enhancing our knowledge of glacier dynamics and their reaction to climate change. This fundamental understanding emphasizes the significance of GPR in glacier research and sets the stage for a deeper exploration of the instrumentation and parameters that govern its effective application.

#### 4.2.2 Instrumentation

Ground Penetrating Radar (GPR) data collecting equipment consists mostly in a transmitting antenna, a receiving antenna, and a control unit for data management and recording. The transmitting antenna emits high-frequency electromagnetic pulses, while the receiving antenna captures the waves reflected by the various interfaces present underground. The received signals are processed by the control unit and converted into profiles revealing the internal structure of the investigated material. Usually coupled with a global positioning system (GPS), this system lets the information collected be georeferenced so guarantees spatially correct analysis.

The transmitter sends high-frequency electromagnetic pulses, with an average power of 50 W, into the substance for examination at intervals of approximately 1 nanosecond. These pulses traverse the medium and expand until they encounter electromagnetic discontinuities, where a portion of the energy undergoes reflection and refractive action. The refractive index of the involved materials determines the reflection and refraction characteristics (and so the portion of energy reflected and transmitted), and the portion of reflected and transmitted energy can find their mathematical representations:

$$R = \left(\frac{n_2 - n_1}{n_2 + n_1}\right)^2 \quad (3)$$

$$T = 1 - R \quad (4)$$

where  $n = \sqrt{\varepsilon}$  represent the refractive indices of the material passed through ( $\varepsilon$  is the electrical permittivity of the material).

The reflecting component comes back to the surface and is captured by the receiving antenna. The later amplifies the collected signal and processes it through a reading system, then sends it to the display for graphic data presentation as radargrams.

Generally equivalent to around 6 cm in glaciological applications, the antenna configuration—known as "constant offset"—offers a fixed distance between transmitter and receiver. While this compact arrangement provides practical advantages in the field, it also poses a risk of noise generation if the antennas lack adequate shielding.

Selected depending on the aims of the research, the GPR antennas can operate over a large spectrum of frequencies, usually between 10 MHz and 2 GHz. Typically, the antennas operate within a frequency band, where the central frequency is characterized by the highest energy. The surveys get more resolution but also experience greater signal attenuation as the bandwidth and frequency rise.

Choosing the above-mentioned frequency band based on the desired depth and resolution allows for a reasonable penetration into the ground, maintaining a constant wave velocity even in low-conductivity environments.

These factors aid in the general classification of antennas:

- Low frequencies (10-100 MHz): Suitable for deep investigations, such as mapping the glacier bed, due to their higher penetration capacity.
- Medium frequencies (200-500 MHz): Offer a balance between investigation depth and resolution, making them ideal for most glaciological applications.
- High frequencies (500 MHz - 2 GHz): Used for detailed analysis of shallow layers or small cavities, providing high spatial resolution.

Additionally, the pulse frequency can be adjusted to control the investigation depth: low frequencies imply higher penetration depth, whereas high frequencies are used for shallow investigations. However, it is important to note that the frequency choice directly affects the wavelength ( $\lambda$ ) of the signal, calculated using the formula:

$$\lambda = \frac{v}{f} \quad (5)$$

where  $v$  is the wave propagation velocity in the medium and  $f$  is the signal frequency. Higher frequencies correspond to shorter wavelengths, leading to greater resolution but reduced penetration depth.

Glaciology extensively applies GPR to estimate ice thickness, locate subglacial cavities, and investigate internal stratifications. Because pure ice has low conductivity, radar signals travel efficiently and allow studies down tens of meters with centimeter-scale resolution. Frequencies between 200 and 500 MHz are often appreciated for their mix between depth and detail.

At last, a cabled connection links the georadar to a computer. From wave emission to capturing the obtained information, the computer runs all processes to enable a real-time field view of the radar image. Especially in remote or difficult areas, the real-time analysis of the gathered data offers a major operational benefit in the field. However, it is crucial to consider the limitations that contaminants in the ice, such as liquid water or sediment, impose on the signal, thereby reducing the effectiveness of the survey.

Generally, the georadar detects heterogeneities by reflecting a portion of the signal upward whenever electromagnetic waves encounter another "target." Selecting the most effective antenna and the wavelength of the produced pulse is crucial, as it depends on the depth to reach, the electromagnetic characteristics of the examined terrain, and the geometric features of the targets. Furthermore, the analysis will rely on the instrument settings the operator imposes depending on their experience, such as the listening time window.

### 4.2.3 Important parameters

The operation of GPR systems is closely related to the electromagnetic properties of the material being investigated, particularly electrical conductivity and dielectric permittivity. These two factors directly influence the reflection, attenuation, and propagation of electromagnetic waves, therefore defining the quality and precision of the obtained data.

## ELECTRICAL CONDUCTIVITY

Expressed in Siemens per meter (S/m), electrical conductivity ( $\sigma$ ) measures the ability of materials to conduct electrical current. High conductivity causes greater attenuation of electromagnetic waves, reducing the signal's ability to penetrate the material; so Ground Penetrating Radar technology returns more significant information if applied to low conductivity materials, as the signal is able to penetrate deeper into the investigated medium.

Three basic groups of materials can be distinguished depending on conductivity:

- Conductors: with  $\sigma > 10^{-2}$  S/m, materials including metals or salt-saturated soils. These materials greatly attenuate GPR signals.
- Semiconductors: materials having  $\sigma$  between  $10^{-4}$  S/m and  $10^{-2}$  S/m include moist soils or clay sediments.
- Insulators: materials with  $\sigma < 10^{-4}$  S/m that permit good signal propagation could be pure ice or dry rocks.

The material is more dissipative the more electrically conductive it is, and the attenuation coefficient is higher. Moreover, conductivity determines the length of the wave propagation; low conductivity will restrict the attenuation and result in large depths reached by the material. However, to have more precise information on the depth of investigation, it is necessary to also take into consideration the frequency at which the wave is emitted.

## ELECTRICAL PERMITTIVITY

Electrical permittivity ( $\epsilon$ ) represents a material's ability to store electrostatic energy in the presence of an electromagnetic field. It is defined by the relation:

$$\epsilon = \epsilon_r \cdot \epsilon_0 \quad (6)$$

where:

- $\epsilon_r$  is the relative permittivity (dimensionless) of the material;
- $\epsilon_0$  is the vacuum permittivity, equal to  $8.854 \cdot 10^{-12}$  F/m.

Materials have different relative permittivity; for example, pure ice has  $\epsilon_r \approx 3.2$ , while liquid water has  $\epsilon_r \approx 80$ . The density of the studied medium is strongly associated with relative permittivity. In glaciology, this link is especially helpful for empirical equation-based snow and ice density estimate using:

$$\epsilon_r = 1 + 1.7 \cdot \rho_r \quad (7)$$

where  $\rho_r = \frac{\rho_{snow}}{\rho_{ice}}$  is the material relative density [39]. Higher density implies higher permittivity, influencing the propagation and reflection of electromagnetic waves.

In the case of snow, the density value is variable and depends on the degree of porosity that characterizes it. Solid precipitation, in fact, undergoes a slow transformation process before becoming ice, according to the following steps:

- seasonal snow
- non-seasonal snow, i.e. snow that has resisted ablation for a year hydrological
- firn, defined by very dense non-seasonal snow (with density equal to 650 – 800 kg/m<sup>3</sup>)
- ice (with density between 830 and 900 kg/m<sup>3</sup>)

Electromagnetic wave propagation velocity ( $v$ ) depends on the relative permittivity of the medium and is:

$$v = \frac{c}{\sqrt{\epsilon_r}} \quad (8)$$

where  $c$  in a vacuum is the speed of light ( $3 \cdot 10^8 \text{ m/s}$ ). This formula makes exact computation of wave velocity possible in a homogeneous and isotropic medium.

Below are the density, relative permittivity and velocity values referring to some materials present in nature, particularly in the glacial and periglacial environment.

Material	Density ( $\text{kg/m}^3$ )	Relative permittivity ( $\epsilon_r$ )	Velocity (m/ns)
Air	1	1.0	0.300
Fresh snow	50-100	1.2-1.4	0.285-0.254
Dry snow	200-300	1.5-1.7	0.245-0.230
Compact snow	400-500	1.8-2.0	0.224-0.212
Firn	500-600	2.0-2.2	0.212-0.202
Pure ice	917	3.2	0.170
Water	1000	81	0.033

*Table 1 - Density, relative permittivity and velocity values referring to some materials present in nature*

#### CORRELATION BETWEEN THE SPEED OF THE WAVES AND THE DEPTH OF THE INVESTIGATED MEDIUM

Wave velocity is correlated with the depth that the radar can probe. Deeper penetration is possible in low-relative-permittivity materials (such as pure ice) because of faster propagation velocity. On materials with high permittivity or conductivity, including water-saturated soils, velocity lowers and signal attenuation rises, therefore lowering penetration depth.

The depth ( $\delta$ ) reachable by the signal can be estimated using the relation:

$$\delta = \frac{v \cdot t}{2} \quad (9)$$

where  $t$  is the round-trip travel time measured by the GPR system.

The analysis of the reflection times allows the depth of the discontinuity to be calculated, thanks to a constant value of the speed with which the radar pulse propagates in the investigated medium. Particularly, the reflection of the signal depends on the distance between the antenna and the detected discontinuity, computed as a function of the delay between the emitted pulse and the reflected pulse returning to the surface. Thus, geophysical studies take into account the Two Way Travel time ( $t_{twt}$ ), which is the sum of the outgoing and return times of the signal itself [40].

Conductivity and permittivity together govern GPR system performance in terms of depth and resolution. In glaciology, where pure ice offers perfect conditions for wave propagation, these factors enable exact measurements of glacier thickness and subglacial cavity discovery. But the existence of contaminants or water layers can greatly affect signal transmission, so thorough investigation of the electromagnetic characteristics of the studied media is necessary.

## 4.3 DATA COLLECTION

Data collection on a glacier using Ground Penetrating Radar (GPR) requires both careful logistical and technical planning since topographical features and extreme environmental conditions might provide major obstacles. This section discusses the data collection techniques, the operating principles of the used equipment, and the logistical problems, along with their solutions.

Data acquisition on the glacier is carried out by controlled movement of a GPR system, which includes a transmitting and receiving antenna mounted on a sled or portable support. Dielectric discontinuities within the ice, such as layers of compacted snow, air bubbles, subglacial cavities, or the glacier bed, reflect the electromagnetic waves emitted by the transmitting antenna. The GPR system is dragged along predefined linear profiles or grids, allowing continuous data collection along the path. Adjustments in movement speed and pulse frequency guarantee the best sampling of the surface and internal stratifications of the glacier. Data collecting comprises grid networks for thorough studies in areas of particular interest and linear profiles for mapping certain sections of the glacier, including ridges or crevasses.



*Fig. 15 - Ground Penetrating Radar (GPR) prospecting for the determination of the thickness of the Ciardoney glacier, by Imageo Srl (f. SMI)*

### 4.3.1 Operating Principles and Radargram Creation

The GPR operates according to principles previously described: electromagnetic energy reflected from discontinuities is recorded as a signal, producing a radargram once processed. This offers a graphical depiction of the interior strata of the glacier, therefore revealing thicknesses, inclinations, and structural anomalies.

The GPR system is dragging along the study's profile; thus, the radargram is created. Regular movement lets the produced electromagnetic waves create coherent information, hence transforming reflections into a two-dimensional image. Every emitted pulse generates a one-dimensional trace, commonly referred to as "A-scan," that shows the reflected signal's amplitude over time.

An ideal transmitting antenna would emit a point-like signal in a single direction; however, in practice, electromagnetic waves propagate at an angle of about 45°-60° relative to the vertical. Reflections produced by this propagation depend on the discontinuities in the medium being crossed, such as variations in density or electrical characteristics. While a point-like object, such as a rock or void, causes diffraction hyperbolas, the reflections in the radargram become horizontal lines if the wave impacts a continuous layer.

Diffraction hyperbolas occur when the electromagnetic signal interacts with the object at different times, contingent on the location of the GPR relative to the object. The return time of the signal decreases as the GPR gets closer to the target and then rises once the system distances itself. This phenomenon creates the reflected point's hyperbolic profile in the radargram. Grayscale or color represents the amplitude of the reflections; darker tones indicate higher reflections. Comprising a sequence of consecutive traces (A-scans), the radargram forms a two-dimensional vertical segment ("B-scan"). Computed as the product of the number of traces and the constant spacing between them, the x-axis shows the distance the GPR has travelled. The y-axis displays the reflection time, which can be translated into depth based on the wave propagation velocity in the studied media [41]. From the slope of the hyperbola it's possible to calculate the wave velocity in the material, but the one outside the hyperbola, so we can just hypothesize what is the object:

$$\text{slope} = \frac{2}{v} \quad (10)$$

To correctly identify glacier features, stratifications, or anomalies, radargrams must be processed correctly using specialized software like Matlab to get rid of noise and make the images easier to read.

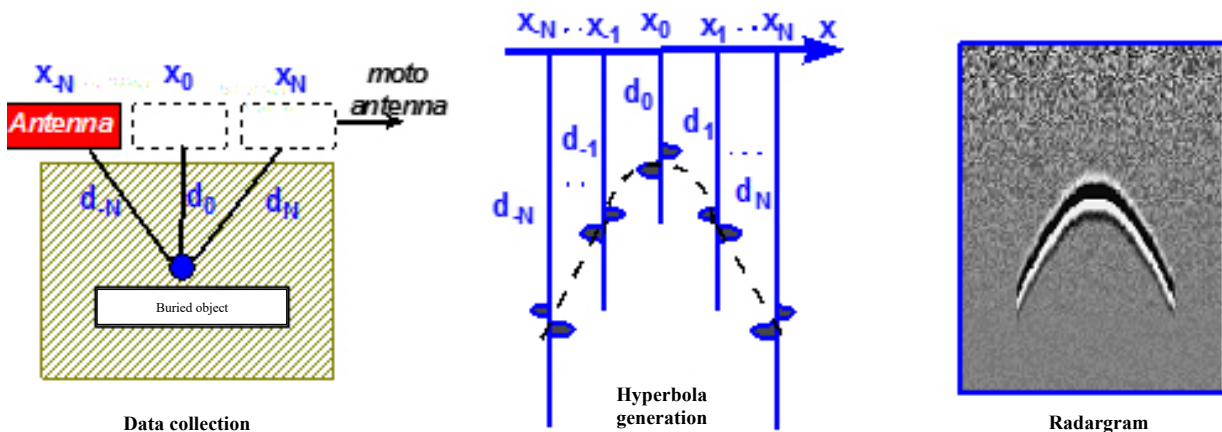
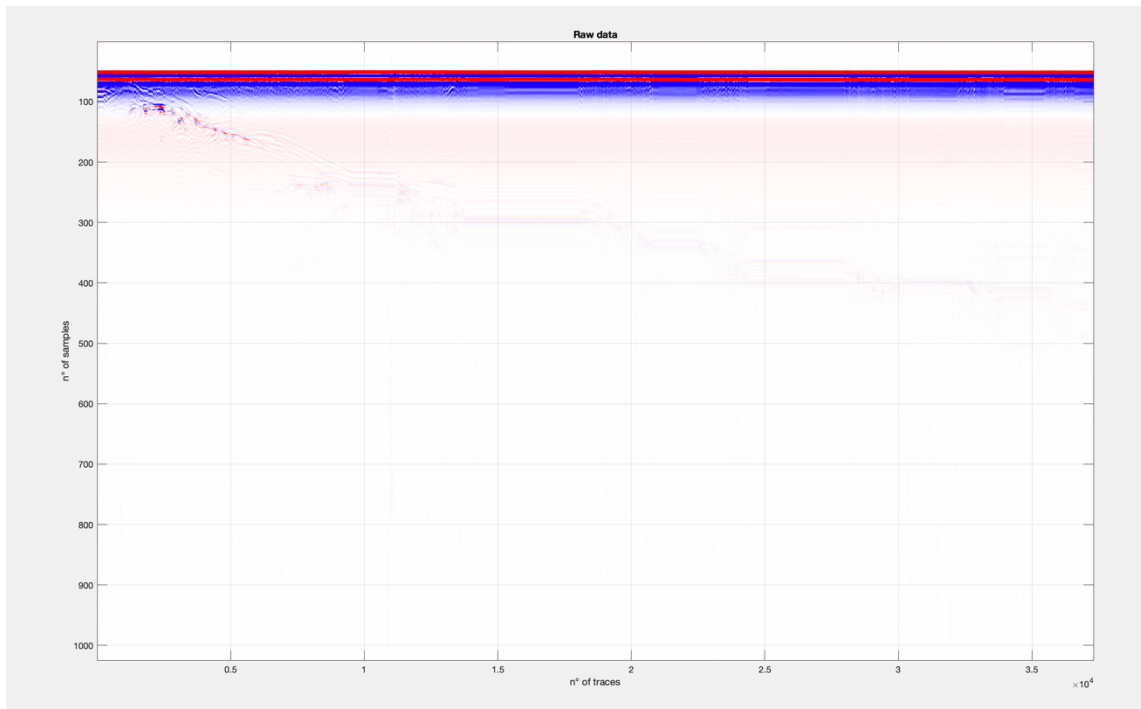


Fig. 16 – Radargram generation. Source: [http://www.gpradar.it/ind\\_georadar.html](http://www.gpradar.it/ind_georadar.html)



*Fig. 17 – Raw radagram generated, before the modification and interpretation using Matlab*

### 4.3.2 Influence of Glacier Internal Characteristics

The interior properties of glaciers can significantly affect both the acquisition and interpretation of GPR data.

- **Crevasses:** They are discontinuities that can reflect or scatter radar signals, so distorting the radargram or producing areas of intense return that make it challenging to separate underlying stratification.
- **Cavities:** Within the ice, cavities form voids that change the refractive index, producing hyperbolas and sometimes difficult-to-understand reflections.
- **Water fractures and water pockets:** Because of their high electrical conductivity, liquid water within fractures or pockets greatly lowers the penetration depth of radar signals. Signal attenuation and a loss of stratification features follow from this.

Some problems in the data interpretation arise from these aspects:

- Multiple reflections between overlapping layers produce artifacts in the radargram, therefore confounding interpretation; layers of snow and ice can trigger scattering events.
- Reduced penetration depth: Areas high in liquid water or contaminants in the ice weaken the signal, therefore restricting the GPR's capacity to identify deep strata.
- Internal glacier characteristics, including the presence of mixed layers or very heterogeneous zones, can influence the reliability of thickness estimates. This calls for rigorous calibration as well as the application of propagation models that consider the local media properties.

### 4.3.3 Logistic Difficulties and Solutions

Data collection in a glacial environment presents various logistical difficulties, including accessibility, safety, and weather conditions.

- **Accessibility:** Glaciers are often located in remote and hard-to-reach areas, with steep slopes, crevasses, and unstable surfaces. This makes transporting equipment, which can be bulky and heavy, particularly challenging.

**Solution:** Helicopters often transport personnel and equipment to acquisition sites. By allowing quick access to otherwise unreachable places, helicopters reduce operator danger and increase operational efficiency. Once on the glacier, the tools are put together and raised on the acquisition support, or the data can be acquired directly from the helicopter.

- **Weather conditions:** Strong winds, low temperatures, and poor visibility all complicate data collection in situations that change quickly. Fresh or wet snow could weaken the radar signal, therefore lowering the data quality.

**Solution:** Acquisition missions are carefully scheduled based on weather forecasts, taking advantage of stable weather windows. Additionally, water- and cold-resistant casings protect GPR equipment, ensuring operation even in adverse conditions.

- **Irregular surfaces:** The equipment's mobility may be limited by irregular glacier surfaces, including crevasses or areas of snow accumulation, therefore endangering operator safety.

**Solution:** Lightweight and robust sleds for moving the GPR help to reduce problems with uneven ground. Moreover, prior analysis of the acquisition region using aerial photos or satellite images helps find the safest and best routes.

## 4.4 DATA PROCESSING

After the data acquisition phase, where raw radargrams are generated, the collected GPR data require further processing to become more readable and interpretable. The processing was conducted using MATLAB code, following several steps to enhance the quality of the radargrams and eliminate noise and artifacts.

### 4.4.1 Steps in Data Processing

1. **Defining the speed of electromagnetic waves:** The first step involves setting the speed of electromagnetic waves in the investigated medium. Since the medium is ice, the speed is defined as 0.17 m/ns.
2. **Adjusting the start time:** The second step consists of moving the start time to correct for the delay caused by the first reflection, known as the "main bang," which occurs during the acquisition phase. This adjustment ensures that the air-ground interface aligns with time zero.

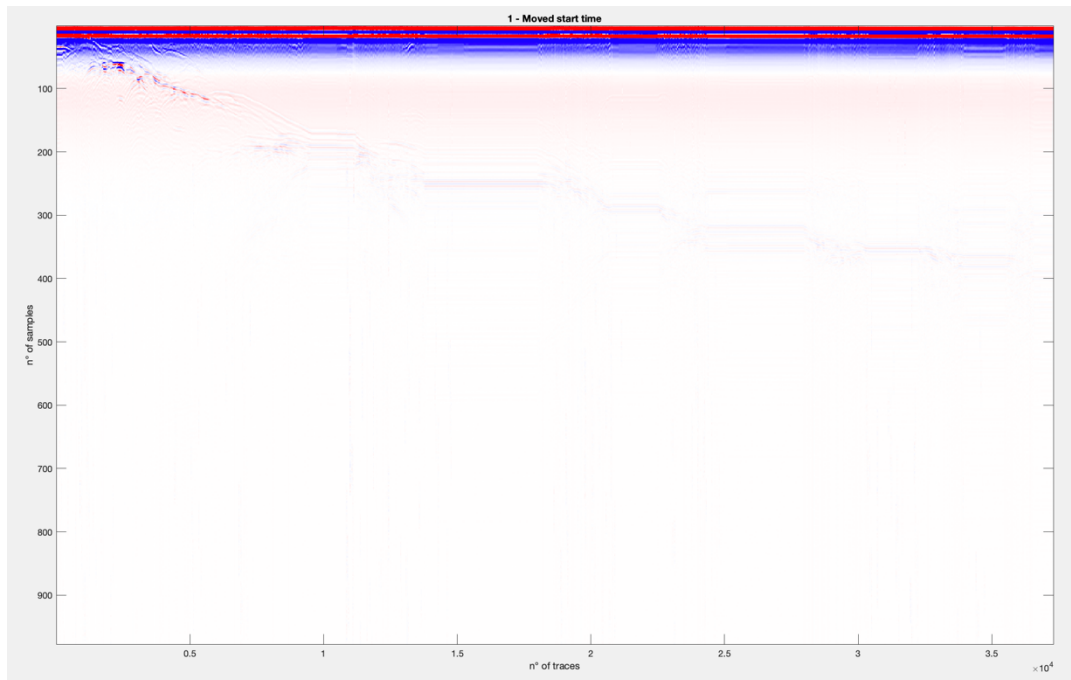


*Fig. 18 – GPR processing Grapillon 2016 line 1, moved start time*

3. Background removal: GPR data often exhibit clutter, which appears as horizontal stripes in the radargram. This effect is caused by system noise, ground bounce, uneven surfaces, and reflections from external anomalies. By subtracting the average trace from the dataset, these constant horizontal events are attenuated, improving the clarity of the radargram.

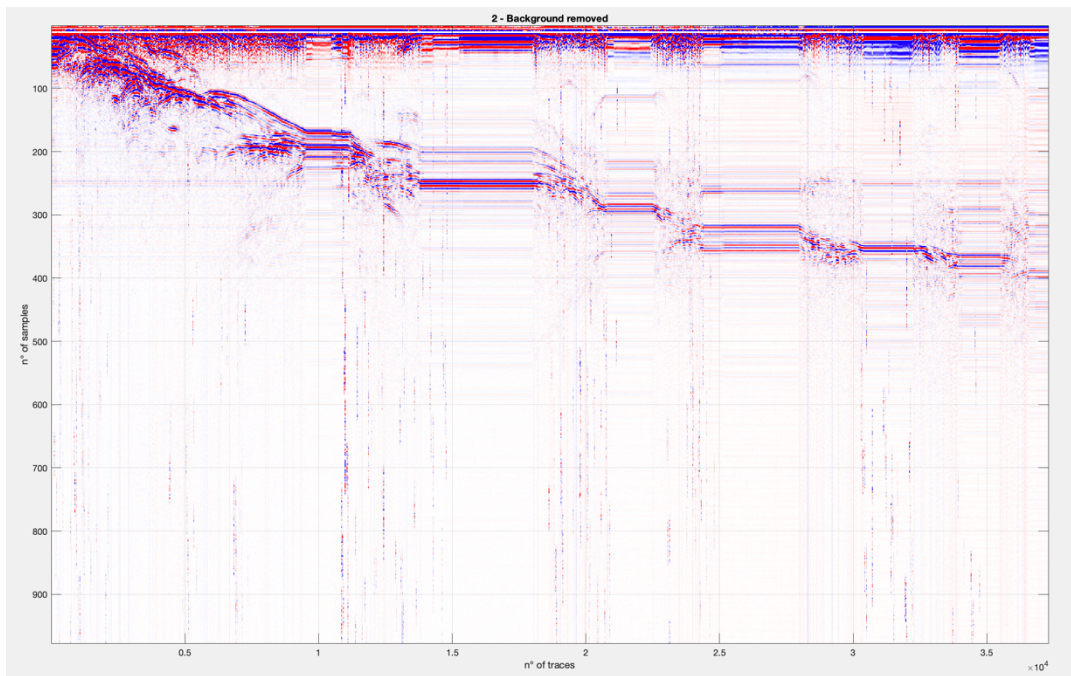


*Fig. 19 – GPR processing Grapillon 2016 line 1, background removed*

4. Removing stationary traces at the edges: Stationary traces at the edges of the radargram are removed to ensure that only relevant data are retained for interpretation.

5. Band-Pass filtering: A band-pass filter is applied to retain only the frequency content centered around the central frequency of the antenna while removing low and high-frequency noise. This step eliminates unwanted noise and enhances the signal quality. The cutoff frequencies were defined as follows:
- For glaciers where data were acquired with 300 MHz antennas (all except Pré de Bar), the cutoff frequencies were set to 85 MHz and 500 MHz.
  - For Pré de Bar, where data were acquired with a 900 MHz high-frequency antenna, the cutoff frequencies were set to 400 MHz and 1300 MHz.

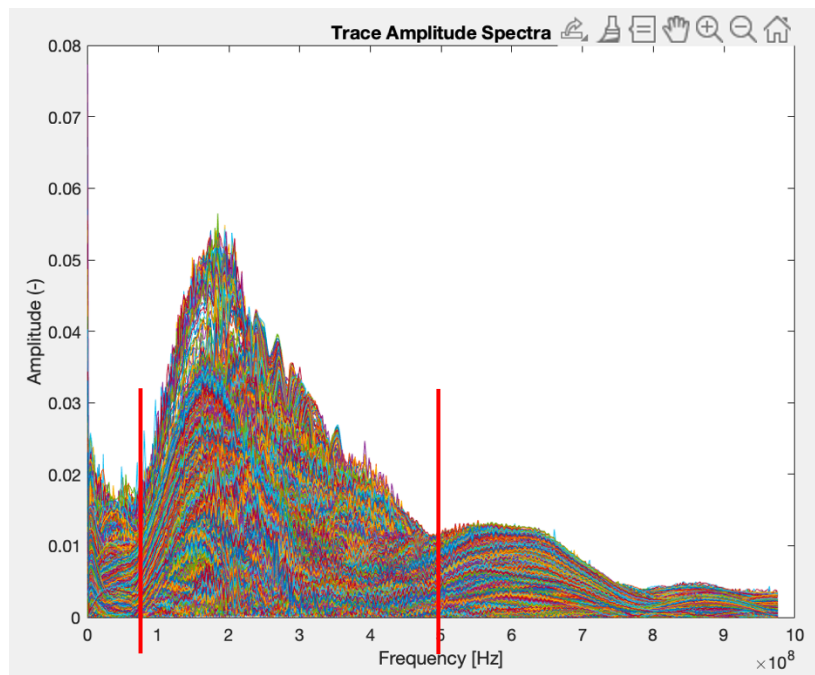


*Fig. 20 – Trace Amplitude Spectra, Grapillon 2016 line 1*

6. Geometrical spreading recovery: To correct for amplitude attenuation with depth, traces were adjusted for geometrical spreading. As the distance from the source increases, the amplitude of the signal decreases. A linear compensation was applied, where each sample was multiplied by the distance from the source. This could be adjusted to quadratic or cubic compensation if needed.

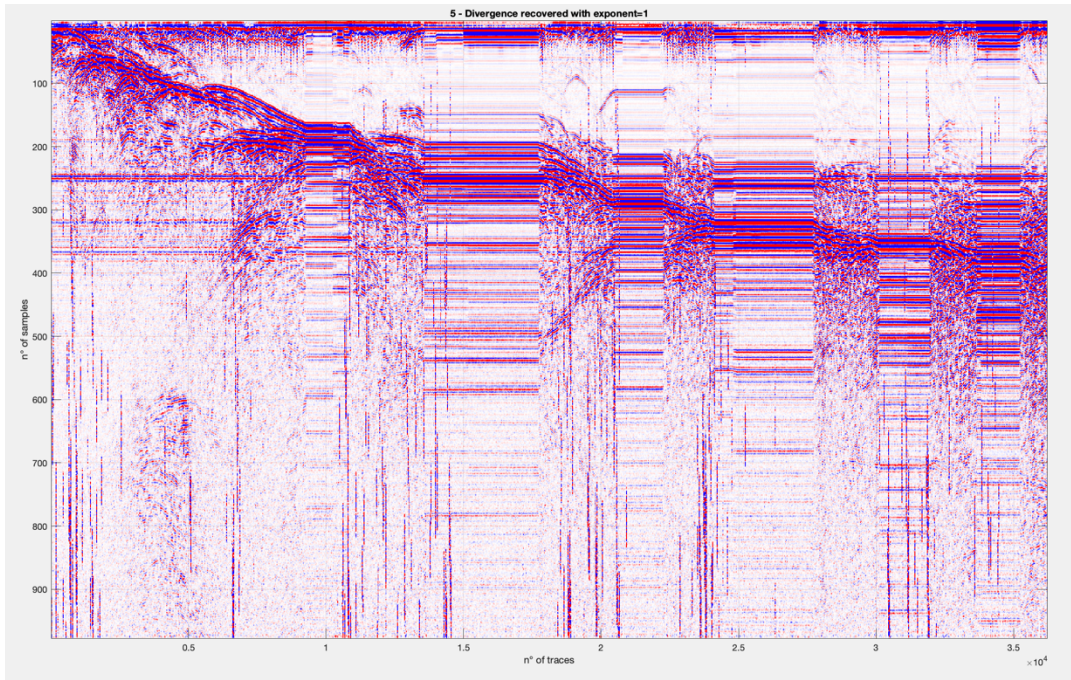


*Fig. 21 – GPR processing Grapillon 2016 line 1, geometrical recovery*

7. Removing stationary traces within the radargram Any stationary traces present within the radargram, caused by continuous recording during instrument downtime, were removed. These traces could lead to incorrect depth localization and interfere with the interpretability of the radargram.

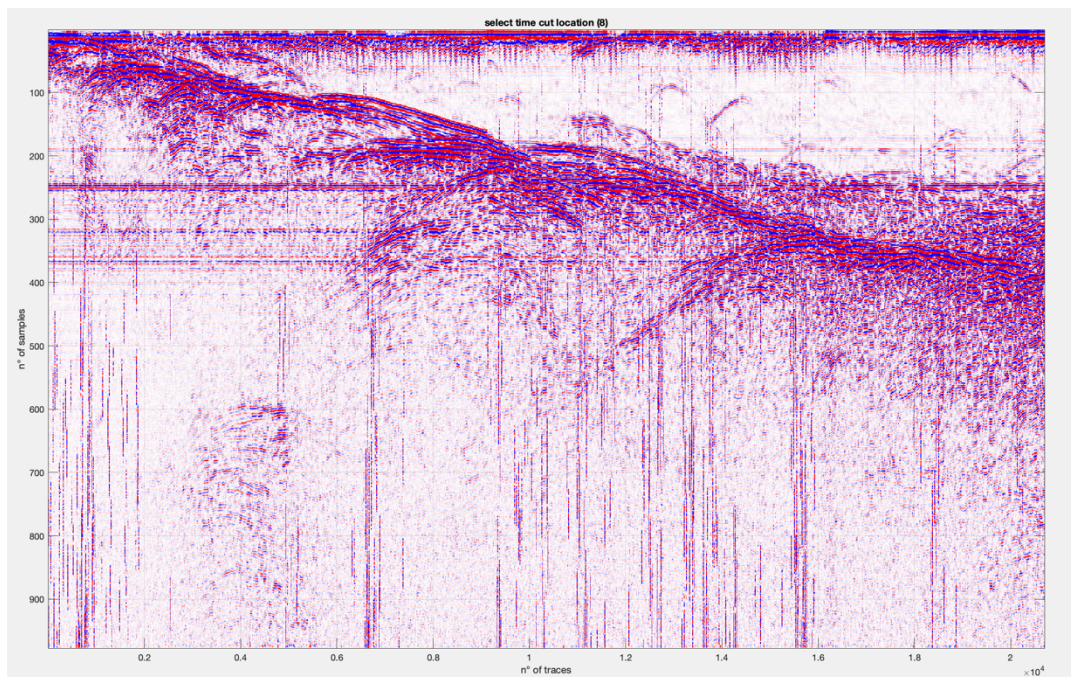


*Fig. 22 - GPR processing Grapillon 2016 line 1, stationary traces removed*

8. Time cut: The final step involved cutting the longest times where no useful information was present. This ensured that only relevant data were included, reducing the size of the dataset and improving visualization.

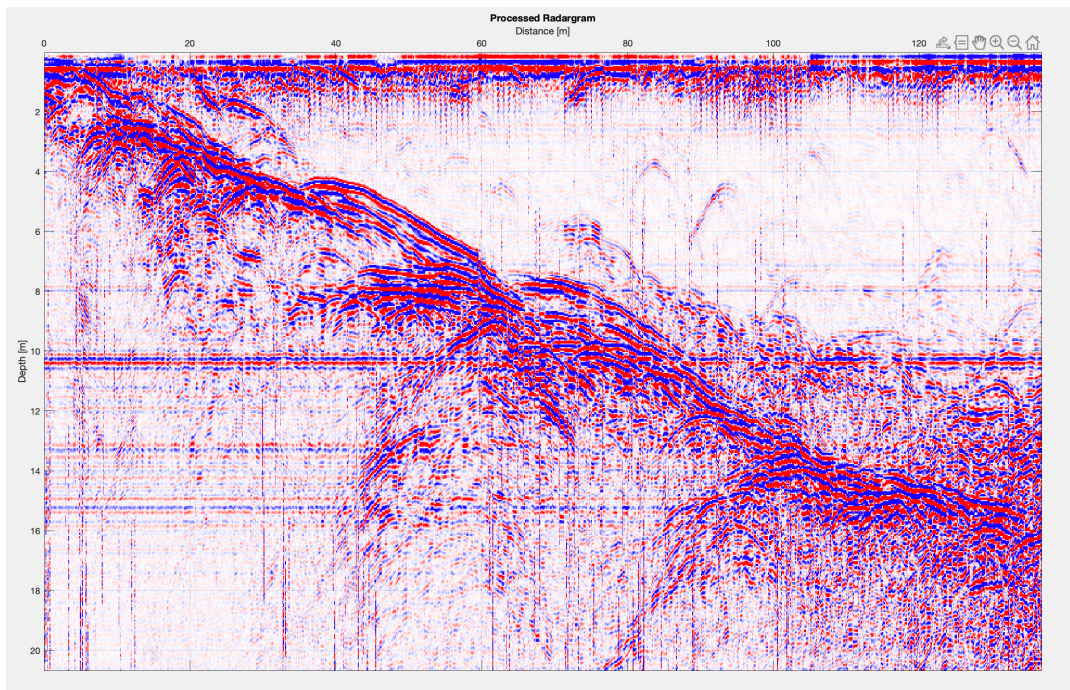


*Fig. 23 - GPR processing Grapillon 2016 line 1, time cut*

By following these processing steps, the raw radargrams were transformed into clean, interpretable images, facilitating the accurate analysis of glacier internal structures and features.

#### 4.4.2 Processing and problems with Val Ferret glaciers

The dataset included the following profiles:

- Grapillon 2016: 12 profiles
- Grapillon 2012: 16 profiles
- Pré de Bar 2010: 11 profiles
- Col del Gigante 2010: 6 profiles
- Planpincieux 2019: 12 profiles
- Planpincieux 2021: 8 profiles
- Whymper 2021: 6 profiles

Due to various issues, such as missing .gps files or data unreadability, not all profiles were usable. After the processing methods outlined in the previous section, the final radargrams were generated. A visual inspection enabled the extraction of ice thickness at the specified locations by manually picking out areas of elevated amplitude contrast which correspond to the bedrock (highlighted in green in the following images).

#### 4.4.2.1 Grapillon

For Grapillon, the data were generally of good quality for both 2012 and 2016, making these datasets a substantial part of the project. Some crevasses are clearly visible, characterized by a diffraction hyperbola.

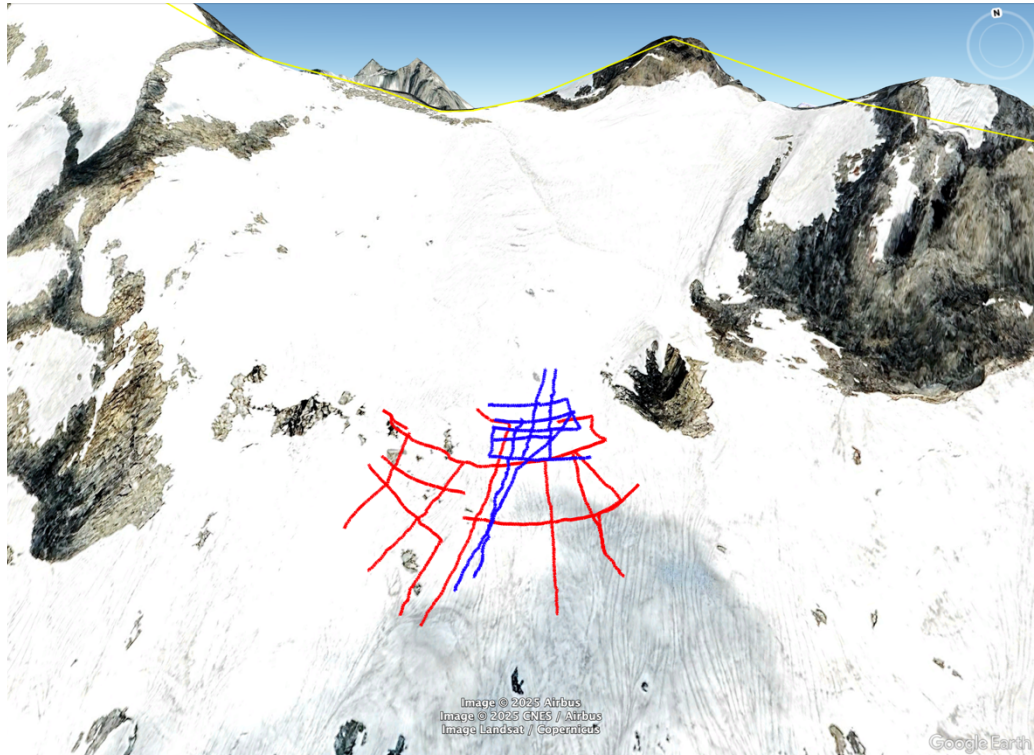


Fig. 24 – Original GPR lines available; data of Grapillon 2012 are red, while data of Grapillon 2016 are blue. Source: Google Earth, 2025

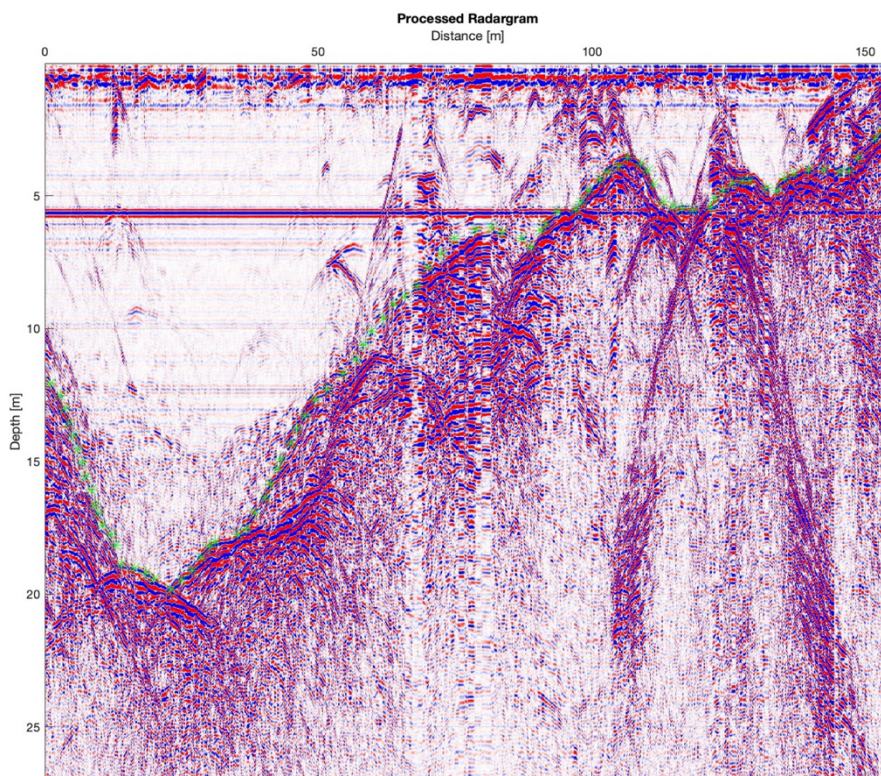
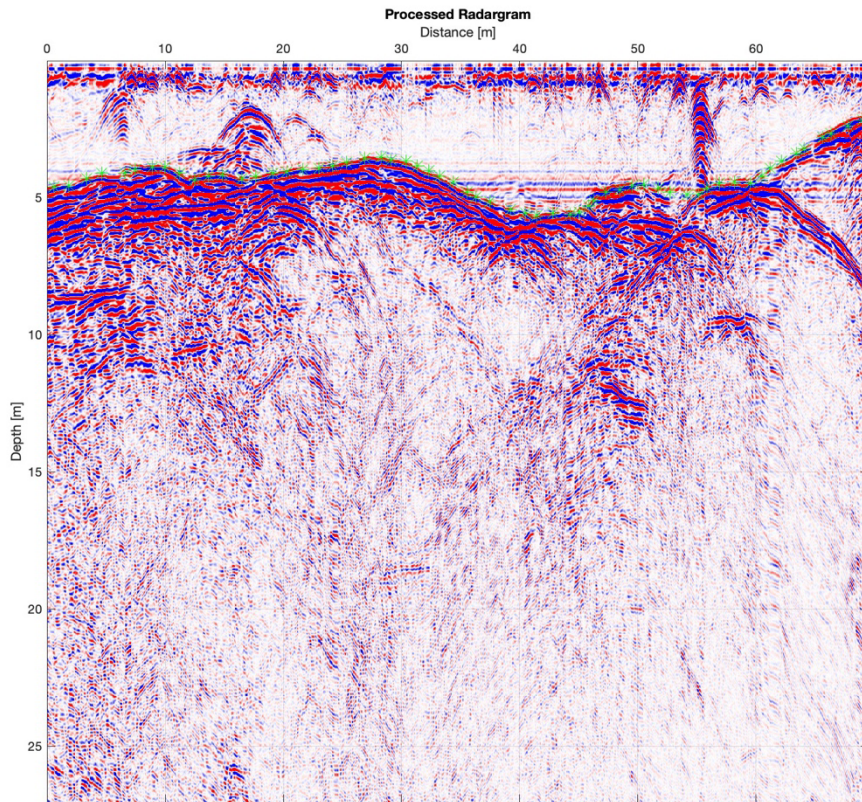
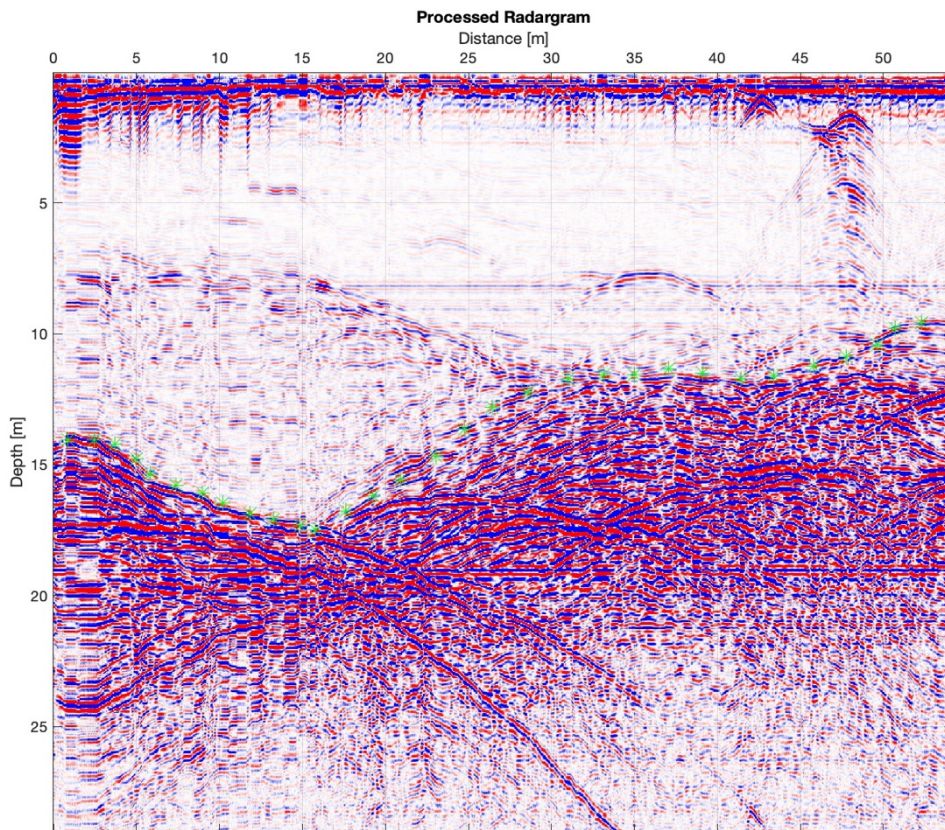


Fig. 25 - Grapillon 2012 line 4 bottom picked



*Fig. 26 - Grapillon 2012 line 8 bottom picked*



*Fig. 27 - Grapillon 2016 line 4 bottom picked*

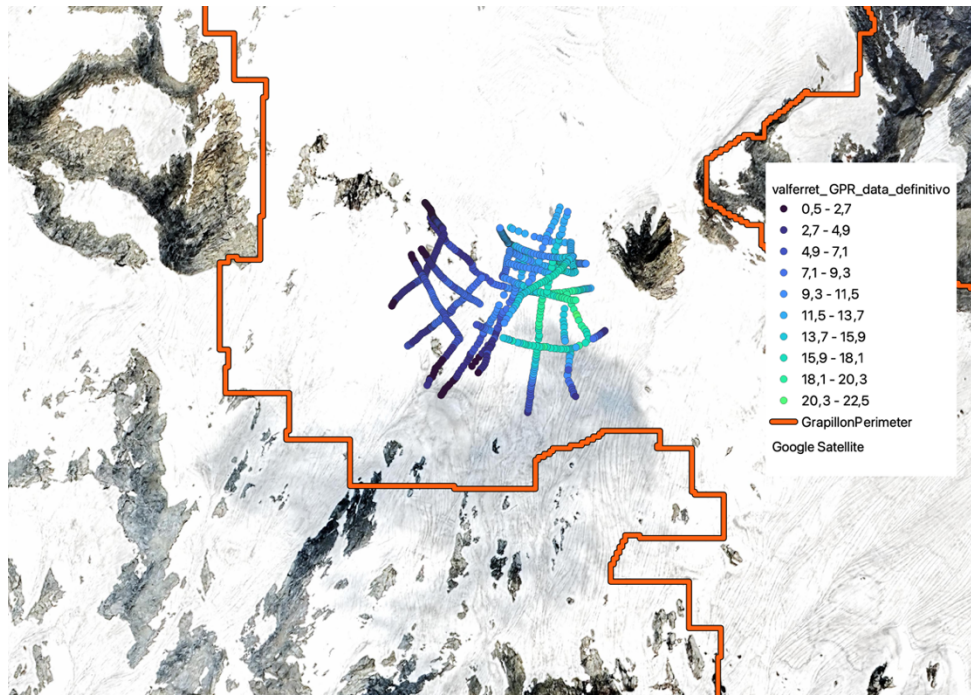


Fig. 28 - Grapillon 2012 and 2016 ice depth

#### 4.4.2.2 Pré de Bar

The measurements for Pré de Bar 2010 were conducted using a high-frequency 900 MHz antenna, which has low penetration depth and is typically used for measuring snow thickness. By applying the correct cutoff frequencies (400 MHz and 1300 MHz), some profiles were readable. From these radargrams, it appears that water infiltration or cavities may be present, disturbing the GPR signal, as discussed in the previous subsection. However, comparing the ice thickness derived from these data (60/100 meters), and the locations of the profiles, with the GlabTop 2008 model (160/180 meters), the Pré de Bar data were excluded due to a lack of congruence.

In the following figure, it can be seen that most of the GPR traces overlap, while for some traces, the GPS files are missing; as a result, only a few GPR traces are visible in the image.

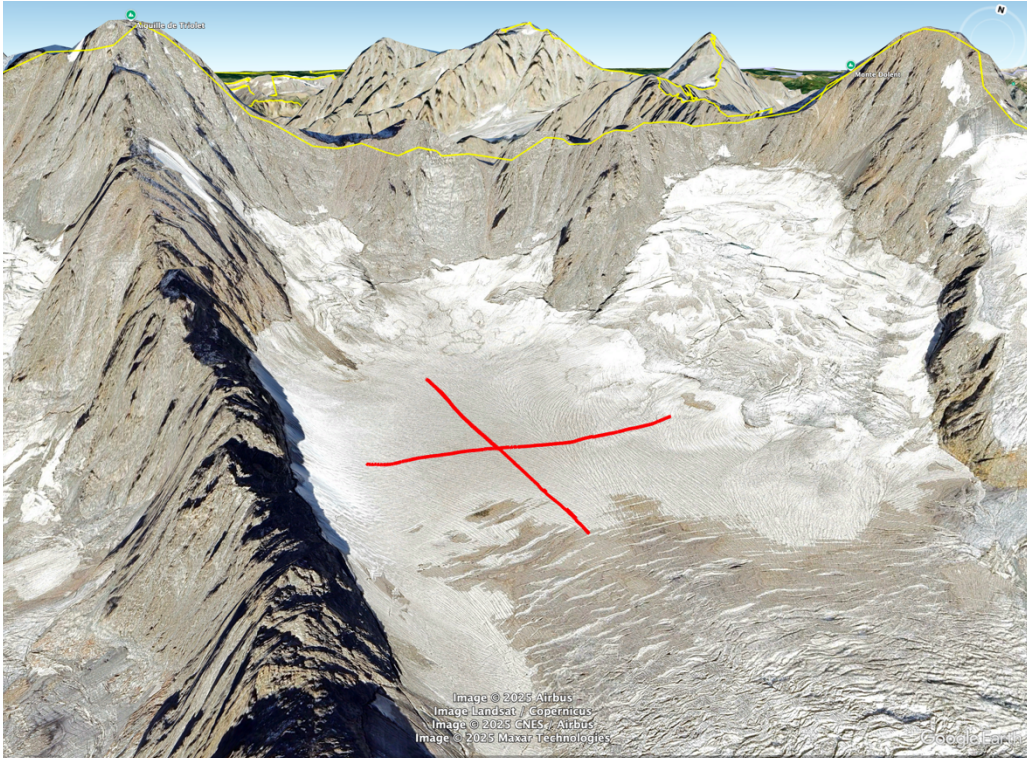


Fig. 29 - Original GPR lines available of Prè de Bar 2010. Source: Google Earth, 2025

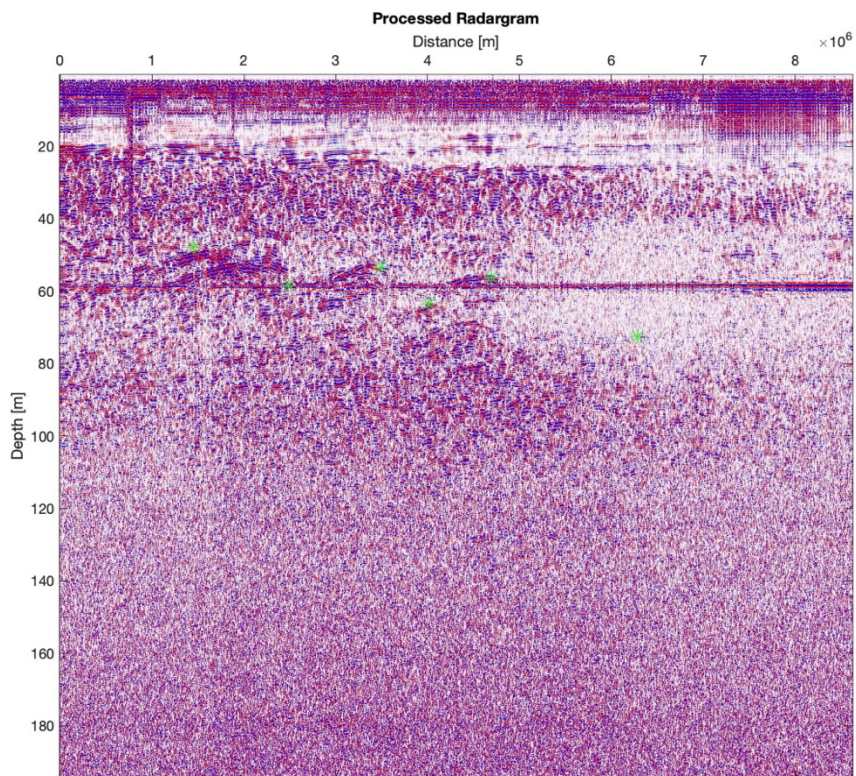


Fig. 30 - Prè de Bar 2010, signal disturbed from water infiltration

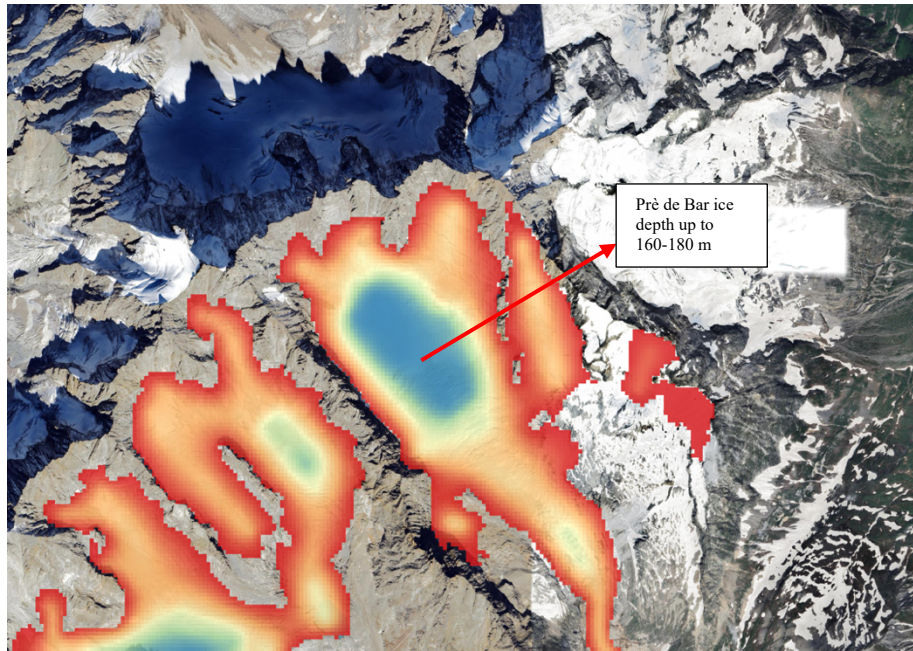


Fig. 31 - Glims 2008 ice depth, mismatch with our GPR data

#### 4.4.2.3 Planpincieux

The data acquisition for Planpincieux was conducted via helicopter, as the glacier surface was impassable (highly crevassed area and ice in critical condition). The 2019 data were unusable, while acceptable results were obtained from 2 profiles of the 2021 data after subtracting 7.5 meters to account for the helicopter's flight altitude and verifying consistency with the GlabTop 2008 model.



Fig. 32 - Original GPR lines available; data of Planpincieux 2019 are red, while data of Planpincieux 2021 are blue.  
Source: Google Earth, 2025

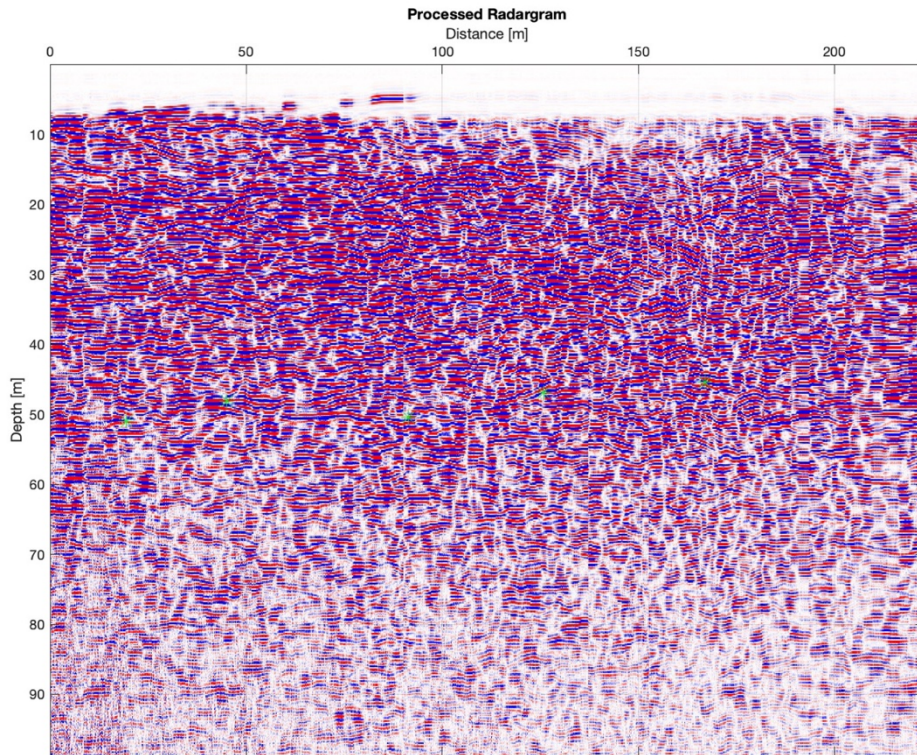


Fig. 33 - Planpincieux 2021 line 4

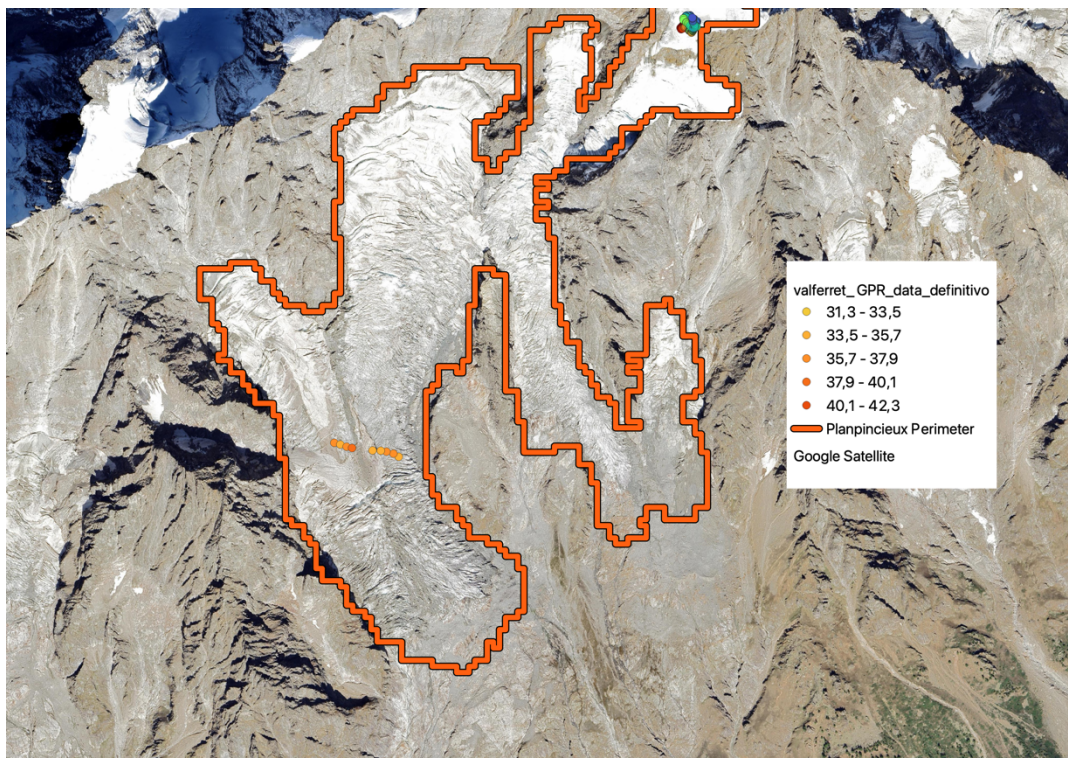


Fig. 34 - Planpincieux 2021 ice depth

#### 4.4.2.4 Col del Gigante

Radargrams from the Col del Gigante glacier are characterized by multiple stratifications, indicating transitions between snow, firn, and different types of ice. Moreover, due to the shallow ice depth, the signal becomes trapped and bounces multiple times before reaching the receiving antenna, generating repetitive band-like signals. The bottom has been picked on the first repetition of the signal.

In the following figure, it can be seen that most of the GPR traces overlap, while for some traces, the GPS files are missing; as a result, only a few GPR traces are visible in the image.

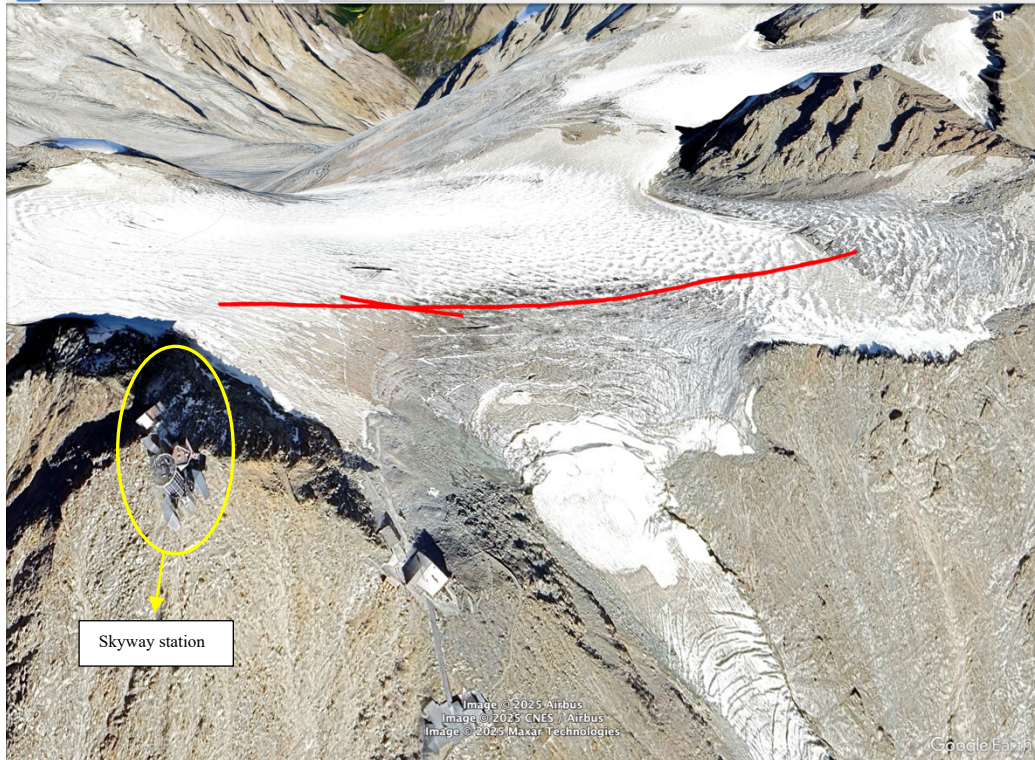
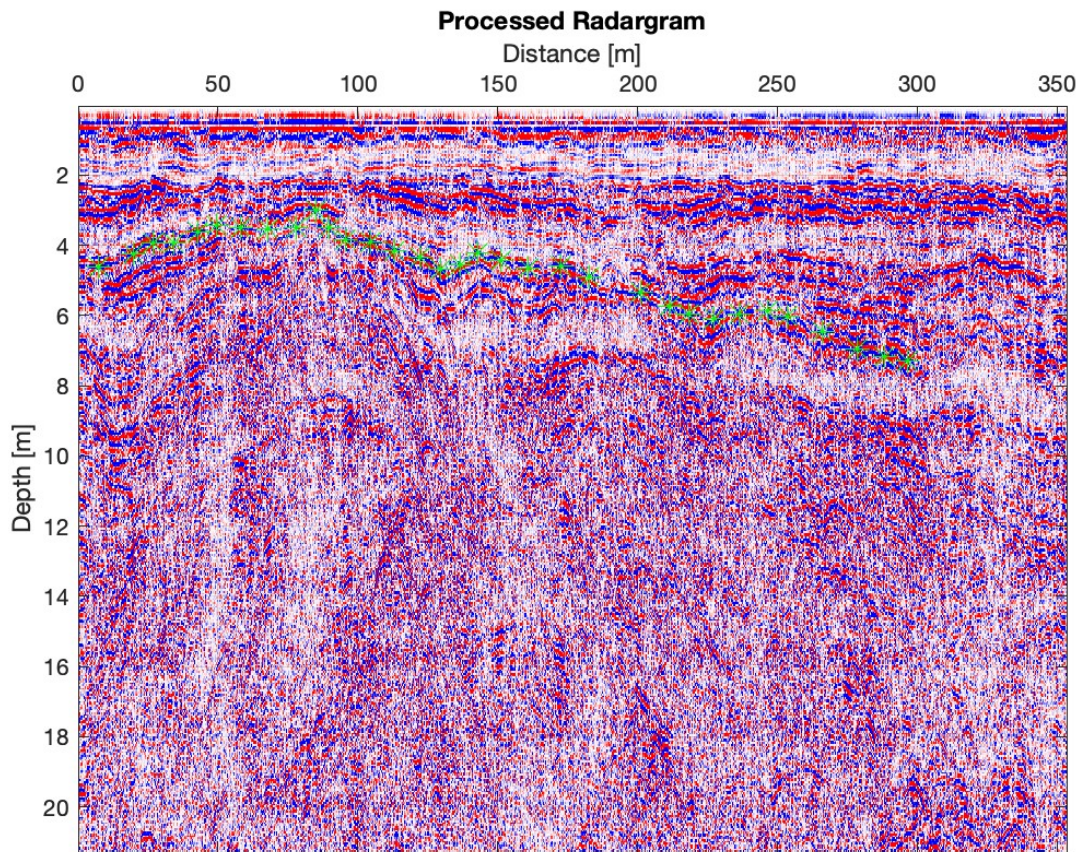
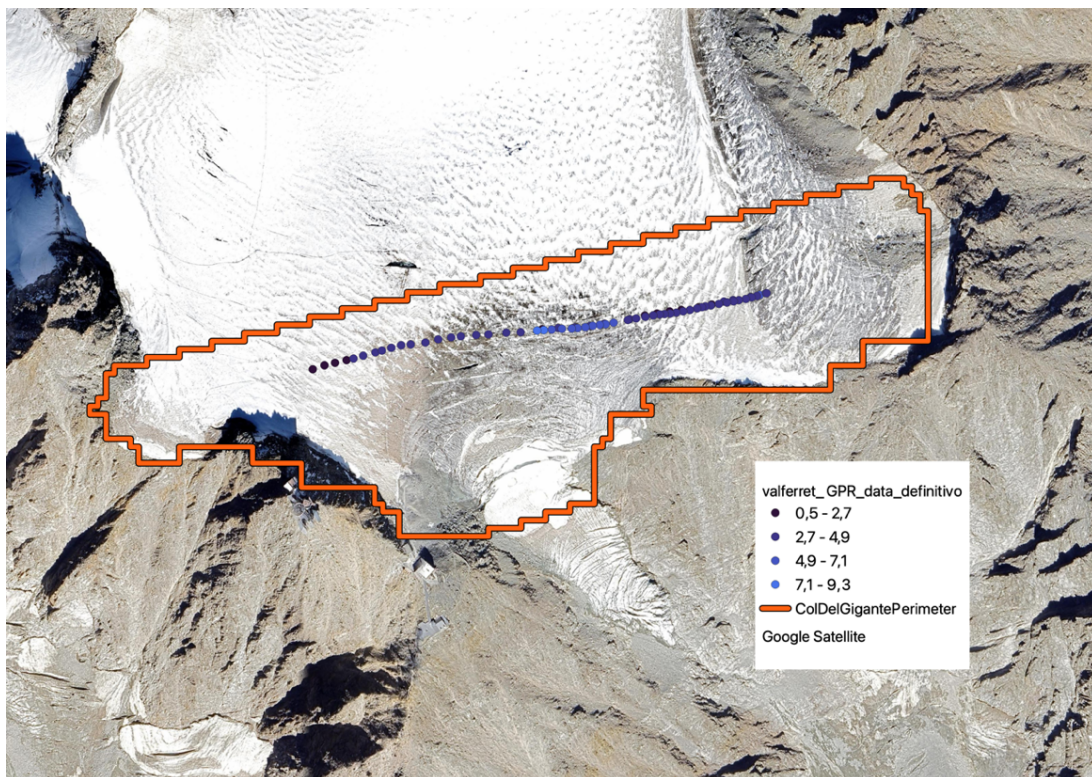


Fig. 35 - Original GPR lines available of Col del Gigante 2010. Source: Google Earth, 2025



*Fig. 36 - Col del Gigante line 4; stratifications and repetitions are visible*



*Fig. 37 - Col del Gigante 2010 ice depth*

#### 4.4.2.5 *Whympser serac*

For the Whympser serac, additional data processing was performed. Due to the serac's steep slope, the initial ice thickness data were picked vertically relative to the topographic surface. These data were then reprojected perpendicular to the topographic surface to obtain a more realistic simulation of the serac. The following figure demonstrates this process, with the initially picked data shown in black and the reprojected data in red:

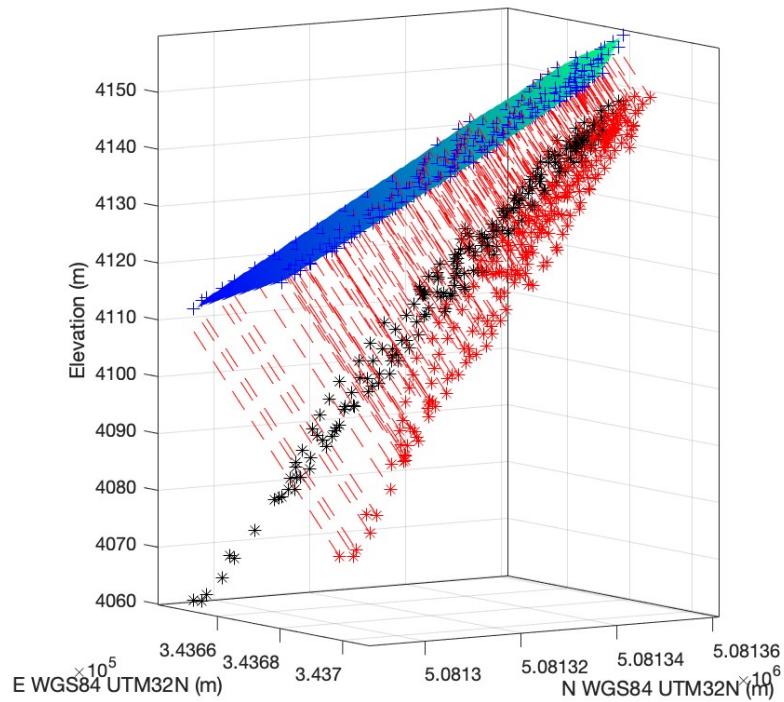


Fig. 38 - Reprojection of the bedrock data picked for Whympser Serac

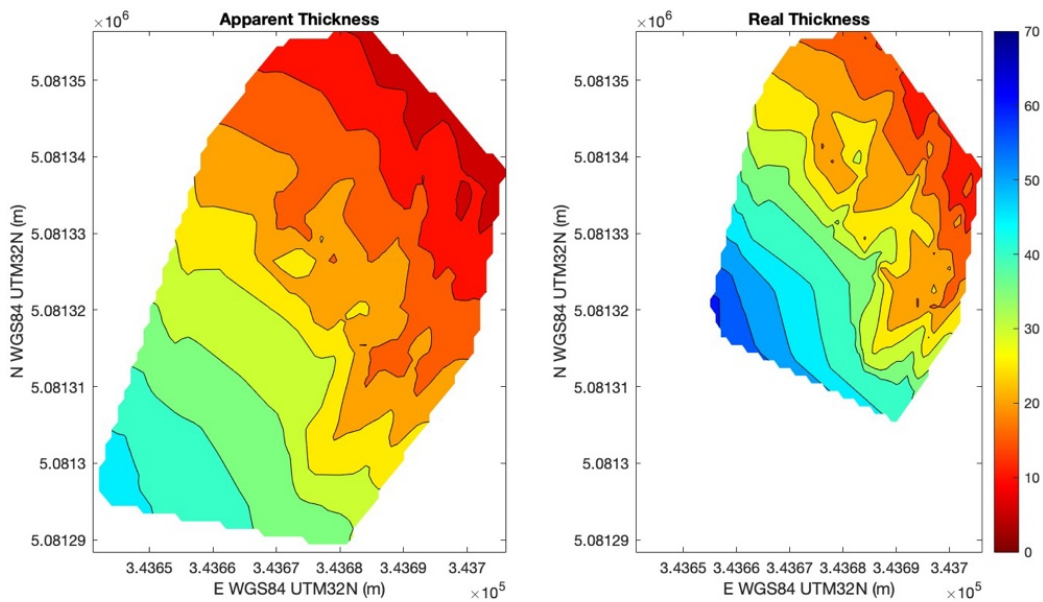


Fig. 39 - Thickness reconstruction of Whympser Serac after the reprojection of the data



Fig. 40 - Original GPR lines available of Whympet serac 2021. Source: Google Earth, 2025

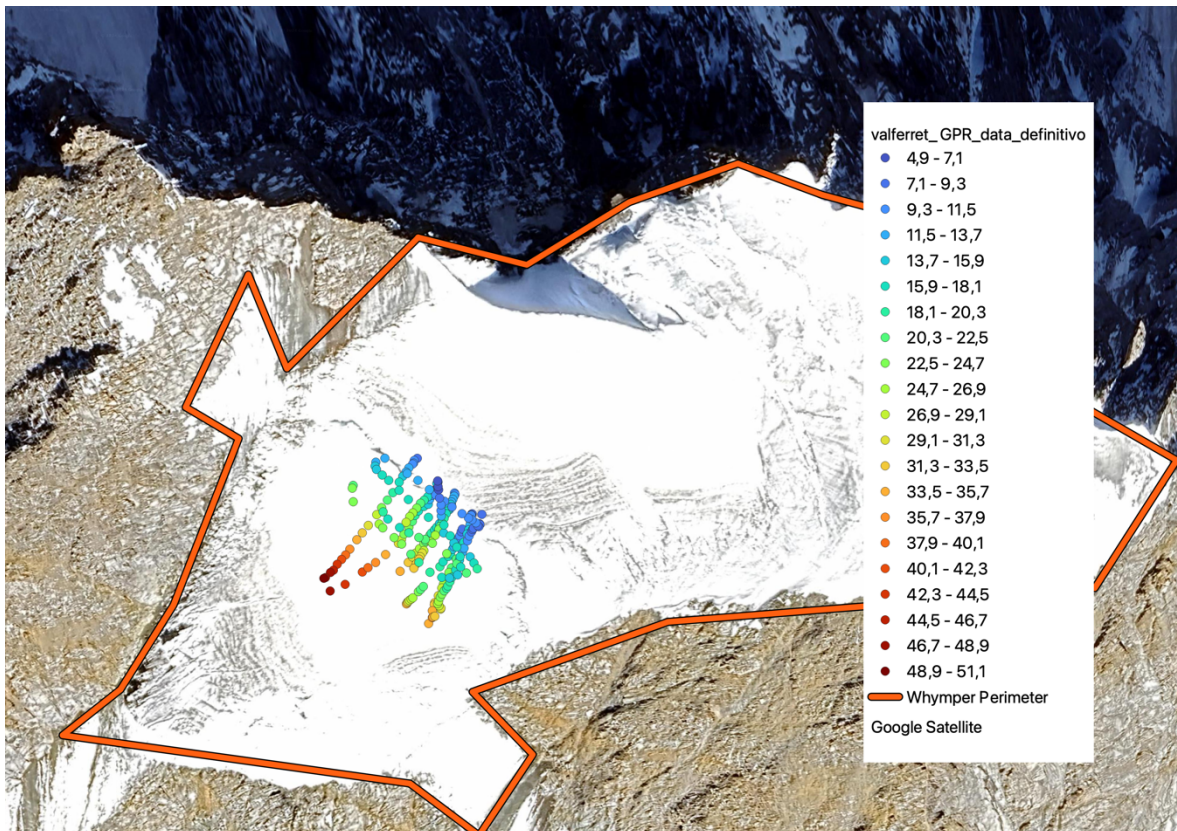


Fig. 41 - Whympet 2021 ice depth

# 5 APPLICATION OF THE GLATE MODEL

## 5.1 MODEL DESCRIPTION

Some glacial models have been created during the last years to estimate the ice thickness of a glacier starting from observable surface conditions, including the slope. In recent years, the literature has published new models that take into account additional mass conservation restrictions and basic shear stress parameters. These models, however, are always dependent on some simplifications, which can cause considerable outcome uncertainty. Developed by Langhammer et al. (2019), the Glacier Thickness Estimation Algorithm enables the constraining of a glaciological model with the ice thickness determined by means of GPR surveys and obtains the general thickness distribution via an inversion process. This guarantees a better degree of accuracy in the acquired outcomes [42]. Apart from the GPR restrictions, this model combines a set of other constraints linked with the GPR one to generate a coherent system of equations. The next paragraph will quickly outline the primary constraining criteria and the relative formulas considered by the authors of this model.

### 5.1.1 GPR data constraint

All constraints are formulated, such that they can be integrated into a single system of equations, which can be solved with an appropriate solver.

The first type of constraints includes the GPR data. They can be written in the form of :

$$Gh^{est} = h_{GPR} \quad (11)$$

Where:

- $G$  is a  $NGPR \times M$  matrix, with ones on the main diagonal and zeros outside;
- $NGPR$  is the number of available GPR data points;
- $M$  is the location of the points defined over a regular grid,  $R$ ;
- $h^{est}$  is a vector containing the ice thickness at all the  $M$  locations, also including the ice thickness estimation for the unknown points.
- $h_{GPR}$  is a vector containing the ice thickness of GPR data.

### 5.1.2 Glaciological constraint

The second constraint is related to the glaciological model. To this aim, the authors proposed the method used by Clarke et al. (2013), connecting the surface slope and ice thickness to the basal shear stress of the glacier. This requires the DEM of the region as well as the mask specifying the glacier's outline. The mask of the glacier consists of a matrix of the same size as the DEM, with zeroes elsewhere and ones when ice cover is present. First the algorithm must split the glacier into flow sheds, which are "glacier flow units defined by their ice catchment," in order to apply this second constraint [43], The Matlab TOPO-Toolbox will assist in this task. By applying the ice volume conservation concept, each of them achieves apparent mass balance once the flow sheds are established.

$$\tilde{b} = \dot{b} - \frac{\partial h}{\partial t} \quad (12)$$

with  $\dot{b}$  being the mass balance rate  $[\frac{m}{yr}]$  and  $\partial h/\partial t$  the thickness change rate  $[\frac{m}{yr}]$ .

In the next step, the flow sheds are partitioned into a prescribed number of elevation zones  $D_i$  ( $i = 1 \dots$  number of elevation zones), for which the ice discharge  $Q_i$  [ $\frac{m^3}{yr}$ ] through its lower boundary is computed using

$$Q_i = \int_{\Omega_{D_i}} \mathfrak{b} \quad (13)$$

where  $\Omega_{D_i}$  is the area of zone  $D_i$ .

Following Clarke et al. (2013), the basal shear stress  $\tau$  can then be obtained via the relationship

$$\tau = \left[ \frac{(n + 2)\rho g \sin(\varphi) 2 \xi q}{2A} \right]^{\frac{1}{n+2}} \quad (14)$$

where:

- $g$  is the gravitational acceleration;
- $n$  is Glen's flow law's ice exponent;
- $\rho$  is the ice density;
- $\xi$  represents the creeping contribution in relation to the basal sliding of the ice flux, ranging from 0 to 1;
- $\varphi$  is the surface slope averaged along the lower boundary of  $D_i$ ;
- $A$  is the creep rate factor;
- $q$  is the specific ice discharge  $q_i = Q_i/l_i$ , where  $l_i$  is the length of the lower boundary of  $D_i$  and  $Q_i$  is the average of  $Q_i$  within  $D_i$ .

At this point, by averaging the basal shear stress in the longitudinal direction,  $\tau^*$  can be calculated, allowing for the determination of the glacial model ice thickness:

$$\hat{h}^{glac} = \frac{\tau^*}{\rho g \sin(\varphi)} \quad (15)$$

Certain parameters in the basal shear stress calculation may exhibit significant uncertainty. The parameter  $\xi$  is frequently inadequately acknowledged, and the values of parameters  $A$  and  $n$ , typically sourced from literature, are not assured to be precise. Generally,  $n$  is well restricted, whereas  $A$  may fluctuate across several orders of magnitude. Consequently, the overall magnitudes of  $\hat{h}^{glac}$  may be much exaggerated or underestimated. This can be evaluated with an additional factor  $\alpha_{GPR}$ , resulting in

$$h^{glac} = \alpha_{GPR} \hat{h}^{glac} \quad (16)$$

$\alpha_{GPR}$  can be computed with an optimization procedure that minimizes

$$\|h_{GPR} - \alpha_{GPR} \hat{h}^{glac}\|^2 \quad (17)$$

The correction factor  $\alpha_{GPR}$  addresses certain inadequacies, however systematic discrepancies between  $h_{GPR}$  and  $h^{glac}$  may still exist. To prevent resultant differences, we focus not on the absolute value of  $h^{glac}$  but rather on the spatial gradient  $\nabla h^{glac}$  as glaciological restrictions, yielding

$$Lh^{est} = \nabla h^{glac} \quad (18)$$

where L is a difference operator of dimension  $M \times M$ .

Further constraints may be established through the glacier boundaries identifiable from aerial or satellite imagery or terrestrial measurements. They are represented by the following equation:

$$Bh^{est} = 0 \quad (19)$$

where B is a  $M \times M$  matrix with ones in its main diagonal and zeros elsewhere.

The discretization of glacier models may enable the resulting system of equations to be solved unambiguously. However, in most cases, the system remains significantly underdetermined, meaning there are many solutions that fit the data equally well. To address this, regularization constraints are applied, often following Occam's razor, which selects the "simplest" solution. Here, "simplicity" is defined in terms of structural complexity, aiming for a smooth model. This is achieved through smoothing equations of the form

$$Sh^{est} = 0 \quad (20)$$

where S is an  $M \times M$  smoothing matrix.

### 5.1.3 Definitive model and weighting coefficients

Ultimately, all the constraints can be consolidated into a singular matrix:

$$\begin{pmatrix} \lambda_1 G \\ \lambda_2 L \\ \lambda_3 B \\ \lambda_4 S \end{pmatrix} h^{est} = \begin{pmatrix} \lambda_1 h^{GPR} \\ \lambda_2 \nabla h^{glac} \\ 0 \\ 0 \end{pmatrix} \quad (21)$$

Where  $\lambda_1$ ,  $\lambda_2$ ,  $\lambda_3$ , and  $\lambda_4$  are weighting coefficients dependent upon the confidence in each individual input. The authors made various considerations for this objective. Typically, a constant value is assigned to  $\lambda_3$  (e.g., 1). An iterative process derives values  $\lambda_1$ ,  $\lambda_2$ , and  $\lambda_4$ , making the system of equations solvable. Initially,  $\lambda_1$  is assigned a value of 1, while a small value is designated for  $\lambda_2$ , resulting in a high  $\lambda_1/\lambda_2$  ratio. This indicates a strong confidence in the GPR data and a diminished confidence in the projected ice thickness derived from the glaciological model. A significant value is allocated to  $\lambda_4$  for excessively smoothed ice thickness. A preliminary GlaTE inversion is executed using these parameters. Consequently, the value of  $\lambda_4$  is progressively diminished until a specified proportion of  $h^{est}$  aligns with  $h_{GPR}$  within its accuracy constraints ( $\pm \epsilon_{GPR}$ ) or until the subsequent condition is satisfied:

$$\lambda_4 = \lambda_{4min} \quad (22)$$

Where  $\lambda_{4min}$  is a predetermined lower limit for the weighting factor. The new smoothing coefficient,  $\lambda_4$ , is determined, with an anticipated high value due to the elevated ratio of  $\lambda_1$  to  $\lambda_2$ . Thus, to enhance the significance of the glaciological model constraint, the  $\lambda_1/\lambda_2$  ratio is reduced, and the previously indicated stages are reiterated in an iterative process. The ultimate values of the weighting components are determined when  $\lambda_4$  equals  $\lambda_{4min}$  without achieving the specified data correspondence or when the ratio  $\lambda_1/\lambda_2$  attains a predetermined lower threshold.

## 5.2 APPLICATION OF THE MODEL TO VAL FERRET GLACIERS

The DTM used is the 2005-2008 aggregated version, downloaded directly from the Geoportal of the Valle d'Aosta region. The 1999, 2005, and 2008 versions were also available separately, but the aggregated version was chosen for greater accuracy, with a 2 m resolution.

The DTM has been downloaded discretized into cells and then merged together.

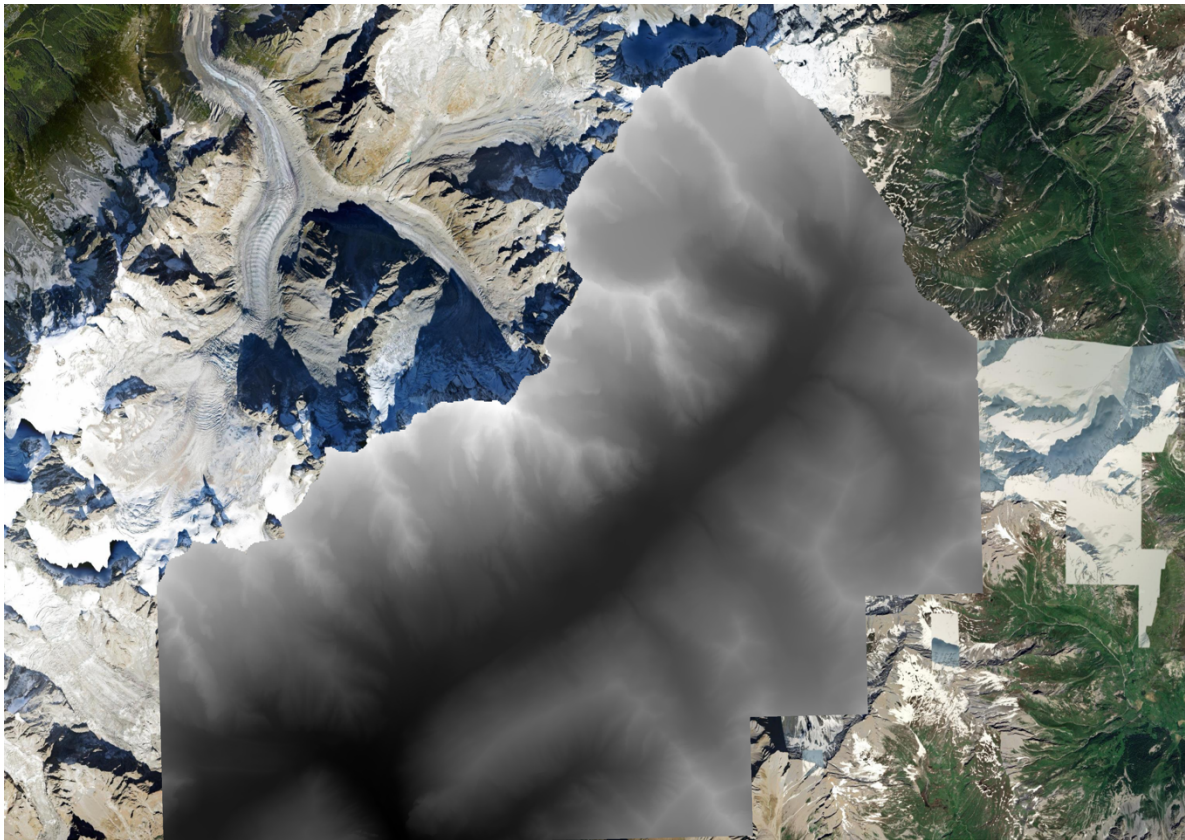


*Fig. 42 - DTM 2005/2008 aggregated for Val Ferret*

In addition to the DTMs, the perimeters of the glaciers in question, downloaded from GLIMS (Global Land and Ice Measurements from Space) and dating back to 2015, were used for the GlaTE model. The mask, with ones inside the glaciers areas and zeros elsewhere, is based on these perimeters. To conduct comparative analysis on the various files (DTMs and perimeters), they needed to be developed within the same reference system. QGIS was utilized to convert all dataset coordinates to WGS84 UTM zone 32N – ED50 (EPSG: 23032).

In summary, to implement the GlaTE model for the Val Ferret scenario, three input datasets were necessary: 1) GPR data, 2) DEM of the region of interest, and 3) a mask of the glacier's perimeter.

Due to the extensive size of the study area, the DTM was resampled to a reduced resolution. This step was necessary as the DTM's initial high resolution would have required excessive processing time for the model.

It is important to remember that the mask must have the same resolution and extent as the DTM. In our study, the model has been run with different values of resolution and smoothing factor (changing the interpolation smoothness).

The resolution chosen is:

1. 10 m
2. 15 m
3. 20 m

The smoothing factor used is:

1. 20
2. 40
3. 60

### 5.3 POTENTIAL LIMITATIONS AND ASSUMPTIONS OF THE MODEL

Using field-collected GPR data to constrain the GlaTE model to simulate glacier dynamics is a useful and new way to look at how glaciers change over time. However, in a critical assessment of the outcomes, it is important to discuss the inherent limitations and assumptions of the data collection and interpretation as well as the modeling technique.

#### 1. Quality and Resolution of GPR Data

GPR data serves as the foundation for all modeling procedures. The reliability of the simulations directly depends on their resolution and correctness. Still, many elements can cause mistakes:

- Data noise: Unclear signals or interference may impede the identification of the substrate's shape and ice boundaries.
- Restricted coverage: Data collecting may be sporadic or fail to cover the whole glacier surface in some places, therefore compromising the capacity of the model to capture local details.
- Environmental conditions: Variations in the measurements' quality may result from fresh snow or crevasses observed during data collecting.

#### 2. Assumptions of the GlaTE Model

Although advanced, the GlaTE model depends on certain simplifications required to control the complexity of glacial dynamics. These include:

- Ice behavior: The ice is considered a linear viscous medium, so nonlinear behaviors under extreme conditions—such as fast flows or large basal pressure variations—are ignored.
- Simplified boundary conditions: Often assuming either an idealized glacier geometry or steady-state flow, the model ignores seasonal changes or major episodic occurrences.
- Averaged parameters: Often averaging physical metrics (such as ice viscosity or basal sliding coefficients) fails to adequately depict local variation within the glacier.

### 3. Sensitivity to Climate Projections

The model estimates the effect of temperature and precipitation fluctuations on glacier mass balance using specified climate scenarios. However, regional climate projections, particularly in mountainous areas where local climatic events can significantly diverge from global trends, are highly questionable. Thus, the quality and resolution of the climate models applied directly affect the dependability of long-term projections.

### 4. External and Unconsidered Factors

Despite its robustness, the model ignores—or barely takes into account—many outside elements that might greatly affect glacier dynamics:

- Ice-sediment interactions: The representation of the glacial substrate's influence, including the deformation of underlying sediments, is incomplete.
- Extreme occurrences: Models do not explicitly account for phenomena like avalanches, landslides, or heavy precipitation events, which can significantly alter the glacier's mass balance.
- Hydrological feedback: simplified interaction between the glacier and local water flows ignores potentially important feedback effects on glacier dynamics.

### 5. Computational Complexity

Using models such as GlaTE requires significant computer resources for both time simulations and geographic resolution. Particularly in research on greater glacier areas, this can result in trade-offs between accuracy and computing time.

Despite these limitations, the chosen modeling technique offers a useful instrument for analyzing Val Ferret's glacier dynamics. Accepting these limitations helps to identify possible future developments and enables better contextualizing of the results. Key areas for additional research to make the analysis even more accurate and dependable are specifically incorporating new data, raising spatial and temporal resolution, and using more exact regional climate models.

## 6 RESULTS

After exploring various combinations of spatial resolutions and smoothing factors, as explained in the previous chapters, a resolution of 15 meters and a smoothing factor of 40 were selected for the analysis. This configuration was deemed optimal to balance spatial detail and simulation stability, ensuring the best representation of the glacial dynamics under study.

In this chapter, the results will be presented and discussed for each glacier considered, highlighting the main morphological characteristics and evolutionary trends obtained using the selected parameters. The aim is to provide a clear and comprehensive overview of the simulations performed and their implications for studying the glacial dynamics of Val Ferret.

### 6.1 PRESENTATION OF SIMULATION RESULTS

To facilitate understanding of the results, the following images are divided into four panels, each illustrating a key phase and outcome of the analysis.

1. Top Left:
  - This panel shows the theoretical glaciological model results for glacier thickness ( $h^{\text{glac}}$ ).
  - These results are derived from an unconstrained simulation, representing a purely theoretical estimate of glacier thickness based on the initial model parameters and configuration.
  - The primary goal is to evaluate how these results change when constrained by GPR data.
2. Top Right:
  - This panel displays the GPR data used to constrain the model.
  - The thickness shown here results from an interpolation between the GPR measurement points to create a continuous surface ( $h^{\text{GPR}}$ ).
  - It is important to note that these interpolated values should not be considered "real" thickness but rather an artifact of the interpolation process necessary for comparison with the model.
3. Bottom Left:
  - This panel shows the results of the model constrained by the GPR data ( $h^{\text{est}}$ ).
  - By integrating the radar data into the theoretical model, a more accurate estimate of glacier thickness is achieved.
  - The incorporation of GPR data allows the theoretical estimates to be corrected and refined based on direct field measurements.
4. Bottom Right:
  - This panel presents the difference between the model constrained by radar data and the thickness of the theoretical model ( $h^{\text{est}}-h^{\text{glac}}$ ).
  - It highlights the discrepancies between the unconstrained simulation and the corrected results.
  - Areas with significant differences may indicate zones where the theoretical model overestimates or underestimates thickness, providing valuable insights for further model improvements.

This visualization allows for a comparative analysis of the differences between the theoretical model and the constrained model, offering a clear representation of how the integration of GPR data modifies

the results. Additionally, the image underscores the contribution of observational data in refining glacier thickness estimates and identifying potential areas for further improvement in the model.

### 6.1.1 Prè de Bar and Grapillon

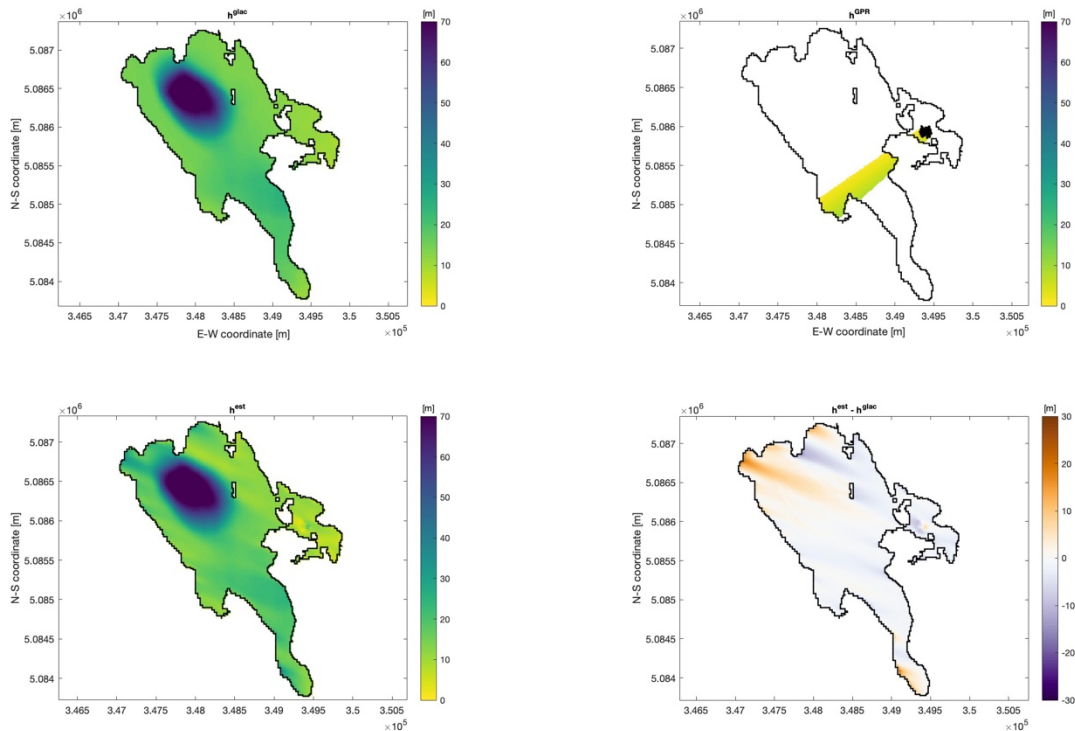


Fig. 43 - Ice thickness results, focus on Prè de Bar and Grapillon glaciers. Top left panel: thickness obtained using only the theoretical glaciological model. Top right: GPR constraint. Bottom left: thickness obtained from the model constrained by the GPR data. Bottom right: difference between the model constrained by radar data and the thickness of the theoretical model Results obtained for a smoothness factor equal to 40 and resolution equal to 15.

The upper-left panel displays the theoretically computed thickness without constraints from observational data. The Prè de Bar glacier reaches a maximum thickness of around 70 meters, exhibiting a homogeneous distribution in its middle region and a decrease toward the periphery zones. The theoretical thickness of the Grapillon glacier, the almost separated protuberance to the right, is significantly lower, approximately 10 meters. This estimate reflects a minimal presence of ice or snow in the region.

The upper right panel presents the interpolated GPR data, which provide a continuous estimation derived from measured radar points. The GPR measurements utilized cover only a limited section of the Grapillon glacier, whereas the interpolation generates a continuous surface that extends into unmeasured regions. This interpolation fails to accurately reflect the true thickness, yielding values considerably lower than those predicted by the theoretical model, with local discrepancies arising from the sparse distribution of radar locations.

The bottom-left panel displays the outcomes of the theoretical model following the integration of the GPR data. The greatest thickness in the center region of the Prè de Bar glacier remains approximately 70 meters, consistent with the theoretical model; however, enhanced precision appears in the outlying regions, which now exhibit diminished thicknesses. The central region of the glacier remains largely unaltered by the radar data, however the areas analyzed by the GPR data exhibit changes in thickness, enhancing its precision.

The bottom-right panel delineates the distinctions between the theoretical model and the constrained model. The Prè de Bar glacier has significant discrepancies mostly in the peripheral regions, where the theoretical model overestimates thickness relative to the constrained model, with negative values of 15–20 meters. Nevertheless, in the glacier's center region, the two models converge more closely. The theoretical model exhibits a significant overestimation for the Grapillon glacier, with maximum discrepancies of up to 20 meters. The dark blue areas signify locations where the theoretical model overestimates thickness, especially in outer zones lacking GPR data coverage. The orange areas indicate regions where the theoretical model underestimates thickness around the radar spots, necessitating substantial corrections from data integration.

A detailed investigation of the Grapillon glacier identifies regions of near-zero thickness, indicated by the yellow color in the "Constrained Model" panel. This feature is visually confirmed by images from Google Earth, which depict exposed rocks or areas barely covered by a thin layer of snow. This discovery highlights that the limited model utilizing radar data precisely reflects the actual conditions of the area, enhancing the estimates offered by the theoretical model. From a geomorphological point of view, the near-zero or minimal thickness indicates that the Grapillon constitutes a peripheral component of the glacial system, with little active ice contribution. This region seems to be more susceptible to ablation or direct melting processes, in accordance with the observed findings.

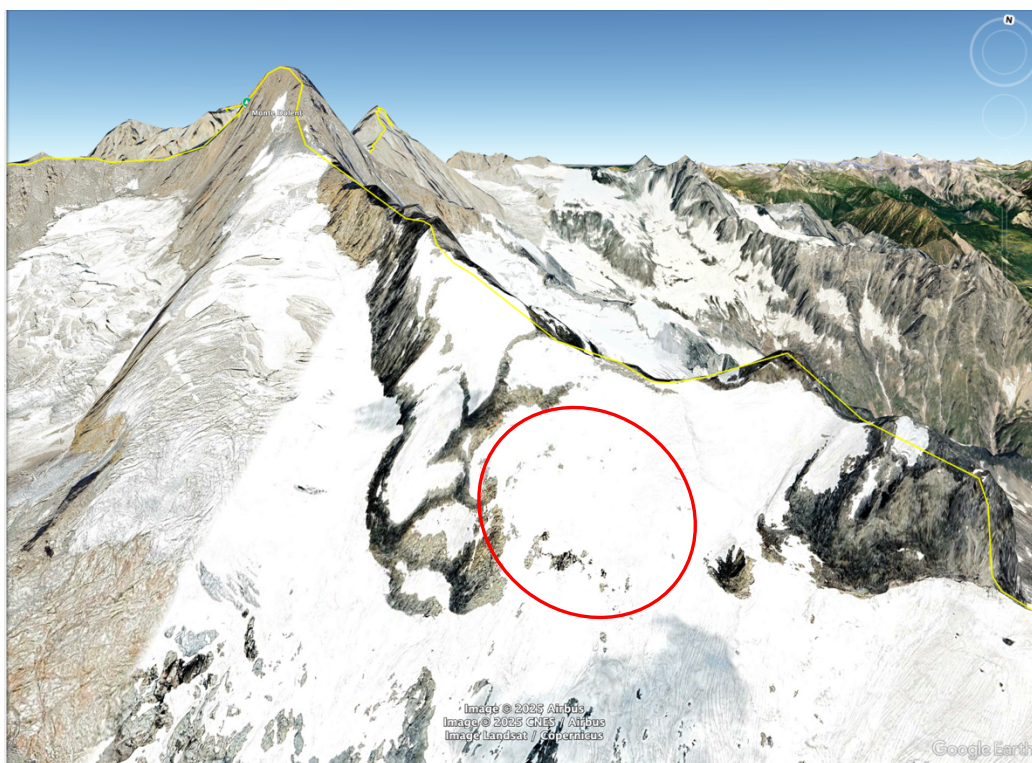


Fig. 44 – Focus on Grapillon glacier, with near-zero thickness rounded in red. Source: Google Earth, 2025

From an overall viewpoint, the GPR data markedly enhance the precision of the theoretical model, especially in regions encompassed by radar points. Substantial discrepancies, reaching up to 20 meters, are observed in areas where the theoretical model lacks empirical validation. The thickness in the center region of the Prè de Bar glacier stays uniform, reaching maximum values of approximately 70 meters in both theoretical and constrained models. Peripheral regions, inversely, are more susceptible to inaccuracies in the theoretical model, which often overestimates thickness in areas lacking radar data.

This analysis underscores the significance of GPR data in refining the theoretical model, diminishing differences, and enhancing accuracy in regions encompassed by radar points. Nevertheless, in unmeasured regions, the theoretical model sometimes overestimates the thickness, highlighting the necessity for expanded GPR coverage to attain additional enhancements.

Panel	Maximum thickness	Maximum difference ( $\pm$ )
Theoretical model	$\sim 70$ m	-
Constrained model	$\sim 70$ m	-
Difference	-	-15/20 m (overestimation) / +20 m (underestimation)

Table 2 - Maximum thickness and Maximum differences for Prè de Bar-Grapillon Glacier

### 6.1.2 Planpincieux glacier and Whympy serac

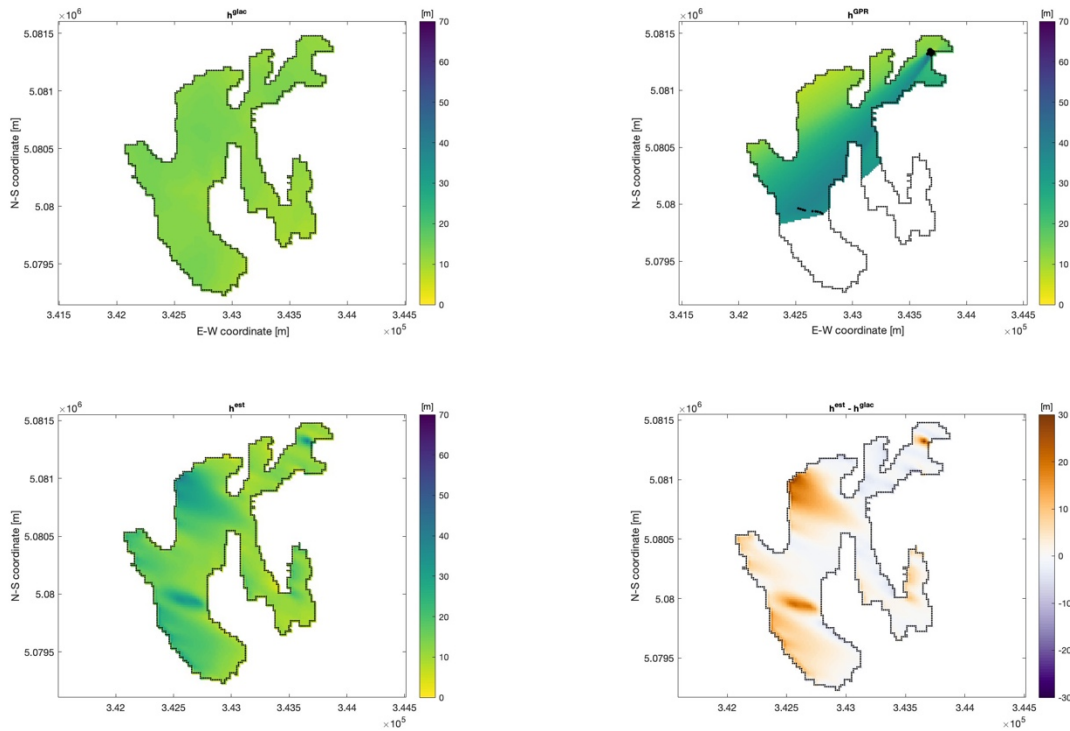


Fig. 45 - Ice thickness results, focus on Planpincieux glacier. Top left panel: thickness obtained using only the theoretical glaciological model. Top right: GPR constraint. Bottom left: thickness obtained from the model constrained by the GPR data. Bottom right: difference between the model constrained by radar data and the thickness of the theoretical model. Results obtained for a smoothness factor equal to 40 and resolution equal to 15.

The top-left panel represents the thickness estimated by the theoretical model, unconstrained by radar data. For the Planpincieux glacier, the maximum thickness, according to the color scale, never exceeds 20 meters. The central areas of the glacier show the highest thicknesses, while the edges display reduced values, close to 5–10 meters. The theoretical model provides a rather uniform distribution of thickness, without accounting for the local variations introduced by the presence of crevasses and water infiltration. In areas covered by GPR data, the theoretical model tends to underestimate the thickness, highlighting a significant margin of error compared to the constrained model.

As the analysis moves toward the Whymper serac, the theoretical model shows a slight overestimation of thickness in peripheral areas. For the serac itself, a general underestimation is evident, particularly pronounced in the lower sections where the serac is thicker. In contrast, the discrepancies diminish towards the upper sections, where the serac gradually thins. This discrepancy suggests that the theoretical model fails to accurately represent the gradual transition in thickness of the serac, emphasizing the need for corrections based on observational data.

The top-right panel shows the interpolated GPR data, which represent an estimate of thickness based on measured radar points. The distribution of interpolated data is limited to areas covered by radar points, while the white regions indicate zones without measurements. GPR data are concentrated on the Whymper serac and along two main lines on the Planpincieux glacier. However, in areas without radar measurements, the interpolation introduces approximate values that do not accurately capture local variations in thickness.

The bottom-left panel shows the results of the theoretical model constrained by GPR data, where radar measurements have been integrated into the model. For the Planpincieux glacier, the integration of radar data introduces significant corrections, especially in the central and southern areas, where the maximum thickness reaches approximately 40 meters, consistent with GPR data. Even in areas without measurements, the constrained model shows notable differences in thickness compared to the theoretical model. These differences can be attributed to the presence of crevasses and water infiltration, which introduce local heterogeneity in thickness and influence radar wave propagation. For the Whymper serac, the constrained model improves the representation of thickness by correcting the underestimation of the theoretical model in the lower sections, where the serac is thicker. Additionally, the gradual thinning of the serac toward the upper sections is better represented in the constrained model, making it more consistent with real observations. It is important to note that, as a cold glacier with minimal water infiltration or melting, the Whymper serac is less influenced by hydrological factors. The discrepancies observed are therefore mainly due to the intrinsic limitations of the theoretical model.

The bottom-right panel highlights the differences between the theoretical model and the constrained model based on radar data. For the Planpincieux glacier, the largest differences are observed in areas covered by radar data, where the theoretical model tends to underestimate thickness, with discrepancies reaching approximately 30 meters, as indicated by the color scale (orange zones). This underestimation is most evident in the central and southern areas of the glacier, which benefit significantly from the integration of radar data. In the case of the Whymper serac, a combination of overestimations and underestimations can be observed. In the peripheral and upper sections, the theoretical model slightly overestimates thickness compared to the constrained model. However, in the lower sections, where the serac is thicker, the theoretical model significantly underestimates thickness compared to the constrained model, with differences reaching 15–20 meters.

The analysis shows that the theoretical model generally underestimates thickness compared to the constrained model based on radar data, with significant discrepancies of up to 30 meters. GPR data have proven crucial for improving thickness estimates, particularly in the central and southern areas of the Planpincieux glacier. The presence of numerous crevasses and water infiltration in the Planpincieux glacier introduces significant local heterogeneity, which the theoretical model struggles to accurately capture. Crevasses, in particular, create substantial variations in thickness, while water infiltration influences the glacier's dynamic behavior, promoting movements and complex thickness variations. In contrast, the stability of the cold Whymper serac reduces the influence of hydrological factors, but the constrained model still provides a more accurate representation of thickness due to the use of radar data.



*Fig. 46 - Focus on the bottom part of Planpincieux glacier: the crevasses are evident. Source: <https://www.theguardian.com>*

In conclusion, this analysis demonstrates that the integration of radar data is essential for accurately capturing local variations in glacier thickness, particularly in complex systems like the Planpincieux glacier, characterized by crevasses and water infiltration. For the Whymper serac, the constrained model better captures the transition in thickness, highlighting the need for modeling based on direct observations to improve precision, even in cold glaciers with stable dynamics.

<b>Panel</b>	<b>Maximum thickness</b>	<b>Maximum difference (<math>\pm</math>)</b>
Theoretical model	~20 m	-
Constrained model	~40m	-
Difference	-	-15/20 m (overestimation)/+30 m (underestimation)

*Table 3 - Maximum thickness and Maximum differences for Planplencieux glacier and Whymper serac*

### 6.1.3 Col del Gigante and Toula glaciers

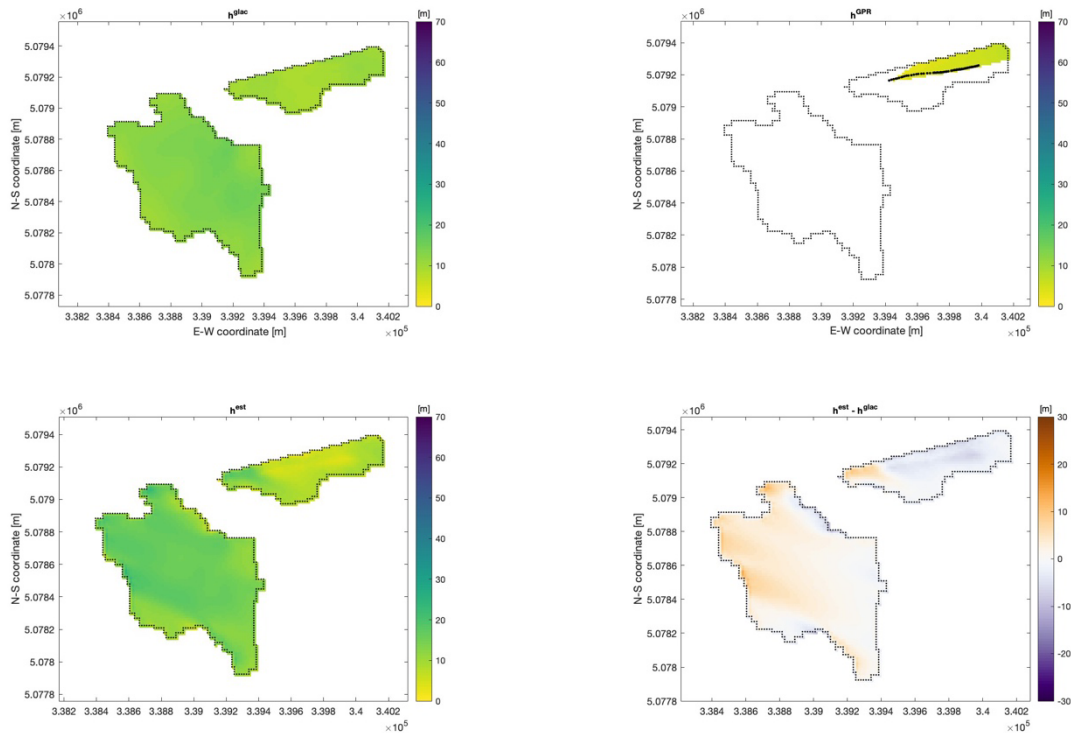


Fig. 47 - Ice thickness results, focus on Col del Gigante and Toula glaciers. Top left panel: thickness obtained using only the theoretical glaciological model. Top right: GPR constraint. Bottom left: thickness obtained from the model constrained by the GPR data. Bottom right: difference between the model constrained by radar data and the thickness of the theoretical model. Results obtained for a smoothness factor equal to 40 and resolution equal to 15.

The examination of the Toula and Col del Gigante glaciers relies on four panels produced by contrasting the theoretical model with the model informed by radar data (GPR). The theoretical model suggests that the Toula glacier (on the left) has a maximum thickness ranging from 15 to 20 meters, gradually diminishing toward the borders, where it approaches 10 meters. The theoretical model for the Col del Gigante glacier (on the right) indicates a comparable maximum thickness of approximately 15 meters, uniformly dispersed across a significant portion of the region. Nevertheless, in both cases, the theoretical model does not account for the local discrepancies in thickness.

The GPR data, displayed in the top-right panel, are missing for the Toula glacier, resulting in a completely blank domain. Radar measurements for the Col del Gigante glacier are focused on the top section, following two GPR lines. These data substantially enhance the accuracy of thickness estimates when incorporated into the model.

The bottom-left panel displays the model findings constrained by GPR data, revealing substantial revisions relative to the theoretical model. Despite the lack of direct radar data for the Toula glacier, the constrained model indicates maximum thicknesses ranging from 20 to 30 meters, while the minimum values approximate 5 meters. This signifies that the model is responsive to various environmental parameters, even without direct radar data. In the case of the Col del Gigante glacier, the incorporation of radar data significantly alters the results, elevating the maximum thickness to roughly 25 meters and decreasing the minimum thickness to approximately 5–6 meters in regions where measurements were taken.

The bottom-right panel, illustrating the difference between the theoretical model and the constrained model, exhibits considerable variances for both glaciers. The theoretical model for the Toula glacier typically underestimates thickness in the middle and western regions by up to 10 meters, while it partially overestimates thickness in certain northern and southern portions by as much as 5 meters. The theoretical model for the Col del Gigante glacier underestimates thickness by up to 10 meters in the western region and overestimates it by up to 10 meters in the eastern region, demonstrating the substantial enhancement in estimate accuracy provided by radar data.

This investigation highlights the importance of integrating radar data to improve our understanding of glacier dynamics. The lack of radar data for the Toula glacier constitutes a limitation; however, the modifications made by the constrained model indicate that more observations could yield significant insights into the glacier's stability. Radar data for the Col del Gigante glacier have facilitated a more precise depiction of glacier thickness, underscoring the necessity of encompassing the entire area with direct measurements.

The location of the Skyway Monte Bianco station between the Toula and Col del Gigante glaciers further emphasizes the strategic significance of this investigation. This infrastructure serves as both a significant tourist attraction and an essential access point for scientific observation and land management in the Alpine region. The closeness of the two glaciers to the station necessitates continuous monitoring of glacier thickness to guarantee infrastructure safety and enhance comprehension of local glacier dynamics. The results illustrate that the incorporation of radar data significantly enhances estimations and establishes a robust basis for the planning of maintenance, preventive, and sustainable management of glacial resources.

To achieve a more comprehensive understanding, it is recommended to expand radar coverage to the Toula glacier and include these data with thermal and hydrological assessments. This method would enhance understanding of local glacier dynamics and improve the safety and management of Alpine infrastructure.

<b>Glacier</b>	<b>Panel</b>	<b>Maximum thickness</b>	<b>Maximum difference (±)</b>
Toula glacier (left)	Theoretical model	~15–20 m	-
	Constrained model	~20–30 m	-
	Difference	-	-5 m (overestimation) / +10 m (underestimation)
Col del Gigante (right)	Theoretical model	~20 m	-
	Constrained model	~25 m	-
	Difference	-	±10 m

*Table 4 - Maximum thickness and Maximum differences for Toula glacier and Col del Gigante glacier*

This analysis unequivocally illustrates that the utilization of radar data is crucial for obtaining more precise glacier thickness measurements, especially in critical contexts like Punta Helbronner. The incorporation of new measurements and the expansion of radar coverage may signify an advancement in comprehending and regulating these complex situations.

## 6.2 COMPARISON BETWEEN DIFFERENT SMOOTHING FACTORS AND RESOLUTIONS

To further explore the behavior of the glaciological model and assess the effects of different configurations, two key comparisons were conducted:

### 1. Comparison between different smoothing factors at the same resolution

The first comparison focuses on the impact of varying the smoothing factor while keeping the spatial resolution constant. Specifically, two smoothing factors were applied, 20 and 60, while the resolution was fixed at 15 m.

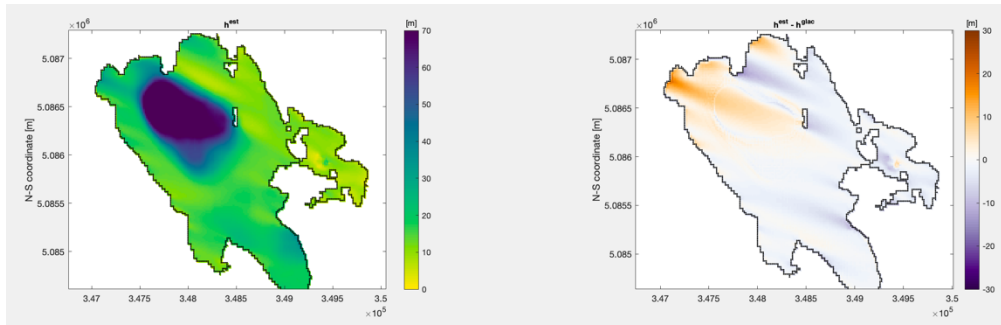


Fig. 48 - Prè de Bar and Grapillon glaciers, smoothing factor 20. Left panel: constrained model. Right panel: difference between constrained and theoretical model

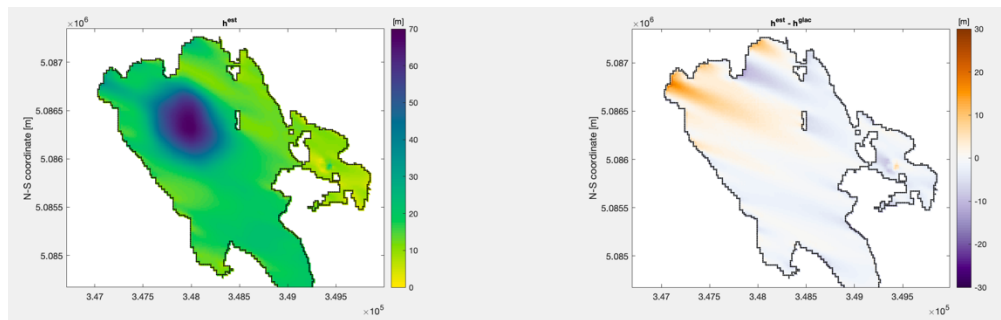


Fig. 49 - Prè de Bar and Grapillon glaciers, smoothing factor 60. Left panel: constrained model. Right panel: difference between constrained and theoretical model

- Observations:
  - As the smoothing factor increases, the difference between the theoretical glaciological model and the model constrained by GPR data decreases.
  - This behavior can be attributed to the increased smoothness introduced into the constrained model, which reduces the variability and sharp transitions caused by localized discrepancies in the GPR data.
  - Higher smoothing factors effectively dampen small-scale anomalies and align the constrained model more closely with the theoretical model.
- Implications:
  - While a higher smoothing factor improves the coherence between the models, it may also lead to a loss of local detail in the constrained model.
  - The choice of an appropriate smoothing factor should balance the need for reducing differences with the requirement to preserve localized features.

## 2. Comparison Between Different Resolutions at the Same Smoothing Factor

The second comparison examines the effect of varying spatial resolution while keeping a smoothing factor constant of 40. Three resolutions were tested: 20 meters, 15 meters, and 10 meters.

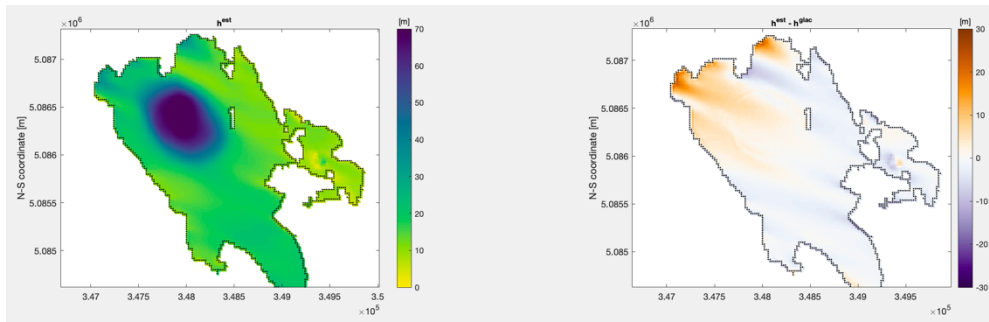


Fig. 50 - Prè de Bar and Grapillon glaciers, resolution 20 m. Left panel: constrained model. Right panel: difference between constrained and theoretical model

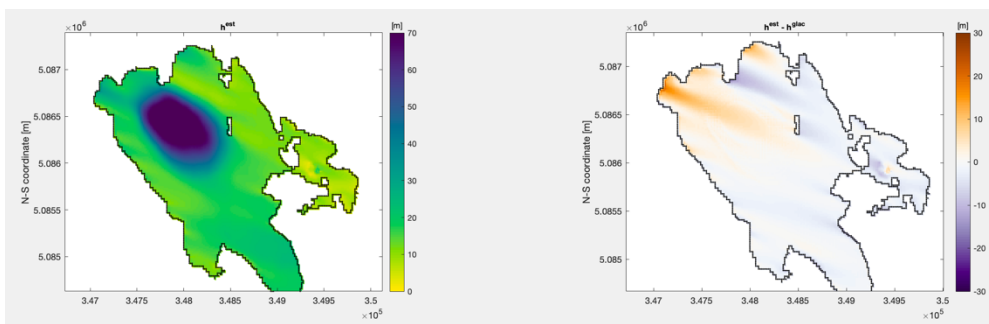


Fig. 51 - Prè de Bar and Grapillon glaciers, resolution 15 m. Left panel: constrained model. Right panel: difference between constrained and theoretical model

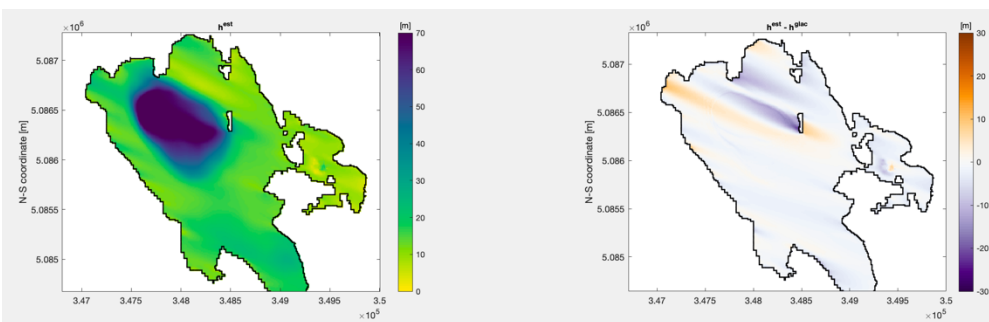


Fig. 52 - Prè de Bar and Grapillon glaciers, resolution 10 m. Left panel: constrained model. Right panel: difference between constrained and theoretical model

- Observations:
  - As the resolution increases (i.e., moving from 20 meters to 15 meters to 10 meters), the difference between the theoretical model and the constrained model change significantly.
  - Higher resolutions allow for a finer representation of the glacier's surface and internal structure, enabling the constrained model to capture more detail from the GPR data and better match the theoretical model.
  - At lower resolutions, certain small-scale features may be smoothed out or misrepresented, leading to larger discrepancies between the models.
  - Additionally, at the same smoothing factor, as resolution increases (from 20 m to 15 m to 10 m), the underestimation of the theoretical model decreases (orange areas

attenuate), while the overestimation increases (blue areas become more pronounced), as shown in Figures 50, 51, and 52.

- In the same figures, to the right of the central void in the Prè de Bar glacier, an inversion of the trend is visible: at 20 m and 15 m resolution, the theoretical model overestimates (appears blue), while at 10 m resolution, it underestimates (appears orange).
- Implications:
  - Increasing resolution enhances the model's ability to integrate GPR data effectively, but it also comes with a computational cost.
  - Higher resolutions are especially useful in areas where detailed analysis is required, such as regions with complex glacier dynamics or steep gradients.
  - The observed inversion in the model behavior could be due to the increased sensitivity of the theoretical model to local variations in ice thickness at higher resolutions. At lower resolutions, the model generalizes more, resulting in an overestimation, while at higher resolutions, the model aligns more closely with local features, leading to localized underestimation.
  - Additionally, the propagation of interpolation errors could explain this trend inversion. At lower resolutions, generalization smooths out discrepancies, while at higher resolutions, abrupt variations in ice thickness data may emerge more clearly, affecting the constrained model's alignment with the theoretical model.

The results of these comparisons highlight the following key points:

1. Smoothing Factor:
  - Increasing the smoothing factor reduces differences between the theoretical model and the constrained model by aligning the results more closely. However, excessive smoothing may sacrifice important localized details.
2. Spatial Resolution:
  - Higher resolutions significantly reduce differences by capturing finer details of the glacier, improving the accuracy of the constrained model at the cost of greater computational demand.

These findings emphasize the importance of carefully selecting both smoothing factor and resolution based on the objectives of the analysis, whether prioritizing coherence with the theoretical model, preserving localized features, or optimizing computational efficiency.

### 6.3 COMPARISON WITH GPR DATA OF GOOD OR POOR QUALITY

The quality of Ground Penetrating Radar (GPR) data is essential in glacier analysis, since it directly influences the model and the subsequent precision of interpretations. This section compares the outcomes derived from high-quality and low-quality GPR data, underscoring the disparities in final results and the influence of data quality on the comprehensive research.

In this case, we have used only the GPR files from Prè de Bar 2010, which, as previously discussed, were excluded due to their low quality and reliability. We have compared them with the complete dataset used earlier (15 m resolution and smoothing factor 40).

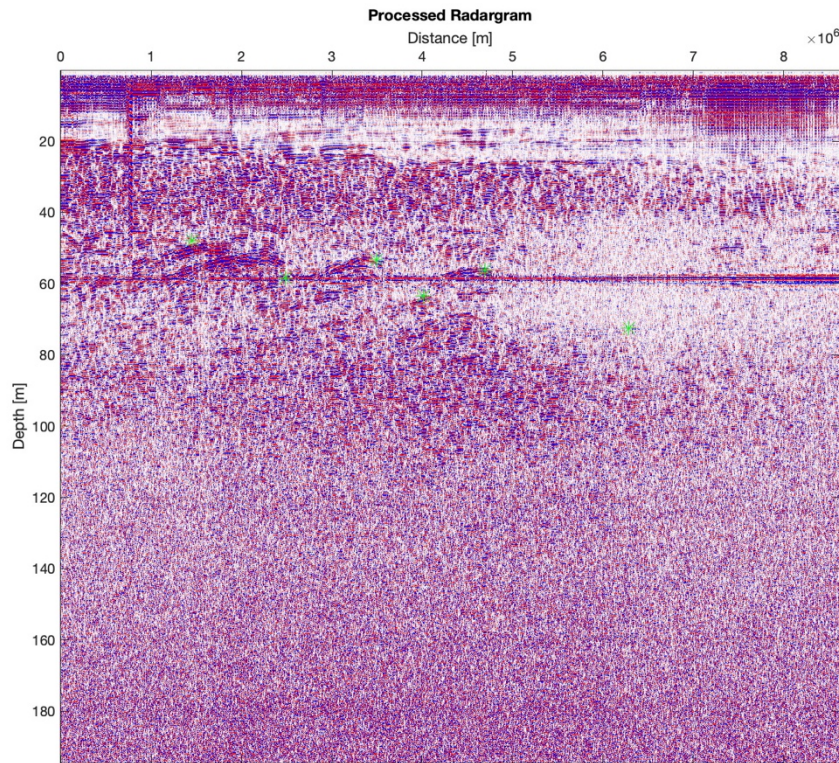


*Fig. 53 – Example of poor quality radargram of Prè de Bar*

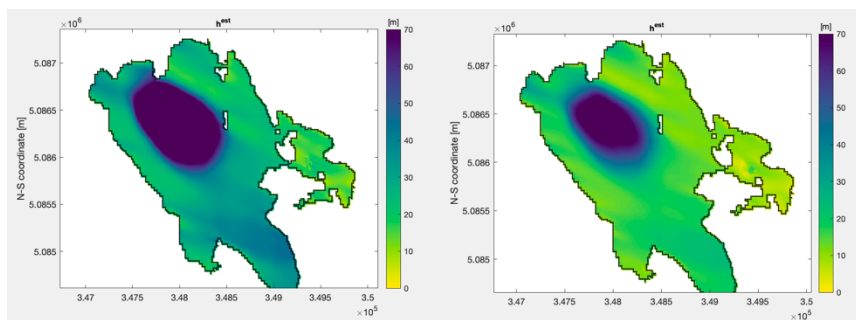


*Fig. 54 – Focus on Prè de Bar-Grapillon glaciers: on the left the results using only poor quality data from Prè de Bar, on the right the results using the correct dataset*

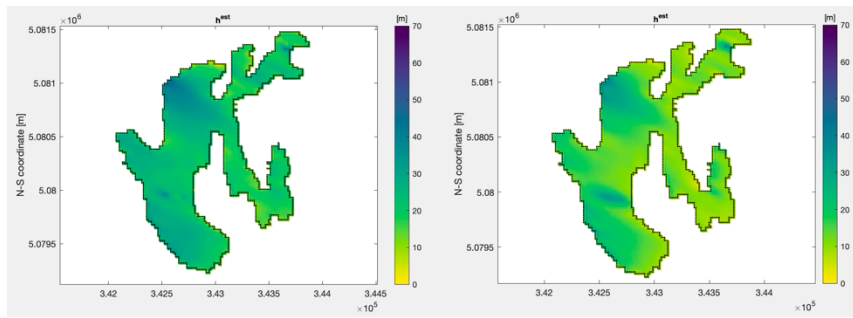


Fig. 55 – Focus on Planpincieux-Whymper glaciers: on the left the results using only poor quality data from Prè de Bar, on the right the results using the correct dataset

High-quality GPR data are defined by:

- High spatial resolution, enabling a clear differentiation of glacier layer boundaries and the glacier substrate.
- Robust and consistent signal: Minimizes interpretative ambiguity and enhances reliability.
- Reduced noise: Enhances processing accuracy and decreases computation duration.
- Precise evaluation of glacier subglacial depth and structure.

For instance, utilizing high-quality data obtained from a meticulously calibrated and appropriately designed equipment, the glacier bed profile is distinctly delineated, allowing for the identification of features such as deep crevasses or debris accumulation zones. These data facilitated precise modeling of glacial dynamics.

Conversely, low-quality GPR data show:

- Limited spatial resolution: Ambiguous boundaries and insufficient information.
- Weak and intermittent signal: Disrupts profile continuity and heightens ambiguity.
- Elevated noise levels: Necessitate more intricate processing and result in inaccuracies.

A notable increase in processing challenges was noticed in instances with poor data. The resultant profiles were disjointed, with missing sections that undermined the integrity of the analysis.

Consequently, the calculated depth lacked precision and the differences arose in the model predictions.

The comparison of the aforementioned results clearly illustrates that the quality of GPR data is essential for the effectiveness of glaciological analysis. High-quality data enhances model correctness and decreases the time needed for future processing. In contrast, worse data result in less dependable models, heightening the likelihood of misinterpretations and undermining the validity of scientific findings.

In conclusion, investing in precise data gathering, utilizing well-calibrated instruments and suitable operating circumstances, is crucial for ensuring the reliability of glacier research. This element is crucial for comprehending glacier dynamics and forecasting their future development.

## 6.4 COMPARISON BETWEEN DIFFERENT EXTENSIONS OF GPR DATA

To further evaluate the impact of GPR data coverage on the glaciological model, the Planpincieux-Whymper glacier area was selected as a case study. This analysis compares the results obtained when GPR data are used on a limited portion of the glacier versus when GPR data cover a larger extent of the glacier.

## 1. Limited GPR Data Coverage

In the first scenario, GPR data are available only for a restricted area of the Whympser serac.

- Observations:
  - Even with limited data, the constrained model exhibits significant changes compared to the theoretical model.
  - The localized integration of GPR data affects the entire glacier model, introducing corrections to the theoretical estimates even in areas not directly covered by the data.
  - However, these corrections are less precise, particularly in regions far from the measured area, as the interpolation process extrapolates information from the limited dataset.
- Implications:
  - Using GPR data on a restricted portion of the glacier demonstrates the sensitivity of the model to observational constraints, emphasizing the value of even partial datasets.
  - Nevertheless, the constrained model in this scenario may still retain inaccuracies in areas not influenced by direct measurements.

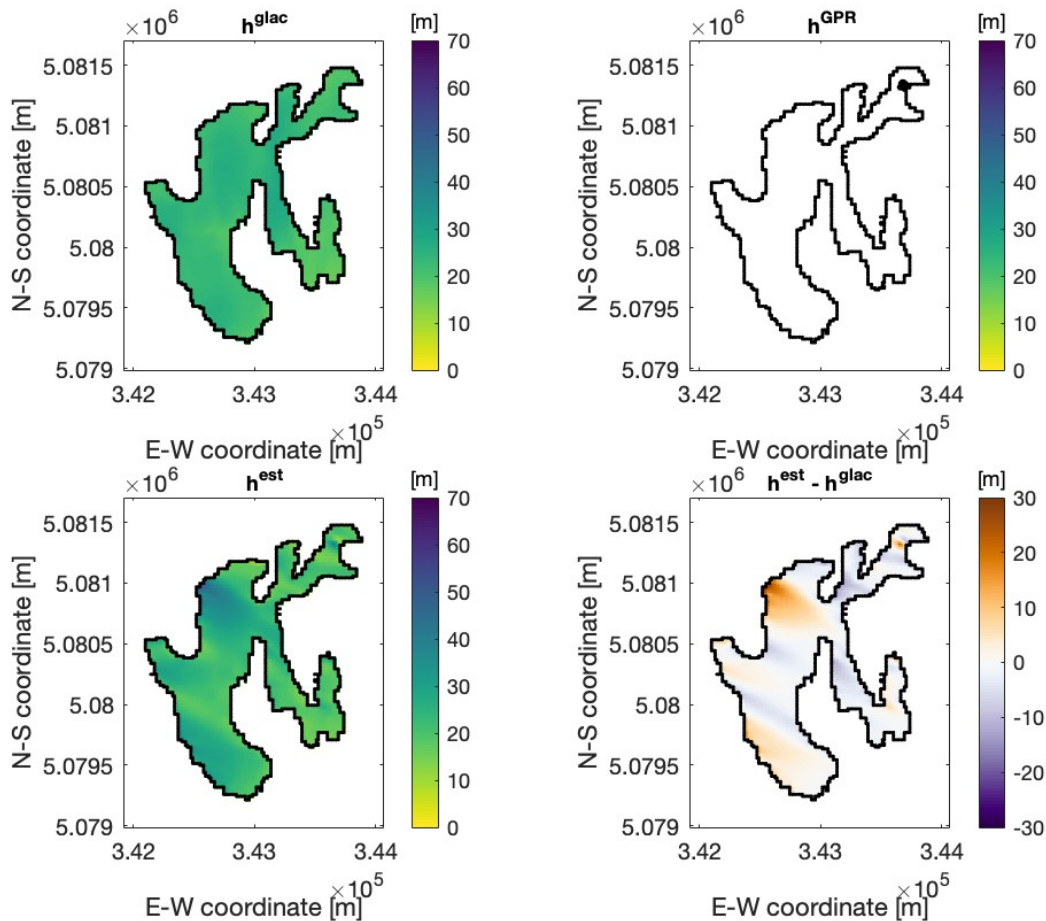


Fig. 56 – Ice thickness results, focus on Planpincieux glacier, using data from a little portion of the Whympser serac. Top left panel: thickness obtained using only the theoretical glaciological model. Top right: GPR constraint. Bottom left: thickness obtained from the model constrained by the GPR data. Bottom right: difference between the model constrained by radar data and the thickness of the theoretical model Results obtained for a smoothness factor equal to 40 and resolution equal to 15.

## 2. Larger GPR Data Coverage

In the second scenario, GPR data are utilized across a larger extent of the glacier, covering a portion of the Planpincieux glacier.

- Observations:
  - With broader data coverage, the constrained model achieves a higher degree of accuracy compared to the theoretical model.
  - The corrections introduced by the GPR data are more evenly distributed, reducing discrepancies across the glacier and improving the reliability of the results.
  - This configuration minimizes the extrapolation required, ensuring that corrections are based on measured data rather than assumptions.
- Implications:
  - Expanding the spatial coverage of GPR data enhances the overall quality of the constrained model, providing a more accurate representation of glacier thickness and dynamics.
  - The addition of data from diverse regions is particularly beneficial in capturing variations in glacier structure and morphology.

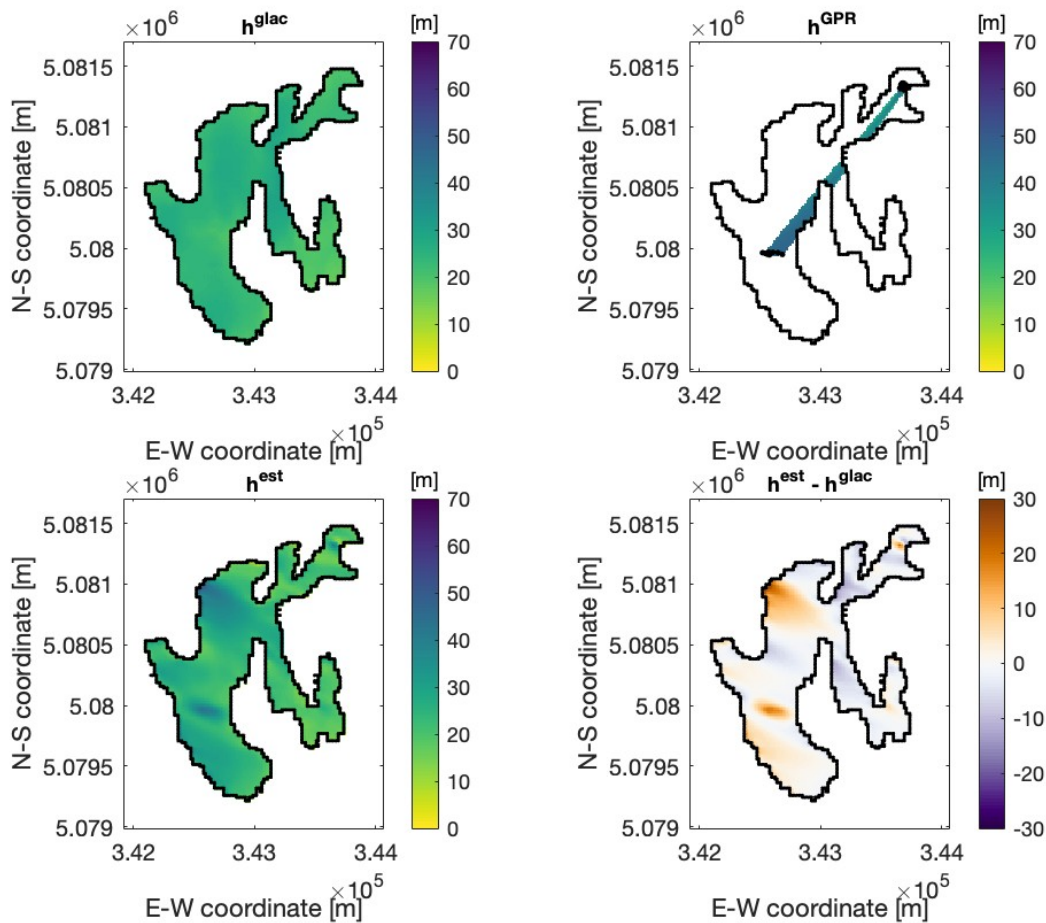


Fig. 57 - Ice thickness results, focus on Planpincieux glacier, using data different zones of the glacier. Top left panel: thickness obtained using only the theoretical glaciological model. Top right: GPR constraint. Bottom left: thickness obtained from the model constrained by the GPR data. Bottom right: difference between the model constrained by radar data and the thickness of the theoretical model. Results obtained for a smoothness factor equal to 40 and resolution equal to 15.

In the first scenario, in particular, the model underestimated the ice thickness in the core zone of the Planpincieux glacier, considering just GPR data from the Whymper area. This is evident when extra GPR data from the Planpincieux area is included into the second scenario. Reflecting better precision, the projected ice thickness increases noticeably in the areas where these extra data are added over the initial scenario. This emphasizes the crucial part data coverage plays in capturing localized changes in glacier structure, therefore guaranteeing that the constrained model more fairly depicts the actual glacier shape.

### 3. Key Insights

- Even with limited GPR data, the constrained model demonstrates notable deviations from the theoretical model, highlighting the value of incorporating observational data, regardless of coverage.
- Broader data coverage significantly improves the model's accuracy and reliability by providing a more comprehensive basis for corrections.

The Planpincieux-Whymper case study underscores the importance of GPR data in improving theoretical glaciological models. While even limited data can introduce meaningful corrections, expanding the spatial coverage of measurements ensures more accurate and reliable results. This highlights the need to balance the extent of data collection with practical constraints, such as time, accessibility, and resources, to optimize the model's performance.

## 6.5 TEMPERATURE ANALYSIS

One of the main climatic elements directly affecting glacier dynamics is temperature, which also controls the mass balance of glaciers and their interactions with the surrounding environment. Analyzing long-term temperature fluctuations in the framework of Val Ferret helps us to better appreciate how local glaciers will react to future climatic changes.

Based on three representative meteorological stations in the area, this subsection investigates the expected temperature patterns over the next years. The aim is to spot any warming trends and evaluate their influence on valley glacier dynamics. By means of a thorough investigation of past data and future estimates, this work emphasizes seasonal fluctuations and their impact on the accumulation of ice and ablation processes. Furthermore, the results give a basis for modeling glacier behavior, allowing a more realistic assessment of how climate change will affect the stability and development of Val Ferret's glacier system.

### 6.5.1 Parameter selection

The stations considered, displayed in Figure 36, which measure temperature are: Ferrachet, Mont de la Saxe and Prè de Bar.

Table 5 in particular provides more specific information on the location and data accessibility of the meteo stations:

Station	Longitude (deg)	Latitude (deg)	Altitude (m asl)	Data availability
Ferrachet	45.8668	7.02754	2290	2002-2024
Mont de la Saxe	45.8170	6.98204	2110	2002-2024
Prè de Bar	45.8843	7.06523	2040	2002-2024

*Table 5 - Detailed summary of the three separate sites*

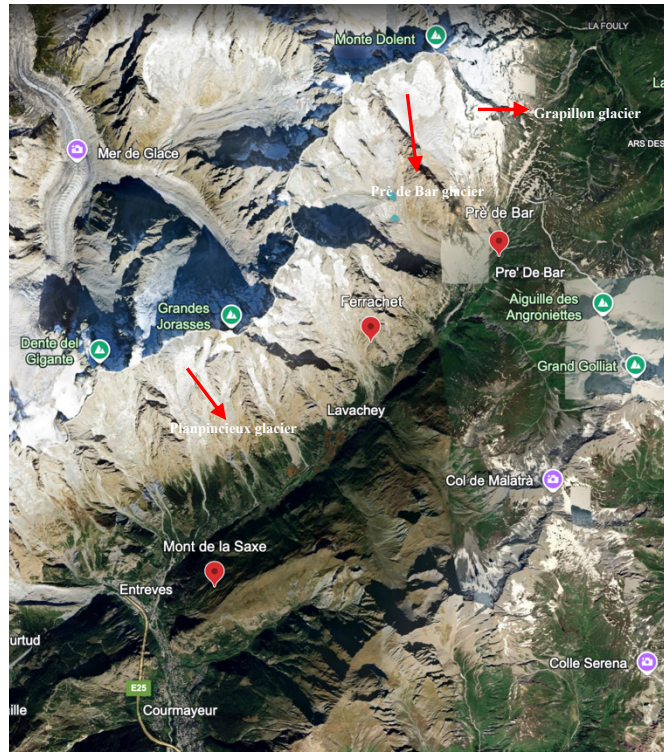


*Fig. 58 - Location of the three meteo stations, respect to Courmayeur*

According to worldwide climatological standards, a high-precision meteorological study should ideally require historical data set spanning at least 30 years. For the assessment of trends and climatic anomalies to be more reliable, this timeframe is required. But in our instance, we have data sets that span roughly 22 years. For the objectives of this study, the results are still acceptable even though the optimal period is not met. With the use of these data, we are able to spot important patterns and offer an initial assessment of how temperature fluctuations affect Val Ferret's glacier dynamics.

The temperature trend was computed for all three stations to have a more complete knowledge of the environment in the area of interest, as we can see in Table 3. The same processing techniques were used for all three datasets for this aim, but the next section describes only the processing carried out especially to the Prè de Bar dataset, for simplicity. The results of Ferrachet and Mont de la Saxe stations are visible in Appendix A.

### 6.5.2 Gap filling

The original temperature dataset recorded at the reference meteorological station are plot in Figure 59.

Usually due to a malfunctioning of the instruments on such days, the dark vertical lines in the graph show the days of the year when the meteorological station was not collecting data.

For those years having measurements, average values computed using the same days of the year substituted this absent data. To get the same daily count, the dataset was also sliced to whole years. Figure 60 shows the results.

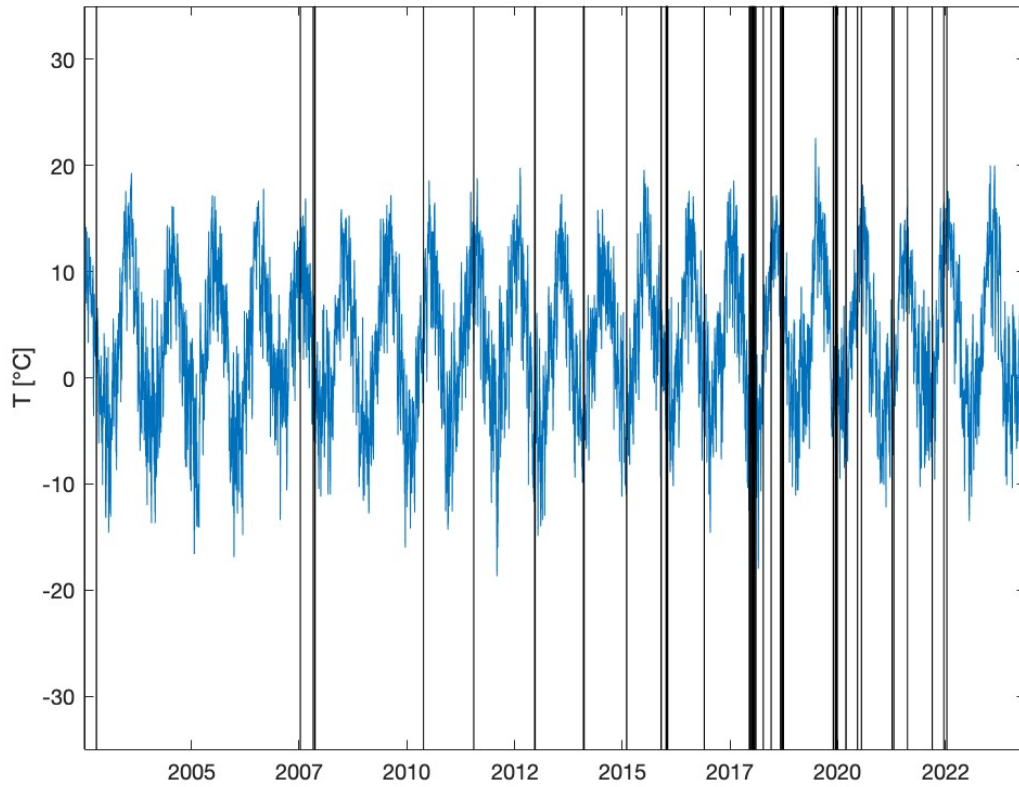


Fig. 59 - Temperature data acquired at Prè de Bar station (2002-2024)

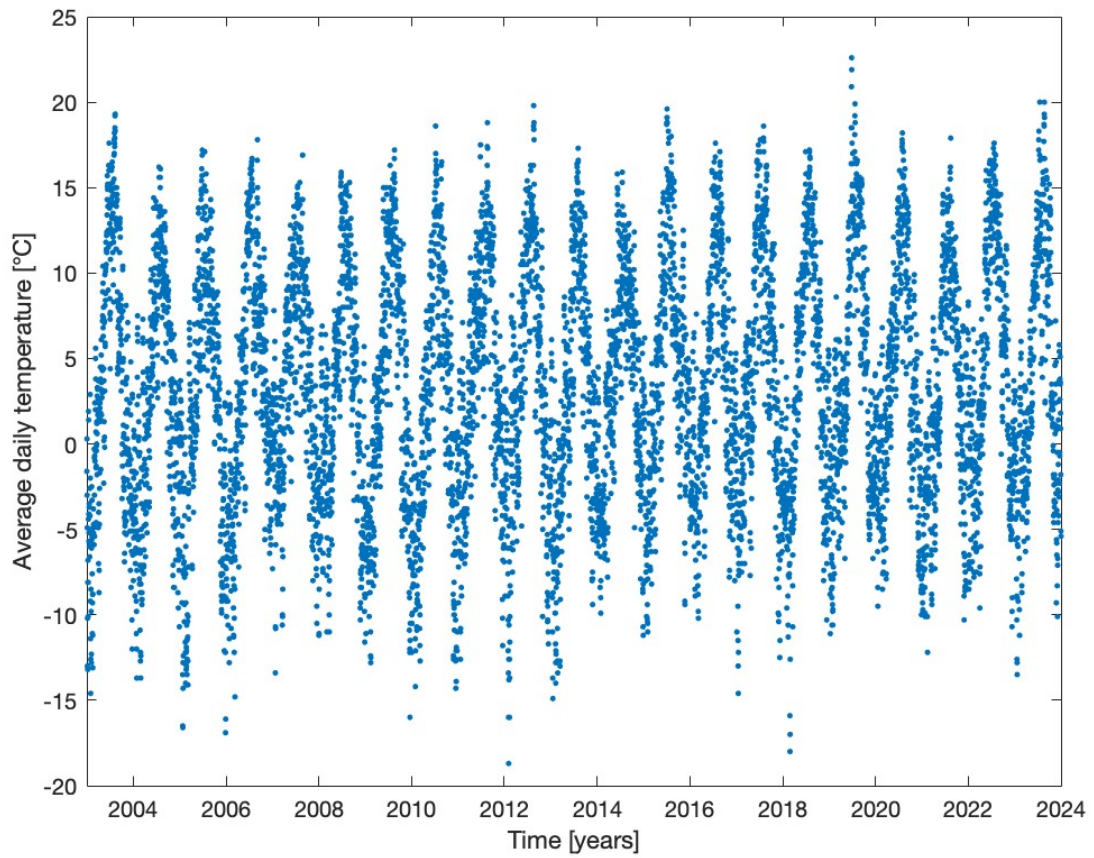


Fig. 60 - Dataset complete and filled

### 6.5.3 Signal processing: Trend enhancement by removal of the periodic component

Quantifying increasing/decreasing trend from the data of the above figure is a difficult task. These data are affected by a marked cyclical component due to the astronomical variations occurring during the year (changes in solar radiation due to Earth's rotation, seasonal variations).

This periodic component can be expressed as:

$$\Psi = A_1 \cos(2\pi f_1 t + \Phi_1) + A_2 \cos(2\pi f_2 t + \Phi_2) + \dots + A_n \cos(2\pi f_n t + \Phi_n) \quad (23)$$

where  $t$  is time (days),  $A$  is amplitude (in °C),  $f$  is frequency (1/days) and  $\Phi$  is phase of the harmonic components. At least one harmonic is detected in the data ( $f_1=1/365.25$  days) but higher ones (2-3) can also be depicted.

$f$ ,  $A$  and  $\Phi$  can be derived from spectral analysis of the dataset (amplitude and phase spectra).

Spectral analysis of the data allowed to recover the amplitude and the phase of  $f_1$ ,  $f_2$ , and  $f_3$ .

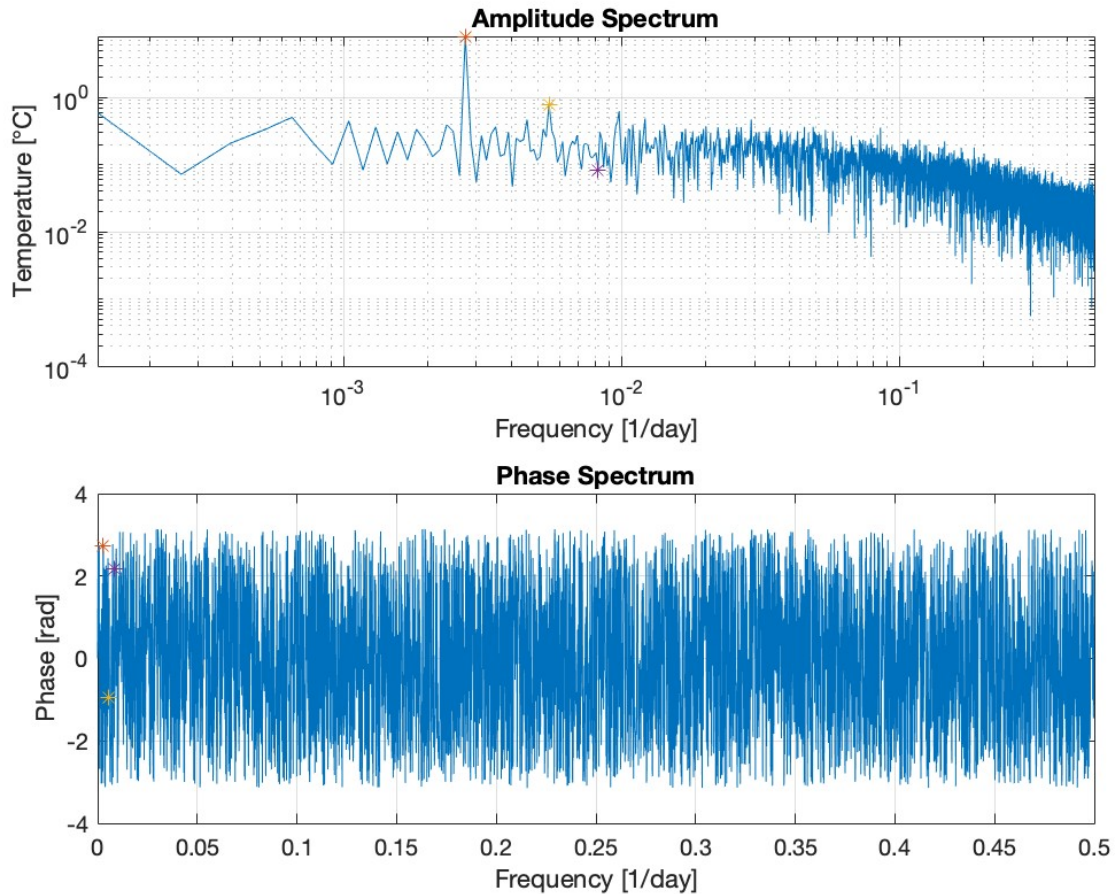


Fig. 61 – Amplitude Spectrum and Phase Spectrum of the recorded temperature data

The next step is the computation of the periodic component, compared with the average daily temperature computed on the whole dataset

After that, the periodic component and the daily average temperatures overlapped to the gap-filled complete-year dataset, as shown in Figure 62.

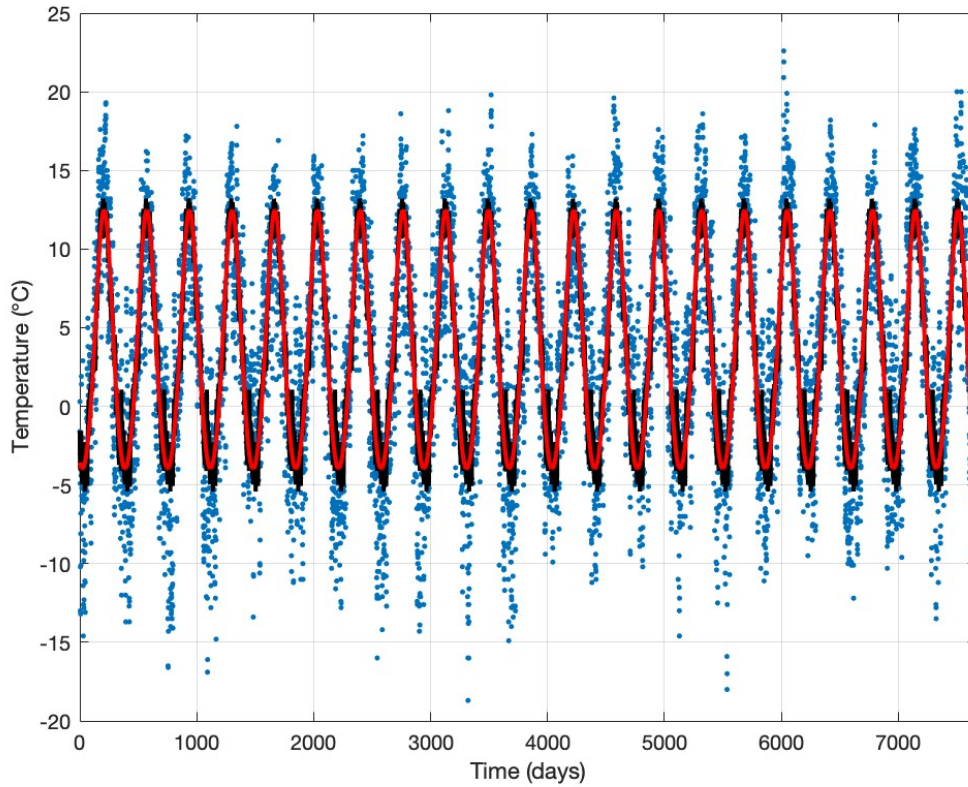


Fig. 62 - Temperature data (blue) with periodic component (red) and daily average temperature (black)

Two residual variations have been calculated: the first ones have been obtained by subtracting the periodic component to the data, in order to analyze the trend caused by atmospheric forcing. The second ones have been obtained by subtracting the average daily temperatures.

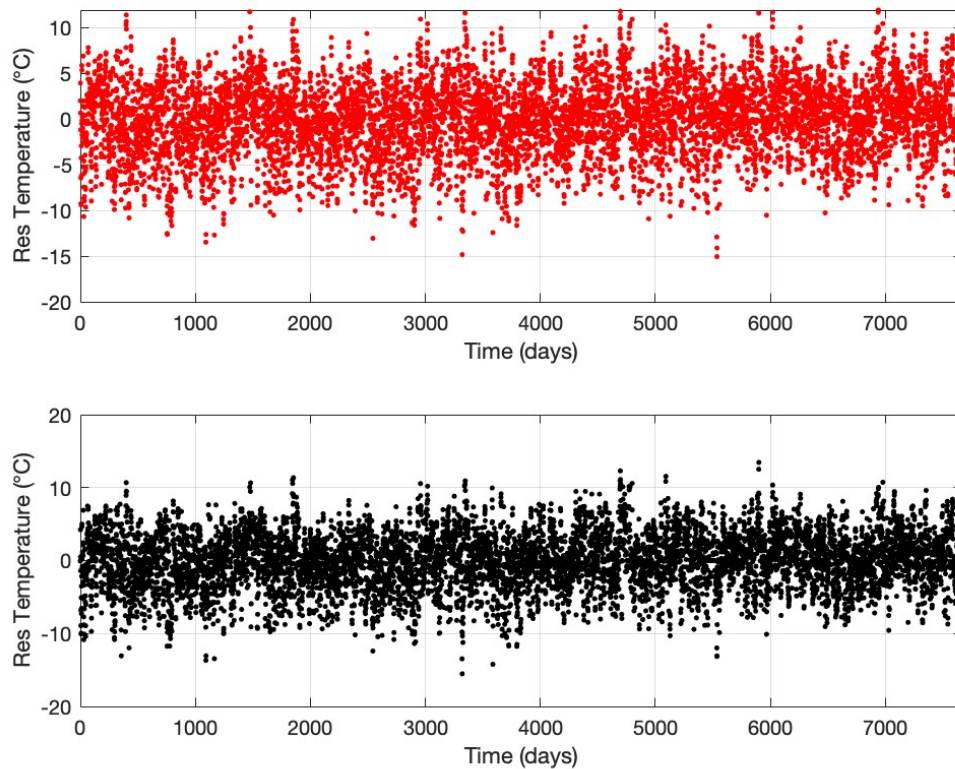


Fig. 63 - Data residuals obtained through the removal of the periodic component (red) and daily average temperature (black)

### 6.5.4 Trend estimation

The residuals can be fitted with linear regression in order to highlight possible increases or decreases of the meteorological parameter along years. In particular, the slope (x1) of the fitting line quantifies the increasing/decreasing trend.

The goodness of the fitting is remarkably quantified by the p-value, corresponding to the probability of a zero-slope fitting line, e.g. p-value=0.05 means that the probability of a zero-slope fitting line is 5%, so the obtained results have a probability of 95% to be reliable.

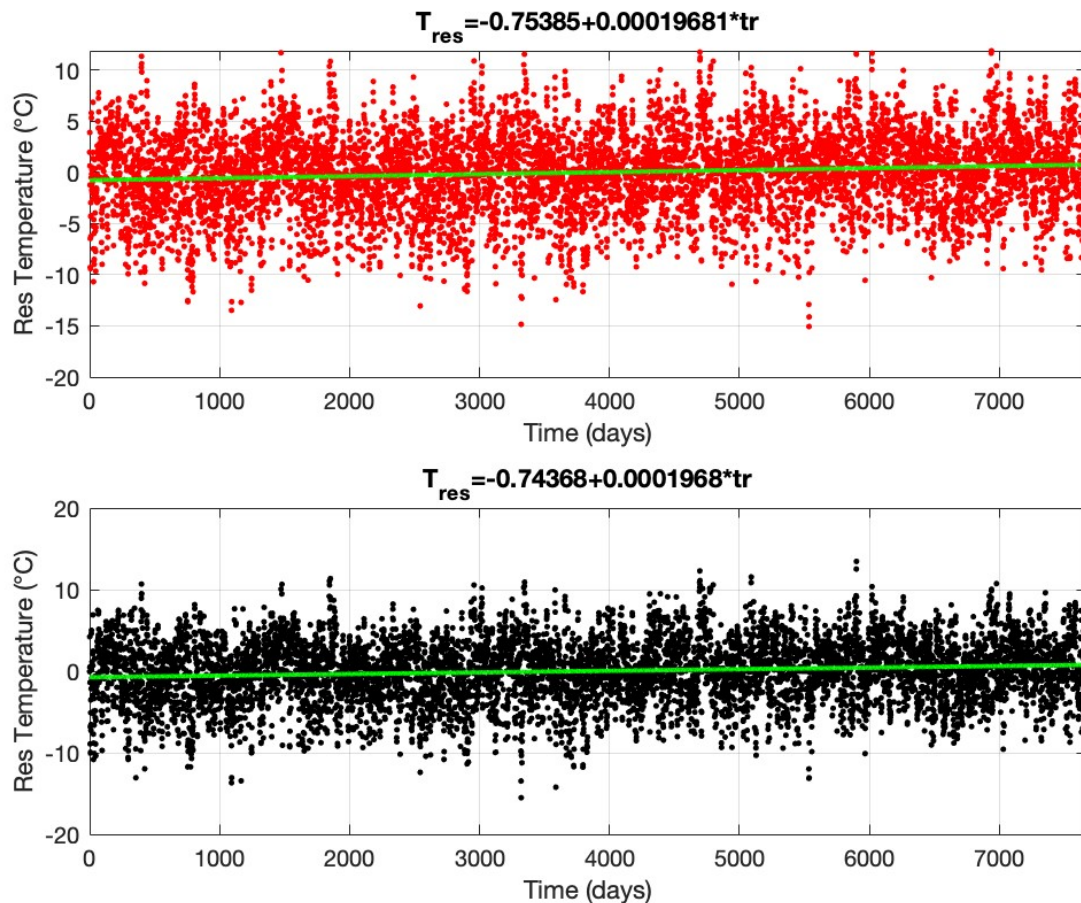


Fig. 64 - Regression lines highlighted

Station	Annual temperature trend by removing periodic component (°C/year)	Standard deviation (°C/year)	pValue	Annual temperature trend by removing daily average temperature (°C/year)	Standard deviation (°C/year)	pValue
Ferrachet	0.009	±0.007	0.194	0.009	±0.007	0.186
Mont de la Saxe	0.072	±0.007	9.3e-23	0.073	±0.007	7.2e-24
Prè de Bar	0.072	±0.007	2.7e-22	0.072	±0.007	2.2e-23

Table 6 - Temperature trend obtained for the three different meteorological stations, with the tolerance and pValue

The analysis of temperature trends yielded interesting and, in some cases, unexpected results that warrant a thorough interpretation. Each meteorological station exhibits unique characteristics, reflecting both local climate variability and the peculiarities of its geographic location.

The Ferrachet station stands out for its nearly null trend, with a value of  $0.009\text{ }^{\circ}\text{C}/\text{year}$ . This result is accompanied by a high pValue, indicating that the data is consistent. This behavior may be attributed to the station's specific placement and location, which could limit its sensitivity to climatic changes or reflect particular microclimatic conditions that dampen temperature variations. In contrast, the Mont de la Saxe and Prè de Bar stations show more pronounced and concerning trends. For both, the maximum trend value, calculated by adding the standard deviation to the mean trend, reaches  $0.079\text{ }^{\circ}\text{C}/\text{year}$ . These results point to significant warming, consistent with global and regional data indicating rapid glacier retreat. The low pValue associated with these trends confirms the reliability and statistical significance of the analysis. These data clearly highlight how thermal warming has a direct impact on glacier dynamics, contributing to the negative mass balance of the Val Ferret glaciers and accelerating their melting processes.

The overall results underscore the importance of detailed, long-term evaluations to fully understand climate dynamics and their local effects. While Ferrachet appears to resist evident changes, Mont de la Saxe and Prè de Bar reveal concerning trends that confirm projections of progressive and significant warming.

## 7 CONCLUSIONS

### 7.1 SUMMARY AND CRITICAL DISCUSSION OF THE RESULTS

The study conducted on the glaciers of Val Ferret has provided a detailed assessment of ice thickness and its spatial variations through the application of the GLATE (Glacier Thickness Estimation) model, constrained by Ground Penetrating Radar (GPR) data collected in the field. The adopted methodology allowed for a more in-depth analysis compared to traditional empirical models, providing a more accurate characterization of glacier thickness and its evolutionary trends.

The results indicate that the retreat of the glaciers in Val Ferret is occurring at an accelerated pace, in line with trends observed across the entire Alpine region. The analysis of glacier thickness has highlighted significant differences between different areas of the glacier basin, with greater thickness in accumulation areas at higher altitudes and a drastic reduction in ablation zones, where ice has fragmented into isolated masses. This distribution reflects the delicate balance between accumulation and mass loss processes, whose balance has now become negative due to climate warming.

One of the most critical aspects emerging from this study concerns the speed at which these transformations are occurring. The comparison between current data and the 2008 GlabTOP ones has revealed an accelerated loss of glacier volume. GPR measurements have shown that some areas, once characterized by significant thickness, now exhibit values below the minimum threshold necessary for the long-term survival of a glacier. This confirms the general trend of glacial degradation in the Alps, with repercussions not only on local hydrology but also on the geomorphological stability of the territory.

The influence of local topography on melting and accumulation dynamics has proven to be a determining factor. In particular, surfaces with high solar exposure show a much more pronounced reduction in glacier thickness compared to those with north-facing or shaded exposure, suggesting that surface energy balance plays a key role in retreat dynamics. The spatial variability of ablation observed in the glaciers of Val Ferret underscores the importance of continuous and detailed monitoring to better understand the interactions between climatic drivers and glacial response.

Another significant element concerns the quality and reliability of the acquired data. The use of Ground Penetrating Radar (GPR) has provided detailed information on the internal structure of glaciers, improving the accuracy of estimates compared to methods based only on surface observations. However, some limitations related to the spatial coverage of radar profiles and their quality have highlighted the need for future acquisition campaigns to further improve model calibration.

From a climatic perspective, the analysis of temperature trends has confirmed the strong impact of global warming on the dynamics of the glaciers in Val Ferret. The available data indicate a constant increase in average temperatures, resulting in a rise in the Equilibrium Line Altitude (ELA) and a reduction of the accumulation zone. This phenomenon is leading to a progressive reduction in the ability of glaciers to supply the local hydrological system, with direct implications for water availability during summer periods.

A particularly relevant aspect is the presence of clear signs of destabilization in some portions of the glacier basin. The formation of crevasses and unstable seracs suggests that glacier retreat does not occur homogeneously but is often accompanied by structural collapse phenomena, which can increase the risk of catastrophic events such as glacial landslides or serac detachments. These phenomena are particularly concerning for the safety of the valley, as they could pose a threat to infrastructure and tourism activities.

Overall, the results of this study provide a clear and detailed picture of the glacial situation in Val Ferret, highlighting the need for monitoring strategies and risk mitigation measures. The ongoing evolution of climatic conditions requires growing attention to water resource management and territorial protection, adopting an approach based on solid and up-to-date scientific data.

## 7.2 POTENTIAL IMPACTS OF GLACIAL CHANGES ON THE VAL FERRET

The observed changes in the glaciers of Val Ferret will have significant consequences on the local environment, with direct and indirect impacts on several aspects:

- **Water resources:** The reduction in glacier volume will compromise the capacity to release water during summer months, affecting rivers and streams that feed into the Dora Baltea, impacting agricultural irrigation, hydroelectric production, and water supply for local communities.
- **Geomorphological risks:** The increasing instability of glacial masses, particularly in hanging glaciers such as Planpincieux Glacier and Whymper Serac, increases the risk of collapses and glacial landslides. These events could damage infrastructure, trails, and settlements, posing a threat to residents and tourists.

- Ecosystem modifications: The reduction in glacier coverage will lead to changes in alpine habitats, affecting biodiversity, vegetation dynamics, and the availability of water for animal and plant species adapted to glacial environments.
- Tourism and economic activities: The reduction of glaciers could have a negative impact on tourism activities related to hiking and winter sports. The loss of iconic landscapes and the threat of catastrophic events could reduce the attractiveness of the valley for visitors and local investors.

These impacts require constant monitoring and adaptation strategies to mitigate the risks associated with glacier retreat. Local institutions will need to implement risk management measures, promote alternative water supply solutions, and develop climate adaptation policies to ensure the sustainability of the region.

### 7.3 COMPARISON WITH SIMILAR STUDIES IN OTHER ALPINE OR GLOBAL AREAS

The behavior of the glaciers in Val Ferret aligns with observations made in other parts of the Alps and in mountain ranges worldwide:

- Studies conducted in the Swiss and Austrian Alps: Show that small and medium-sized glaciers are particularly vulnerable to climatic variations, exhibiting a glacial area reduction trend similar to that observed in Val Ferret [44].
- Glaciers in the Andes and the Himalayas: These regions experience similarly rapid retreat rates, with significant implications for drinking water availability and the risk of catastrophic events such as Glacial Lake Outburst Floods (GLOFs) [45].
- Glaciers in Greenland and Antarctica: Display even higher mass loss rates, with direct effects on rising sea levels. Although geographical scales and climatic conditions differ, the parallels between these phenomena emphasize the global nature of the ongoing glacial crisis.

### 7.4 LIMITATIONS OF THE RESEARCH AND FUTURE PERSPECTIVES FOR MODEL IMPROVEMENT

Despite the results obtained, the research presents some limitations that could be addressed in future studies:

- Spatial coverage of GPR data: The measurements taken do not homogeneously cover the entire study area, limiting estimate accuracy in some zones. Acquiring a greater number of radar profiles could improve the quality of the simulations.
- Integration with satellite data: Using high-resolution satellite images (e.g., Sentinel-1, ICESat-2) could provide complementary information to enhance the accuracy of glacier thickness estimates.
- Dynamic models: The GLATE model currently follows a static approach.
- Integrating dynamic models could allow for more precise simulations of future glacier evolution.

- Subglacial processes: The effects of basal sliding and the presence of subglacial cavities were not considered in detail. Future studies could explore these aspects to improve model calibration.
- Comparison with other survey methods: Integrating complementary geophysical techniques (e.g., seismic surveys, gravimetric measurements) could contribute to more robust glacier thickness estimates.

To enhance the study's accuracy and applicability, future research should:

- Conduct additional GPR measurement campaigns to improve data coverage.
- Integrate the GLATE model with dynamic approaches considering the temporal evolution of glaciers.
- Strengthen comparisons with theoretical models to enhance simulation calibration and validation.

These improvements will allow for a deeper understanding of Alpine glacier dynamics, providing more effective tools for risk management and water resource conservation in mountain regions.

## 8 APPENDIX

### 8.1 APPENDIX A

The subsequent part will discuss the temperature analysis for the Ferrachet and Mont de la Saxe stations, using the identical approach utilized for the Prè de Bar station. Consequently, only the outcomes derived from the various phases of processing will be presented here.

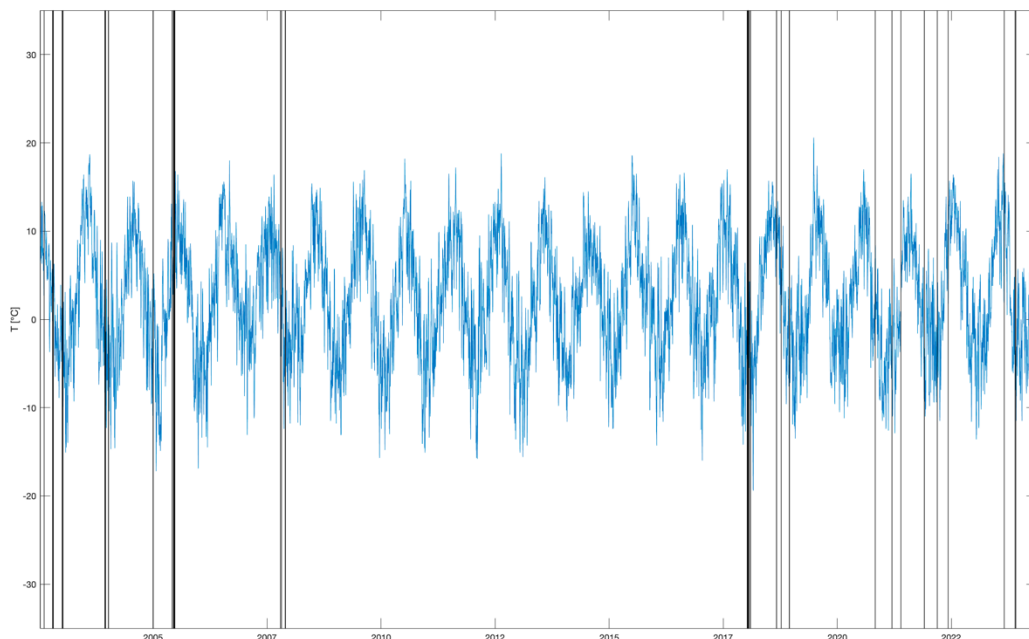


*Fig. 65 - Temperature data acquired at Ferrachet station (2002-2024)*

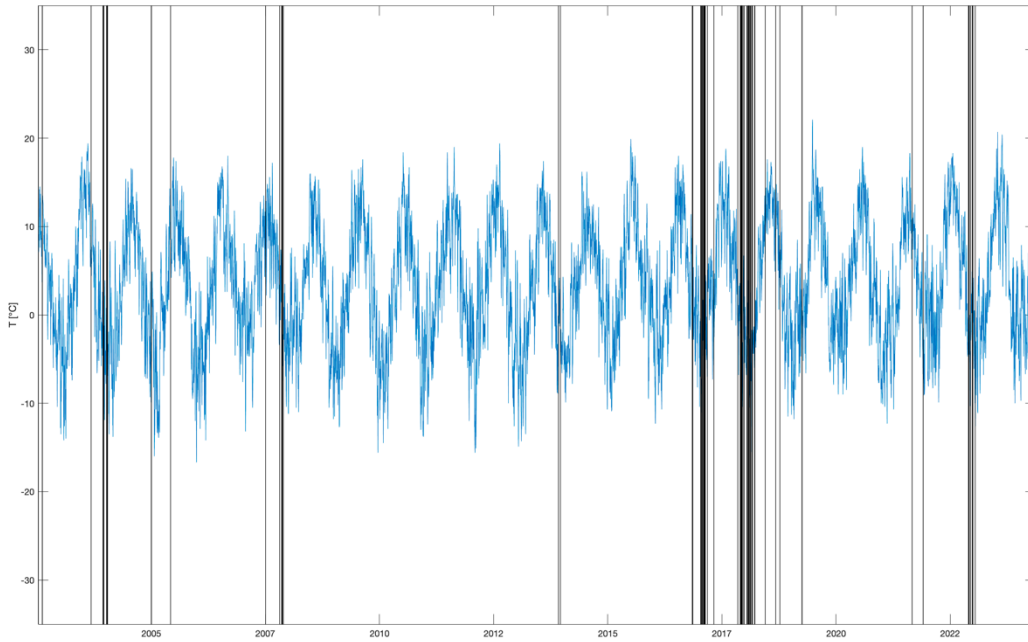


*Fig. 66 - Temperature data acquired at Mont de la Saxe station (2002-2024)*

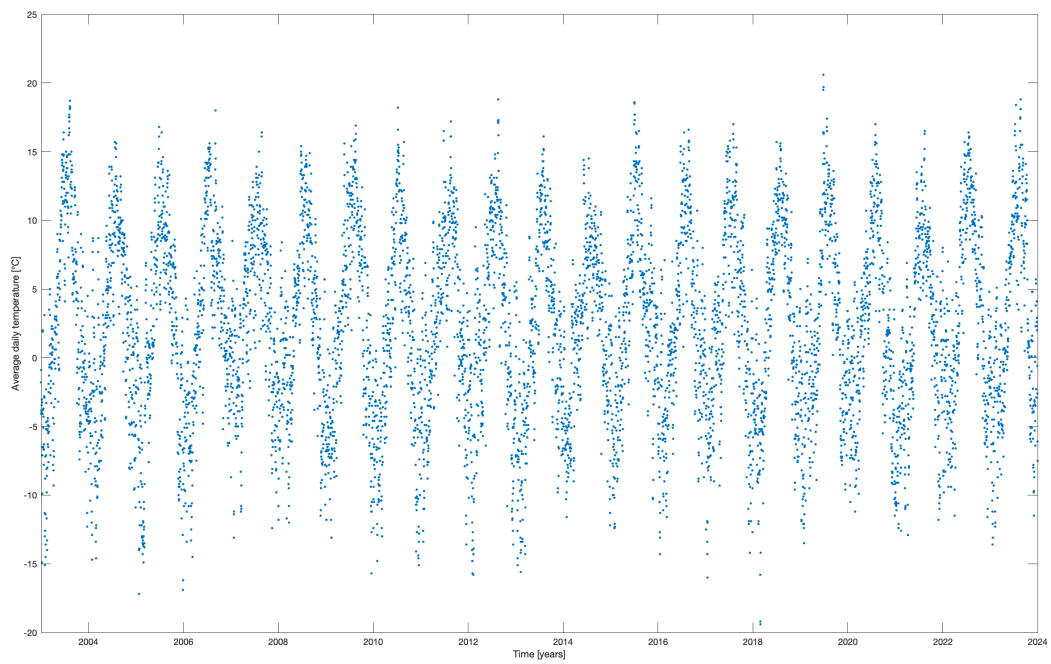


*Fig. 67 - Ferrachet station dataset complete and filled*

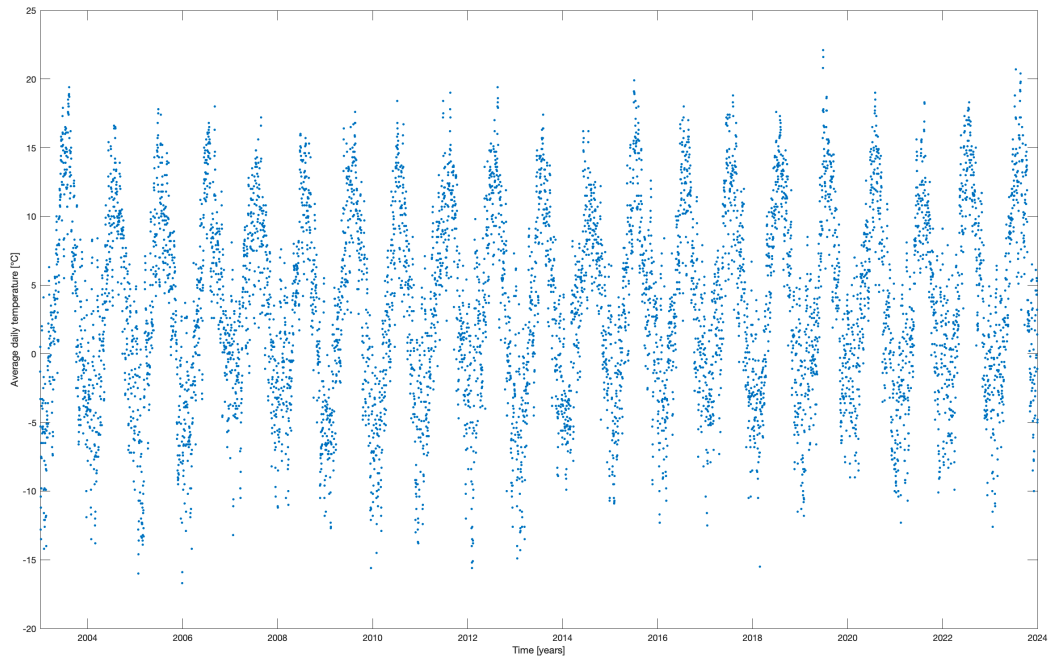


*Fig. 68 - Mont de la Saxe station dataset complete and filled*

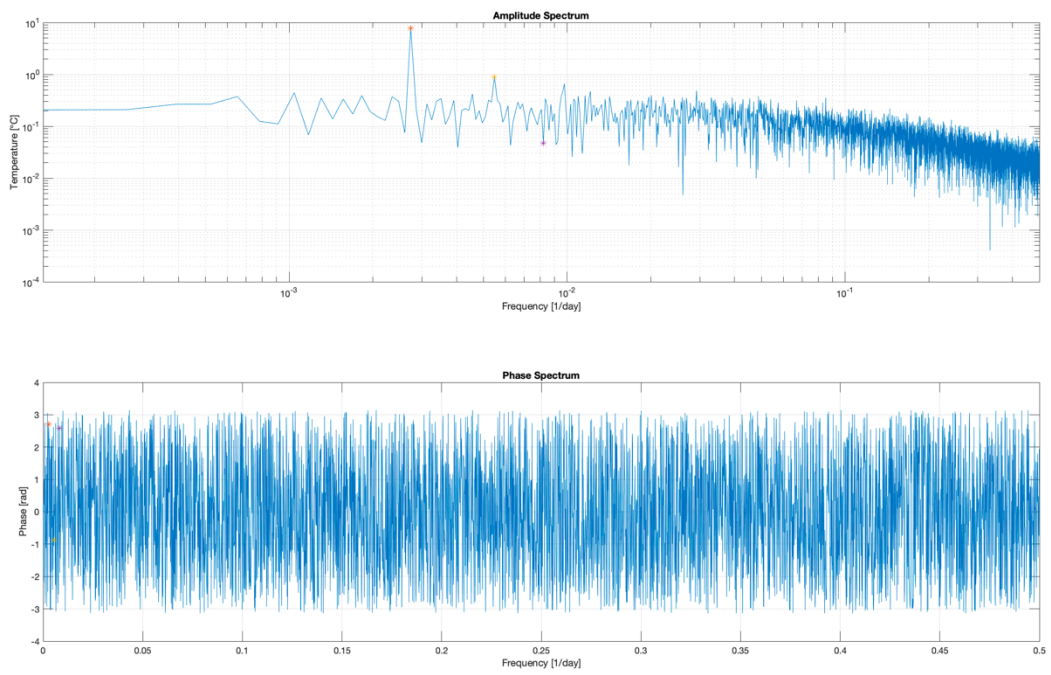


*Fig. 69 - Ferrachet station Amplitude Spectrum and Phase Spectrum of the recorded temperature data*

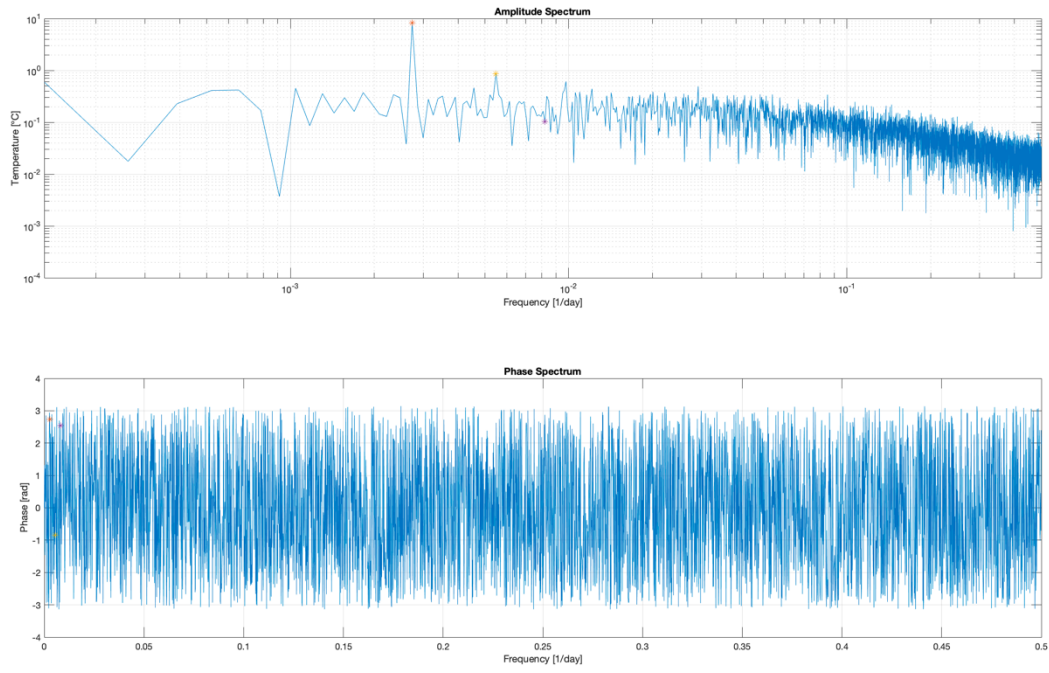


Fig. 70 - Mont de la Saxe Amplitude Spectrum and Phase Spectrum of the recorded temperature data

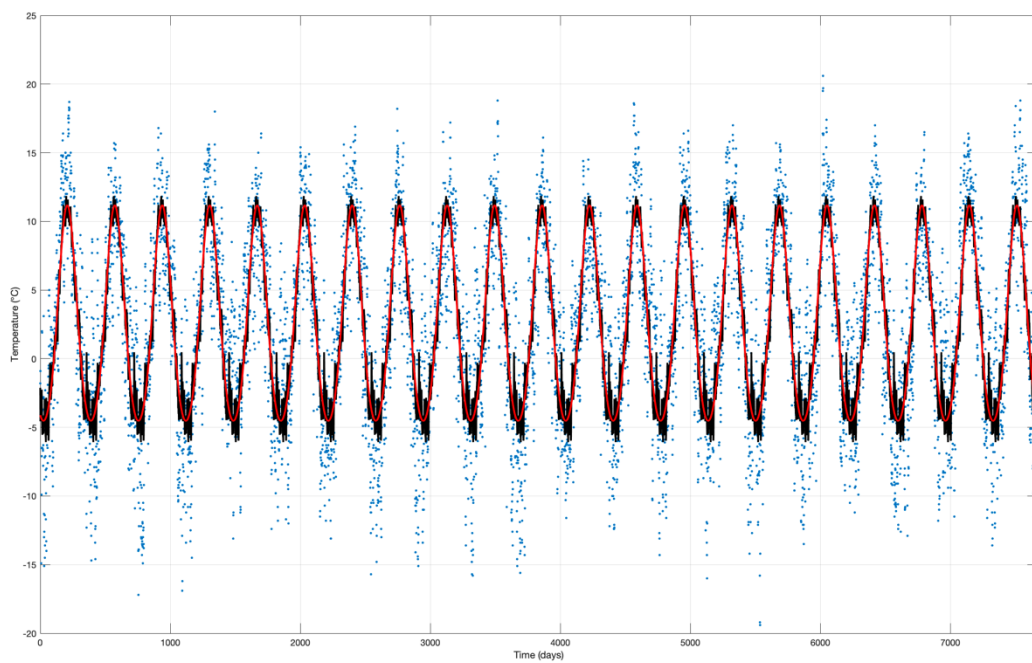


Fig. 71 - Ferrachet station temperature data (blue) with periodic component (red) and daily average temperature (black)

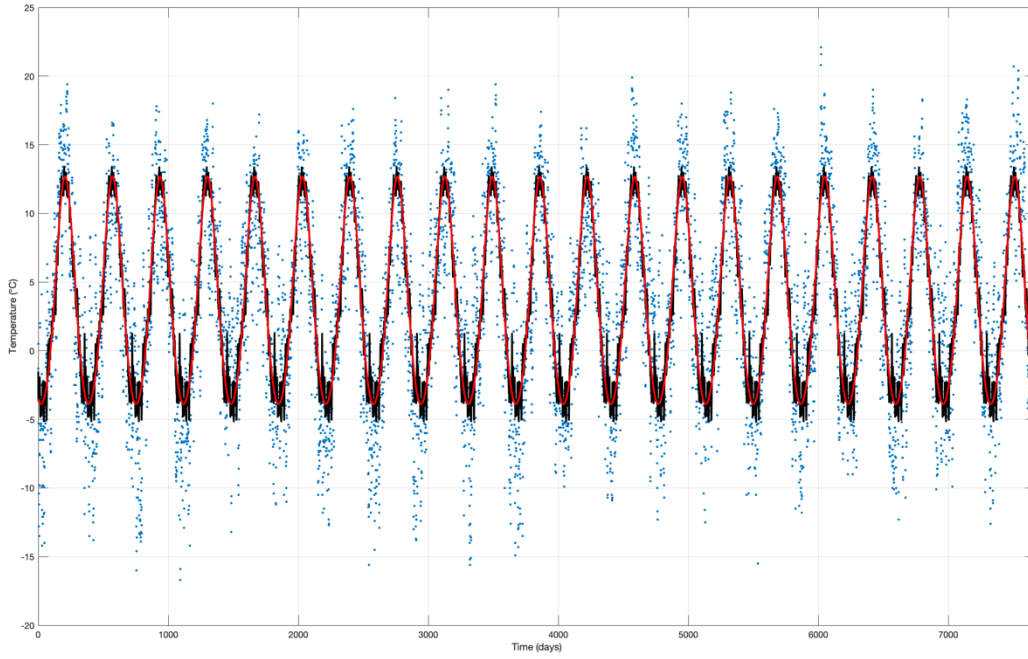


Fig. 72 - Mont de la Saxe station temperature data (blue) with periodic component (red) and daily average temperature (black)

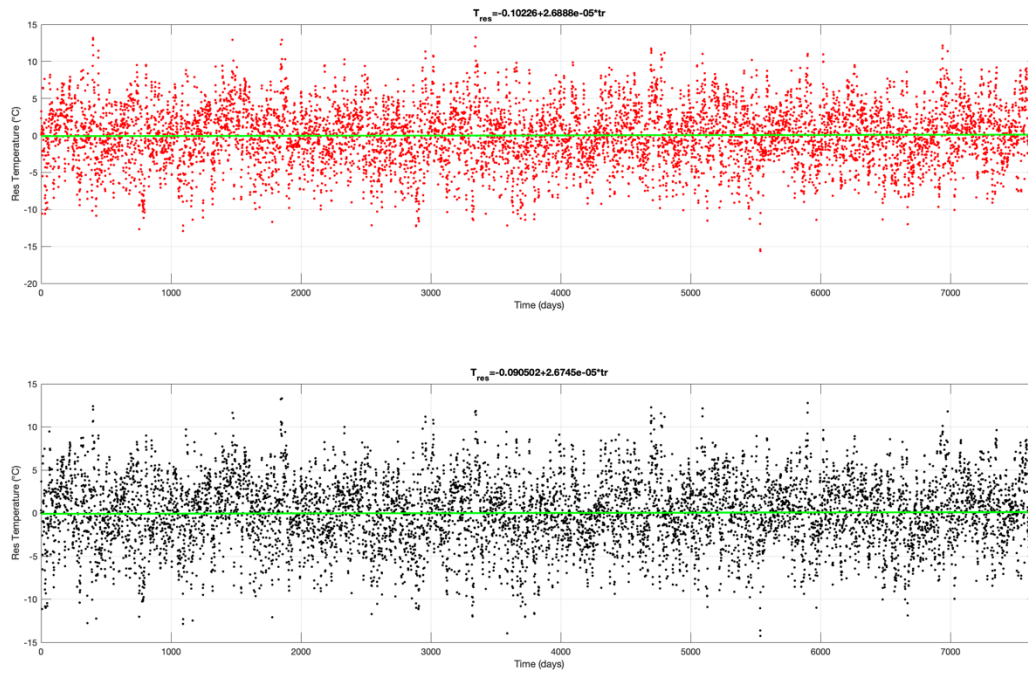


Fig. 73 - Ferrachet station data residuals obtained through the removal of the periodic component (red) and daily average temperature (black), with the regression line highlighted

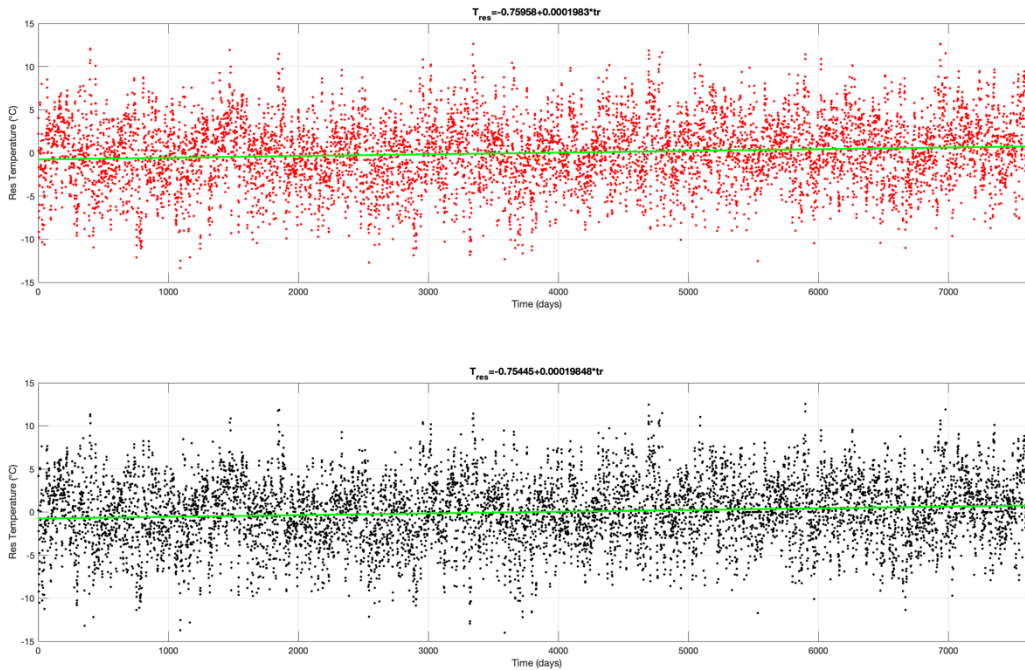


Fig. 74 – Mont de la Saxe station data residuals obtained through the removal of the periodic component (red) and daily average temperature (black), with the regression line highlighted

## 8.2 APPENDIX B

In the following appendix the MATLAB code used for the GPR files processing is shown:

```

%% Select the colorscale for radargram visualization
%%% suggested default colorscales: 'bone','jet','gray'
cmap='gray';
%%% or ad-hoc build colorscale
load('GPRcmap.mat')

%% Import GPR traces
dati=Idsris_read;           % function for reading raw data (*.dt) from IDS GPR
antennas
nusa=dati.n_sampler_y;     % number of samples (time)
nutr=dati.n_sampler_x;     % number of traces (space)
dx=dati.sweep_dx;         % trace distance along the profile
savename=dati.filename;
%% Import profile coordinates .GPS
filename1=[dati.filename '.GPS'];
if isfile(filename1)==1
gpsraw=importdata(filename1);

delimiter = ',';
formatSpec = '%s%s%s%s%s%s%s%s%s%s%s%s%s%s%s%[\n\r]';

fileID = fopen(filename1,'r');
dataArray = textscan(fileID, formatSpec, 'Delimiter', delimiter, 'TextType',
'string', 'ReturnOnError', false, 'EndOfLine', '\n\r');
fclose(fileID);

```

```

raw = repmat({''},length(dataArray{1}),length(dataArray)-1);

for col=1:length(dataArray)-1
    raw(1:length(dataArray{col}),col) = mat2cell(dataArray{col},
ones(length(dataArray{col}), 1));
end
numericData = NaN(size(dataArray{1},1),size(dataArray,2));

for col=[1,2,3,4,5,6,7,8,9,10,11,12,13,14,15]
    % Converts text in the input cell array to numbers. Replaced non-numeric
    % text with NaN.
    rawData = dataArray{col};
    for row=1:size(rawData, 1)
        % Create a regular expression to detect and remove non-numeric prefixes
and
        % suffixes.
        regexstr = '(?<prefix>.*?)(?<numbers>([-
]*(\d+[\,]*)+[\.]{0,1}\d*[eEdD]{0,1}[-+]*\d*[i]{0,1})|([-
]*(\d+[\,]*)*[\.]{1,1}\d+[eEdD]{0,1}[-+]*\d*[i]{0,1}))(?<suffix>.*?);
        try
            result = regexp(rawData(row), regexstr, 'names');
            numbers = result.numbers;

            % Detected commas in non-thousand locations.
            invalidThousandsSeparator = false;
            if numbers.contains(',')
                thousandsRegExp = '^[-/+]*\d+(\,|\d{3})*\.{0,1}\d*$';
                if isempty(regexp(numbers, thousandsRegExp, 'once'))
                    numbers = NaN;
                    invalidThousandsSeparator = true;
                end
            end
            % Convert numeric text to numbers.
            if ~invalidThousandsSeparator
                numbers = textscan(char(strrep(numbers, ',', '')), '%f');
                numericData(row, col) = numbers{1};
                raw{row, col} = numbers{1};
            end
        catch
            raw{row, col} = rawData{row};
        end
    end
end

% Replace non-numeric cells with NaN
R = cellfun(@(x) ~isnumeric(x) && ~islogical(x),raw); % Find non-numeric cells
raw(R) = {NaN}; % Replace non-numeric cells

% Create output variable
coord = cell2mat(raw);

lat=coord(:,3)./100;          % LATITUDE (deg) WGS84
lon=coord(:,5)./100;          % LONGITUDE (deg) WGS84
elev=coord(:,10);            % ELEVATION (m)

% CONVERT LAT, LON (deg) in N, E (m) WGS84 UTM32N
[N,E,Zone]=wgs84_degminTOutmwgs84(lat,lon);

distance(1)=0;

```

```

for i=2:length(N)
    distance(i) = sqrt((E(i)-E(i-1)).^2 + (N(i)-N(i-1)).^2); % COMPUTE THE GPR
TRACE DISTANCES
end

end

%% Import profile coordinates .DST

filename2=[dati.filename '.DST'];

if isfile(filename2)==1
gpsraw=importdata(filename2);

E=gpsraw(:,3);
N=gpsraw(:,4);
elev=gpsraw(:,end);          % ELEVATION (m)

distance(1)=0;

for i=2:length(N)
    distance(i) = sqrt((E(i)-E(i-1)).^2 + (N(i)-N(i-1)).^2); % COMPUTE THE GPR
TRACE DISTANCES
end

end

dist=cumsum(distance);

%%%%%%%%%%%%%%%%%%%%%%%%%%%%%%%%%%%%%%%%%%%%%%%%%%%%%%%%%%%%%%%%%%%%%%%%
% EM wave velocity in the investigated medium
%v=input('EM WAVE VELOCITY (m/ns) = ');
v=0.17; %m/ns
v=v./10^-9; % converted into (m/s)

%%%%%%%%%%%%%%%%%%%%%%%%%%%%%%%%%%%%%%%%%%%%%%%%%%%%%%%%%%%%%%%%%%%%%%%%
T=dati.sweep_time_tot;          % TOTAL LENGTH OF RECORDING (s)
dt=T/(nusa-1);                 % SAMPLING RATE - dt
i=1:nusa;
j=1:nutr;
t=dt*i;
x=dx*j;
z=0.5*v*t; %%%%%%%%%% DEPTH CONVERSION (v*twt/2)
a=(j)*2*pi/(nutr-1);
a=[0 a];
rdrori=dati.MAPPA;

%% %% UNDERSAMPLE THE RAW DATA (they might be too big for your laptop, no
% other reasons)
skip=1; % if skip=1 no undersampling; if skip>1 select the step for keeping the
traces %%%%%%%%%% AUMENTARE NEL CASO
DIVENTASSE LENTO E PESANTE
rdrori=dati.MAPPA(:,1:skip:end);
nutr=length(rdrori(1,:));
j=1:nutr;
disp('File has been correctly read... processing starts... ')
dati.filename

%% 1) MOVE START TIME (remove the delay of the system before the main
%%%%%%%% bang)

```

```

figure (10)
imagesc(rdrori); % RAW RADARGRAM
title('Raw data')
xlabel('n° of traces')
ylabel('n° of samples')
grid
S=size(rdrori);
m=mean(reshape(rdrori,S(1,1)*S(1,2),1));
sd=std(reshape(rdrori,S(1)*S(2),1));
colormap(cmap);
caxis([m-sd m+sd])
disp ('Select delay to be removed... ');
[spa, tim]=ginput(1); %%%%%%%%%%% Manual input of the delay time
%%%%%%%%%%
tim=round(tim);
nusa=nusa-tim;
i=1:nusa;
t=dt*i;
rdrnod=rdrori(tim:(nusa+tim-1),:); % UNDELAYED RADARGRAM
figure (20)
imagesc(rdrnod)
title('1 - Moved start time')
xlabel('n° of traces')
ylabel('n° of samples')
grid
S=size(rdrnod);
%%%%%%%% Define a proper colorscale limit for the displayed radargram
m=mean(reshape(rdrnod,S(1,1)*S(1,2),1)); %average reflection amplitude
sd=std(reshape(rdrnod,S(1)*S(2),1)); % reflection amplitude standard deviation
colormap(cmap);
caxis([m-sd m+sd]) % colorscale limits
grid
%% 2) TRACE AVERAGE REMOVAL = BACKGROUND REMOVAL
%subav=input('Background removal? (0=NO ; 1=YES) ');
subav=1;
if subav==1
    meanoftr= repmat(mean(rdrnod,2),1,nutr);
    radr=rdrnod-meanoftr;
    rdr=radr;% YES - background removal
    figure (25)
    imagesc(rdr)
    title('2 - Background removed')
    xlabel('n° of traces')
    ylabel('n° of samples')
    grid
S=size(rdr);
m=mean(reshape(rdr,S(1,1)*S(1,2),1));
sd=std(reshape(rdr,S(1)*S(2),1));
colormap(cmap);
caxis([m-sd m+sd])

else
    rdr=rdrnod; % NO - background removal
end
%% 3) Cut traces start/end of the profile - antenna not moving
taglio=input(['Cut stationary traces at the radargram edges? (0=NO ; 1=YES) ']);
if taglio==1
    display('Select the traces that you want to preserve (start - end points)')
    [loc, t1]=ginput(1);
    [hic, t2]=ginput(1);

```

```

loc=floor(loc);
hic=floor(hic);
rdr=rdr(:,loc:hic); % cut
nutr=hic-loc+1;
j=1:nutr;
a=(j)*2*pi/(nutr-1);
a=[0 a];
else
rdr=rdr; % no cut
end
figure(30)
imagesc(rdr) %(cut/no cut)
xlabel('n° of traces')
ylabel('n° of samples')
title('3 - Stationary traces (@edges) removed')

S=size(rdr);
m=mean(reshape(rdr,S(1,1)*S(1,2),1));
sd=std(reshape(rdr,S(1)*S(2),1));
colormap(cmap);
caxis([m-sd m+sd])
%% 4) Spectral analysis on the GPR traces
f0=1/T;
indfr=(0:floor(nusa/2)); % frequency indexes
fr=f0*indfr;
asprdr=abs(fft(rdr))/nusa; %%%%%%%%%%% Amplitude spectrum (fft)
asprdr1=2*asprdr((1:length(fr)),:); %% true amplitude

figure(40)
hold on
plot(fr,asprdr1)
xlabel('Frequency [Hz]')
ylabel('Amplitude (-)')
box on
title('Trace Amplitude Spectra')
%% 5) BAND-PASS FILTERING
%fsn=input('Band-pass filtering ? 0=NO ; 1=YES ');
fsn=1;
if fsn==1

    %[ffilt]=ginput(2);
    %freq1=ffilt(1,1);
    %freq2=ffilt(2,1);
    freq1=0.4E6;
    freq2=1.3E6;

    disp('Filtering the data... please wait... ')

    [FF, Wn] = buttord(([freq1 freq2])*2*(dt),([0.5*freq1
1.25*freq2])*2*(dt),5,20);
    [B,A] = butter(FF,Wn);
    rdrf = filtfilt(B,A,rdr);

elseif fsn==0
rdrf=rdr; % NO FILT (0)
end

figure (50)
imagesc(rdrf);
title('4 - Band-pass filtered')

```

```

xlabel('n° of traces')
ylabel('n° of samples')
S=size(rdrf);
m=mean(reshape(rdrf,S(1,1)*S(1,2),1));
sd=std(reshape(rdrf,S(1)*S(2),1));
colormap(cmap);
caxis([m-sd m+sd])

%% 6) DIVERGENCE COMPENSATION – recover geometrical spreading
%disp ('Select starting point to recover geometrical spreading... ')
%[spa2, tim2]=ginput(1);
%tim2=round(tim2);
tim2=1;
%ampl=input('Divergence recovery: NO=0; LIN=1; QUAD=2; CUB=3 ');
ampl=1;
dist1=t(1:tim2)*v;
dist2=t(tim2+1:nusa)*v;
for ii=1:nutr
    rdrg(1:tim2,ii)=rdrf(1:tim2,ii);
    rdrg(tim2+1:nusa,ii)=rdrf(tim2+1:nusa,ii).*((1+dist2).^ampl); % divergence
recovery
end
AMP=num2str(ampl);

figure (80)
imagesc(rdrg);
titf5=['5 – Divergence recovered with exponent=' AMP];
xlabel('n° of traces')
ylabel('n° of samples')
grid
title(titf5)
S=size(rdrg);
m=mean(reshape(rdrg,S(1,1)*S(1,2),1));
sd=std(reshape(rdrg,S(1)*S(2),1));
colormap(cmap);
caxis([m-sd m+sd])

%% 9) Remove stationary traces within the radargram
cuttraces=input('Stationary traces within the radargram: NO=0; YES=1 ');
if cuttraces==1
    display('Select the traces that you want to delete')
    figure(90)
    imagesc(rdrg);
    title('select stationary window (1)')
    xlabel('n° of traces')
    ylabel('n° of samples')
    grid
    S=size(rdrg);
    m=mean(reshape(rdrg,S(1,1)*S(1,2),1));
    sd=std(reshape(rdrg,S(1)*S(2),1));
    colormap(cmap);
    caxis([m-sd m+sd])
    [loc1, t1]=ginput(1);
    [loc2, t2]=ginput(1);
    rdrg(:,floor(loc1):floor(loc2))=[]; %remove traces
else
    rdrg=rdrg; %no traces removed
end

jj=length(rdrg(1,:));

```

```

cuttraces=input('Stationary traces within the radargram: NO=0; YES=1 ');
if cuttraces==1
    display('Select the traces that you want to delete')
figure(95)
imagesc(rdrng);
title('select stationary window (2)')
xlabel('n° of traces')
ylabel('n° of samples')
grid
S=size(rdrng);
m=mean(reshape(rdrng,S(1,1)*S(1,2),1));
sd=std(reshape(rdrng,S(1)*S(2),1));
colormap(cmap);
caxis([m-sd m+sd])
[loc1, t1]=ginput(1);
[loc2, t2]=ginput(1);
rdrng(:,floor(loc1):floor(loc2))=[]; % remove traces
else
    rdrng=rdrng; % no traces removed
end

jj=length(rdrng(1,:));

cuttraces=input('Stationary traces within the radargram: NO=0; YES=1 ');
if cuttraces==1
    display('Select the traces that you want to delete')
figure(95)
imagesc(rdrng);
title('select stationary window (3)')
xlabel('n° of traces')
ylabel('n° of samples')
grid
S=size(rdrng);
m=mean(reshape(rdrng,S(1,1)*S(1,2),1));
sd=std(reshape(rdrng,S(1)*S(2),1));
colormap(cmap);
caxis([m-sd m+sd])
[loc1, t1]=ginput(1);
[loc2, t2]=ginput(1);
rdrng(:,floor(loc1):floor(loc2))=[]; % remove traces
else
    rdrng=rdrng; % no traces removed
end

jj=length(rdrng(1,:));

cuttraces=input('Stationary traces within the radargram: NO=0; YES=1 ');
if cuttraces==1
    display('Select the traces that you want to delete')
figure(95)
imagesc(rdrng);
title('select stationary window (4)')
xlabel('n° of traces')
ylabel('n° of samples')
grid
S=size(rdrng);
m=mean(reshape(rdrng,S(1,1)*S(1,2),1));
sd=std(reshape(rdrng,S(1)*S(2),1));
colormap(cmap);

```

```

caxis([m-sd m+sd])
    [loc1, t1]=ginput(1);
    [loc2, t2]=ginput(1);
    rdrv(:,floor(loc1):floor(loc2))=[]; % remove traces
else
    rdrv=rdrv; % no traces removed
end
cuttraces=input('Stationary traces within the radargram: NO=0; YES=1 ');
if cuttraces==1
    display('Select the traces that you want to delete')
figure(95)
imagesc(rdrv);
title('select stationary window (5)')
xlabel('n° of traces')
ylabel('n° of samples')
grid
S=size(rdrv);
m=mean(reshape(rdrv,S(1,1)*S(1,2),1));
sd=std(reshape(rdrv,S(1)*S(2),1));
colormap(cmap);
caxis([m-sd m+sd])
    [loc1, t1]=ginput(1);
    [loc2, t2]=ginput(1);
    rdrv(:,floor(loc1):floor(loc2))=[]; % remove traces
else
    rdrv=rdrv; % no traces removed
end
cuttraces=input('Stationary traces within the radargram: NO=0; YES=1 ');
if cuttraces==1
    display('Select the traces that you want to delete')
figure(95)
imagesc(rdrv);
title('select stationary window (6)')
xlabel('n° of traces')
ylabel('n° of samples')
grid
S=size(rdrv);
m=mean(reshape(rdrv,S(1,1)*S(1,2),1));
sd=std(reshape(rdrv,S(1)*S(2),1));
colormap(cmap);
caxis([m-sd m+sd])
    [loc1, t1]=ginput(1);
    [loc2, t2]=ginput(1);
    rdrv(:,floor(loc1):floor(loc2))=[]; % remove traces
else
    rdrv=rdrv; % no traces removed
end
cuttraces=input('Stationary traces within the radargram: NO=0; YES=1 ');
if cuttraces==1
    display('Select the traces that you want to delete')
figure(95)
imagesc(rdrv);
title('select stationary window (7)')
xlabel('n° of traces')
ylabel('n° of samples')
grid
S=size(rdrv);
m=mean(reshape(rdrv,S(1,1)*S(1,2),1));
sd=std(reshape(rdrv,S(1)*S(2),1));
colormap(cmap);

```

```

caxis([m-sd m+sd])
    [loc1, t1]=ginput(1);
    [loc2, t2]=ginput(1);
    rdrng(:,floor(loc1):floor(loc2))=[]; % remove traces
else
    rdrng=rdrng; % no traces removed
end

%10) Time cut
cuttime=input('Time cut? NO=0; YES=1 ');
if cuttime==1
    display('Select the time cut position')
figure(95)
imagesc(rdrng);
title('select time cut location (8)')
xlabel('n° of traces')
ylabel('n° of samples')
grid
S=size(rdrng);
m=mean(reshape(rdrng,S(1,1)*S(1,2),1));
sd=std(reshape(rdrng,S(1)*S(2),1));
colormap(cmap);
caxis([m-sd m+sd])
    [loc1, tcut]=ginput(1);
    rdrng(round(tcut):end,:)=[]; % remove traces
    t(round(tcut):end)=[];
else
    rdrng=rdrng; % no traces removed
end

jj=length(rdrng(1,:));
display('End of processing... preparing and saving the final results!')

%% DISPLAY THE PROCESSED RADARGRAM
figure (100)
z=0.5*v*t; %final depth
xnew=linspace(0,dist(end),jj);
imagesc(xnew,z,rdrng);
hold on
title('Processed Radargram');
xlabel('Distance [m]')
ylabel('Depth [m]')
set(gca,'XAxisLocation','top')
%colormap('parula');
%caxis([-1 1])
grid
S=size(rdrng);
m=mean(reshape(rdrng,S(1,1)*S(1,2),1));
sd=std(reshape(rdrng,S(1)*S(2),1));
colormap(cmap);
caxis([m-sd m+sd])
saveas(gcf,[savename '_proc.fig'])
saveas(gcf,[savename '_proc.jpg'])

%%%%%%%%%% Attribute analysis (instantaneous amplitude)
rdrgh=abs(hilbert(rdrng));
figure (110)
imagesc(xnew,z,rdrgh);

```

```

title('Istantaneous Amplitude');
xlabel('Distance [m]')
ylabel('Depth [m]')
set(gca,'XAxisLocation','top')
colormap(flipud(hot));
caxis([0 1])
grid
saveas(gcf,[savename '_istA.fig'])
saveas(gcf,[savename '_istA.jpg'])

% save radargram coordinates
[dist, index] = unique(dist);
E1=interp1(dist,E(index),xnew);
N1=interp1(dist,N(index),xnew);
Z1=interp1(dist,elev(index),xnew);

save(savename, 'xnew','z','rdrg','rdrgH','E1','N1','Z1')
cd ..

```

## 8.3 APPENDIX C

In the following appendix the MATLAB code used for the glaciers bedrock picking is shown:

```

[filename, pathname]=uigetfile('*.mat'); % processed file selection
cd(pathname)

load(filename)
savename=[filename(1:end-4) '_bottom']; %%%%% the results will be saved with
this name

%% Select the colorscale for radargram visualization
%% suggested default colorscales: 'bone','jet','gray'
cmap='gray';
%% or ad-hoc build colorscale
load('GPRcmap.mat')

%% Plot the processed radargram on which you want to perform the picking of GPR
features
figure (100)
imagesc(xnew,z,rdrg); %or rdrgH
hold on
title('Processed Radargram');
xlabel('Distance [m]')
ylabel('Depth [m]')
set(gca,'XAxisLocation','top')
grid
S=size(rdrg);
m=mean(reshape(rdrg,S(1,1)*S(1,2),1));
sd=std(reshape(rdrg,S(1)*S(2),1));
colormap(cmap);
caxis([m-sd m+sd])

% manual picking
pick=ginput;

```

```

hold on
plot(pick(:,1),pick(:,2),'*g','MarkerSize',10) % plot the manually picked points

xp=pick(:,1);
depthp=pick(:,2);

% coordinates of the picked points
Ep=interp1(xnew,E1,xp);
Np=interp1(xnew,N1,xp);
Zp=interp1(xnew,Z1,xp);

% save the figure with the picked points
saveas(gcf,[savename '_picked.fig'])
saveas(gcf,[savename '_picked.jpg'])

% plot the picked points in 3D
figure (200)
plot3(E1,N1,Z1,'.k')
hold on
plot3(Ep,Np,Zp-depthp,'*g','MarkerSize',10)
xlabel('X WGS84 UTM32N [m]')
ylabel('Y WGS84 UTM32N [m]')
zlabel('Elevation [m]')
box on
saveas(gcf,[savename '_picked3d.fig'])
saveas(gcf,[savename '_picked3d.jpg'])

% save the picked points in a variable (they can be uploaded later to
% create a map of all the picked features or to interpolate the results of
% all the lines
save(savename, 'xp', 'depthp', 'Ep', 'Np', 'Zp')

```

## 8.4 APPENDIX D

The appendix includes the MATLAB code used for the implementation of the GLATE model, applied to the glaciers of Val Ferret.

```

function glate_wrapper(tag)
pp = '/Users/giacomodalmasso/Desktop/SEMESTREII.2/TESI/Glate/glate-master'; %
Add your location
if (exist('glate.m','file') ~= 2)
    addpath([pp '/matlab']);
end

% hardwired data file names
%tag = 'plaine';
tag='valferret';
DEMfile = [pp '/Data/' tag '_dem.tif']; % q
if exist(DEMfile, 'file') ~= 2
    error('Il file DEM non esiste nel percorso specificato: %s', DEMfile);
end
GlacierMaskFile = [pp '/Data/' tag '_mask.tif']; % Glacier mask (<=0: outside,
1: inside)

GPRData = [pp '/Data/' tag '_GPR_data.mat']; % variables xgpr ygpr hgpr pno
(optional Hgprtop Hgprbot)

```

```

% Add path to topotoolbox and fix ambiguity with the resample function
topo_toolbox_path =
'/Users/giacomodalmasso/Desktop/SEMESTREII.2/TESI/Glate/topotoolbox-master'; %
add your location

if (exist('GRIDObj.m','file') ~= 2)
    addpath(genpath(topo_toolbox_path));
end
pwd = (pwd);
cd([topo_toolbox_path '@GRIDObj']);
my_resample = @resample;
cd(pwd);

% Constants and parameters
CST.stmin = 5.0/180*pi; % minimum slope angle allowed [radians]
CST.stmax = 60.0/180*pi; % maximum slope angle allowed [radians]
CST.smooth_SA = 40; % smoothing of surface geometry factor
[cell units]
CST.gacc = 0.0025; % q gradient in accumulation zone [m w.e.
m-1 yr-1]
CST.gabl = 0.0025*9/5; % q gradient in ablation zone [m w.e. m-1
yr-1]
CST.n = 3; % Exponent of Glen's law [-]
CST.A = 2.4e-24; % creep factor [s-1 Pa-3]
CST.rho = 910; % ice density [kg m-3]
CST.g = 9.81; % earth gravity acceleration [m s-2]
CST.gsi = 0.5; % fraction of creep relative to basal
sliding [fraction]
CST.nbzone = 20; % number of zones of constant AMB rates
within a flowshed [-]
CST.l_factor = 2; % exponential factor for longitudinal
averaging [-]
CST.apriori_smoothing = 0; % smoothing of unconstrained model [cell
units]
CST.target_acc = 0.05; % GPR accuracy, used if no min/max GPR
thickness is given [%]
CST.reg_acc = 0.95; % required minimum GPR points modeled
within top/bottom thickness [fraction]
CST.glacfac_ini = 0.45; % Initial weight for glaciological
constraints [-]
CST.glacfac_min = 0.75; % Minimum value for (final) glaciological
constraints [-]
CST.glacfac_max = 3.0; % Maximum value for (final) glaciological
constraints [-]
CST.glac_adjust = 1.1; % Adjustment of glaciological constraints
factor [fraction]
CST.smoothfac_ini = 12.0; % Initial smoothing factor for inversion
[-]
CST.smoothfac_min = 5.0; % Minimum smoothing factor [-]
CST.smoothfac_min2 = 2.0; % Minimum smoothing factor in case minimum
glacfac_min can not be reached [-]
CST.smooth_adjust = 1.1; % Adjustment of smoothing factor
[fraction]
CST.boundfac_ini = 1; % initial weight for boundary constraints
[-]
CST.nb = 3; % width of boundary region, to which
boundary gradients get applied [cell units]
CST.grdfac = 5; % maximum gradient alteration (1/grdfac <
grad(Glac)/grad(B) < grdfac) [-]

```

```

CST.fdebr          = -1;          % Reduction of AMB in debris-covered
ablation areas [fraction], set fdebr = -1 to ignore debris cover

% Digital elevation model
% if (strcmp(tag,'dom')== 1)
%     DEMfile = [pp 'data/' tag '_dem.tif'];
% else
%     DEMfile = [pp 'data/' tag '_dem.asc'];
% end

% Raster file with debris cover:
if CST.fdebr ~= -1
    DEBfile = [pp 'data\' tag '_debris.asc'];
end

% Read original DEM, glacier mask, and debris mask, and prepare some grid
parameters
DEM = GRIDobj(DEMfile);
DEM.Z = double(DEM.Z); % Converti il DEM a double

DEMX = DEM.refmat(3,1):DEM.refmat(2,1):DEM.refmat(3,1) +
DEM.size(2)*DEM.refmat(2,1);
DEMY = DEM.refmat(3,2):DEM.refmat(1,2):DEM.refmat(3,2) +
DEM.size(1)*DEM.refmat(1,2);
DEMX = DEMX(1:DEM.size(2)) + 0.5*DEM.refmat(2,1);
DEMY = DEMY(1:DEM.size(1)) + 0.5*DEM.refmat(1,2);

[yy,xx] = ndgrid(DEMY,DEMX);
TMP = GRIDobj(GlacierMaskFile);

if CST.fdebr ~= -1
    DEB = GRIDobj(DEBfile);
    DEB.Z = double(DEB.Z);
else
    DEB = [];
end

% Read GPR data
load(GPRData,'xgpr','ygpr','Hgpr');
ngpr = length(xgpr); % no of GPR data points

% Determine gpridx (nearest grid point of DEM of each GPR point)
xidx = zeros(ngpr,1);
xdist = zeros(ngpr,1);
yidx = zeros(ngpr,1);
ydist = zeros(ngpr,1);
for a = 1:ngpr, [xdist(a),xidx(a)] = min(abs(DEMX-xgpr(a))); end
for a = 1:ngpr, [ydist(a),yidx(a)] = min(abs(DEMY-ygpr(a))); end
gpridx = sub2ind(size(DEM.Z),yidx,xidx);

% Exclude GPR points outside of glacier mask
SRF.iig = find(~isnan(TMP.Z)); % areas on glacier
SRF.iing = find(isnan(TMP.Z)); % areas outside of glacier
ii = find(ismember(gpridx,SRF.iig) == 0);
gpridx = gpridx(ii);
xgpr = xgpr(ii);
ygpr = ygpr(ii);
Hgpr = Hgpr(ii);

```

```

% if available, minimum/maximum ice thickness at GPR points according to
% GPR uncertainty. Here we use a 5% GPR uncertainty:
if ~exist('Hgprtop','var'), Hgprtop = Hgpr*(1-CST.target_acc); end
if ~exist('Hgprbot','var'), Hgprbot = Hgpr*(1+CST.target_acc); end

% perform unconstrained (no GPR data) glate inversion and determine gfac
[~,Hgla,~,gfac,~,~,~,~] =
glate_inv(DEM,TMP,CST,DEB,xgpr,ygpr,Hgpr,Hgprtop,Hgprbot,-1,[],[]);

% Perform GlaTE inversion using gfac and the glaciological constraints
[Hall,~,Hgpronly,~,smooth_fac,glac_fac,bound_fac,mi] =
glate_inv(DEM,TMP,CST,DEB,xgpr,ygpr,Hgpr,Hgprtop,Hgprbot,gfac,Hgla,[]);

%DALMASSO MODIFICHE PER ESPORTARE TIF FILE DA METTERE SU QGIS
%DEMx = DEM.refmat(3,1):DEM.refmat(2,1):DEM.refmat(3,1) +
DEM.size(2)*DEM.refmat(2,1);
%DEMy = DEM.refmat(3,2):DEM.refmat(1,2):DEM.refmat(3,2) +
DEM.size(1)*DEM.refmat(1,2);
%DEMx = DEMx(1:DEM.size(2)) + 0.5*DEM.refmat(2,1);
%DEMy = DEMy(1:DEM.size(1)) + 0.5*DEM.refmat(1,2);

% Specifica il codice EPSG per il sistema di coordinate
%epsgCode = 32632; % Cambia con il codice EPSG del tuo sistema di riferimento

% Crea il riferimento spaziale per le celle
%R = maprefcells([min(DEMy), max(DEMy)], [min(DEMx), max(DEMx)], size(Hall));

% Esporta il GeoTIFF con il codice EPSG
%geotiffwrite('Hall_map.tif', Hall, R, 'CoordRefSysCode', epsgCode);

%disp('File GeoTIFF salvato con successo!');

% Plotting parameters
cax1 = [0 70];
cax2 = [-30 30];
clf;

% Determine glacier outline
GRAD = TMP;
GRAD.Z(isnan(GRAD.Z)) = 0;
GRAD = gradient8(GRAD);
dbx =xx(GRAD.Z > 0);
dby =yy(GRAD.Z > 0);

% Plot unconstrained model
plot_results(DEM,Hgla*gfac,dbx,dby,[],[],[],flipud(viridis(100)),2,2,1,'
h^{glac}',cax1);

% Plot GPR only model
F = scatteredInterpolant(xgpr,ygpr,Hgpr,'natural','none');
Hgpronly2 = F(xx,yy);
Hgpronly2(isnan(TMP.Z)) = NaN;
Hgpronly2(Hgpronly2 == 0) = NaN;
plot_results(DEM,Hgpronly2,dbx,dby,[],[],[],flipud(viridis(100)),2,2,2,'
h^{GPR}',cax1);
hold on;
plot(xgpr,ygpr,'k.','markersize',6);

```

```

% Plot GlaTE model and its difference to unconstrained model
plot_results(DEM,Hall,dbx,dby,[],[],[],flipud(viridis(100)),2,2,3,'
h^{est}',cax1);
plot_results(DEM,Hall-
gfac*Hgl,dbx,dby,[],[],[],flipud(brewermap(100,'Pu0r')),2,2,4,'h^{est} -
h^{glac}',cax2);

function plot_results(DEM,inpm,dbx,dby,xgpr,ygpr,Hgpr,cm,sp1,sp2,sp3,tit,cax)

aa = DEM;
aa.Z = inpm;
marksize = 1;

spi = subplot(sp1,sp2,sp3);
imagesc(aa,'AlphaData',~isnan(aa.Z))
hold on
plot(dbx,dby,'k.','MarkerSize',marksize)
h = title(tit);
set(h,'FontSize',9);
colormap(spi,cm)
h = colorbar;
hh = get(h,'title');
set(hh,'string','[m]');
caxis(cax)
if (isempty(xgpr) == 0)
    s = scatter(xgpr(~isnan(Hgpr)),ygpr(~isnan(Hgpr)),'k. ');
    s.MarkerFaceAlpha = 0;
    s.MarkerEdgeAlpha = 0.25; %0.008;
end
marg_x = 0.1 * (max(dbx) - min(dbx));
marg_y = 0.1 * (max(dby) - min(dby));
axis([min(dbx)-marg_x max(dbx)+marg_x min(dby)-marg_y max(dby) + marg_y]);
set(gca,'dataaspectratio',[1 1 1]);
h = xlabel('E-W coordinate [m]');
p = get(h,'Position');
if (sp1 == 1), p(2) = p(2) - 100; end
if (sp1 >= 2), p(2) = p(2) - 200; end
set(h,'Position',p);
ylabel('N-S coordinate [m]');

```

## 9 LIST OF FIGURES AND TABLES

<i>Fig. 1 - Cumulative glacier mass changes in Europe from 1967-2018 for glaciers with long-term ...</i>	7
<i>Fig. 2 - Comparison of Lys Glacier in 1920 and 2019. Source: Umberto Monterin (credit: Famiglia Monterin), Fabiano Ventura (Associazione Macromicro) .....</i>	7
<i>Fig. 3 - Mass balance of Rutor glacier from 2005 to 2018. Source: Arpa VdA (RSA 2018) .....</i>	8
<i>Fig. 4 - Crevasses in Washington Glacier, Alaska. Source: L. Petersen, Crevasses, 2021.....</i>	9
<i>Fig. 5 - Crevasse formation on valley glacier. Source: B. Davies, Structural glaciology, 2023 .....</i>	10
<i>Fig. 6 - Controls on crevasse depth in valley glaciers. Source: B. Davies, Structural glaciology, 2023.....</i>	11
<i>Fig. 7 - The equilibrium line separates the zone of accumulation from the zone of ablation. Source: S. Bate, A reconstruction of ELA of little ice glacier in Linnédalen, 2018 .....</i>	12
<i>Fig. 8 - Geographical location of the study area.....</i>	16

Fig. 9 - Overview of Val Ferret glaciers (the processed ones are in red), Source: 4-valle-daosta.pdf	18
Fig. 10 – Prè de Bar glacier in 1897 (Druetti photo)	19
Fig. 11 - Prè de Bar glacier in 1993 (A. Cerutti photo)	19
Fig. 12 – Prè de Bar glacier in 2012 (L. Mercalli photo)	19
Fig. 13 - Planpincieux glacier and Whymper serac, Source: fondazionemontagnasicura.org	21
Fig. 14 - Skyway station, between Toula and Col del Gigante glaciers. Source: <a href="https://www.montebianco.com/it/funivie/punta-helbronner-the-sky">https://www.montebianco.com/it/funivie/punta-helbronner-the-sky</a>	22
Fig. 15 - Ground Penetrating Radar (GPR) prospecting for the determination of the thickness of the Ciardoney glacier, by Imageo Srl (f. SMI)	29
Fig. 16 – Radagram generation. Source: <a href="http://www.gpradar.it/ind_georadar.html">http://www.gpradar.it/ind_georadar.html</a>	30
Fig. 17 – Raw radagram generated, before the modification and interpretation using Matlab	31
Fig. 18 – GPR processing Grapillon 2016 line 1, moved start time	33
Fig. 19 – GPR processing Grapillon 2016 line 1, background removed	33
Fig. 20 – Trace Amplitude Spectra, Grapillon 2016 line 1	34
Fig. 21 – GPR processing Grapillon 2016 line 1, geometrical recovery	35
Fig. 22 - GPR processing Grapillon 2016 line 1, stationary traces removed	35
Fig. 23 - GPR processing Grapillon 2016 line 1, time cut	36
Fig. 24 – Original GPR lines available; data of Grapillon 2012 are red, while data of Grapillon 2016 are blue. Source: Google Earth, 2025	37
Fig. 25 - Grapillon 2012 line 4 bottom picked	37
Fig. 26 - Grapillon 2012 line 8 bottom picked	38
Fig. 27 – Grapillon 2016 line 4 bottom picked	38
Fig. 28 - Grapillon 2012 and 2016 ice depth	39
Fig. 29 - Original GPR lines available of Prè de Bar 2010. Source: Google Earth, 2025	40
Fig. 30 - Prè de Bar 2010, signal disturbed from water infiltration	40
Fig. 31 - Glims 2008 ice depth, mismatch with our GPR data	41
Fig. 32 - Original GPR lines available; data of Planpincieux 2019 are red, while data of Planpincieux 2021 are blue. Source: Google Earth, 2025	41
Fig. 33 - Planpincieux 2021 line 4	42
Fig. 34 - Planpincieux 2021 ice depth	42
Fig. 35 - Original GPR lines available of Col del Gigante 2010. Source: Google Earth, 2025	43
Fig. 36 - Col del Gigante line 4; stratifications and repetitions are visible	44
Fig. 37 - Col del Gigante 2010 ice depth	44
Fig. 38 - Riprojection of the bedrock data picked for Whymper Serac	45
Fig. 39 - Thickness reconstruction of Whymper Serac after the riprojection of the data	45
Fig. 40 - Original GPR lines available of Whymper serac 2021. Source: Google Earth, 2025	46
Fig. 41 - Whymper 2021 ice depth	46
Fig. 42 - DTM 2005/2008 aggregated for Val Ferret	50
Fig. 43 - Ice thickness results, focus on Prè de Bar and Grapillon glaciers. Top left panel: thickness obtained using only the theoretical glaciological model. Top right: GPR constraint. Bottom left: thickness obtained from the model constrained by the GPR data. Bottom right: difference between the model constrained by radar data and the thickness of the theoretical model Results obtained for a smoothness factor equal to 40 and resolution equal to 15	54
Fig. 44 – Focus on Grapillon glacier, with near-zero thickness rounded in red. Source: Google Earth, 2025	55
Fig. 45 - Ice thickness results, focus on Planpincieux glacier. Top left panel: thickness obtained using only the theoretical glaciological model. Top right: GPR constraint. Bottom left: thickness obtained from the model constrained by the GPR data. Bottom right: difference between the model	

<i>constrained by radar data and the thickness of the theoretical model Results obtained for a smoothness factor equal to 40 and resolution equal to 15.....</i>	<i>56</i>
<i>Fig. 46 - Focus on the bottom part of Planpincieux glacier: the crevasses are evident. Source: <a href="https://www.theguardian.com">https://www.theguardian.com</a>.....</i>	<i>58</i>
<i>Fig. 47 - Ice thickness results, focus on Col del Gigante and Toula glaciers. Top left panel: thickness obtained using only the theoretical glaciological model. Top right: GPR constraint. Bottom left: thickness obtained from the model constrained by the GPR data. Bottom right: difference between the model constrained by radar data and the thickness of the theoretical model Results obtained for a smoothness factor equal to 40 and resolution equal to 15. ....</i>	<i>59</i>
<i>Fig. 48 - Prè de Bar and Grapillon glaciers, smoothing factor 20. Left panel: constrained model. Right panel: difference between constrained and theoretical model.....</i>	<i>61</i>
<i>Fig. 49 - Prè de Bar and Grapillon glaciers, smoothing factor 60. Left panel: constrained model. Right panel: difference between constrained and theoretical model.....</i>	<i>61</i>
<i>Fig. 50 - Prè de Bar and Grapillon glaciers, resolution 20 m. Left panel: constrained model. Right panel: difference between constrained and theoretical model.....</i>	<i>62</i>
<i>Fig. 51 - Prè de Bar and Grapillon glaciers, resolution 15 m. Left panel: constrained model. Right panel: difference between constrained and theoretical model.....</i>	<i>62</i>
<i>Fig. 52 - Prè de Bar and Grapillon glaciers, resolution 10 m. Left panel: constrained model. Right panel: difference between constrained and theoretical model.....</i>	<i>62</i>
<i>Fig. 53 – Example of poor quality radargram of Prè de Bar .....</i>	<i>64</i>
<i>Fig. 54 – Focus su Prè de Bar-Grapillon: on the left the results using only poor quality data from Prè de Bar, on the right the results using the correct dataset.....</i>	<i>64</i>
<i>Fig. 55 – Focus on Planpincieux-Whymper: on the left the results using only poor quality data from Prè de Bar, on the right the results using the correct dataset.....</i>	<i>65</i>
<i>Fig. 56 – Ice thickness results, focus on Planpincieux glacier, using data from a little portion of the Whymper serac. Top left panel: thickness obtained using only the theoretical glaciological model. Top right: GPR constraint. Bottom left: thickness obtained from the model constrained by the GPR data. Bottom right: difference between the model constrained by radar data and the thickness of the theoretical model Results obtained for a .....</i>	<i>66</i>
<i>Fig. 57 - Ice thickness results, focus on Planpincieux glacier, using data different zones of the glacier. Top left panel: thickness obtained using only the theoretical glaciological model. Top right: GPR constraint. Bottom left: thickness obtained from the model constrained by the GPR data. Bottom right: difference between the model constrained by radar data and the thickness of the theoretical model Results obtained for a .....</i>	<i>67</i>
<i>Fig. 58 - Location of the three meteo stations, respect to Courmayeur.....</i>	<i>69</i>
<i>Fig. 59 - Temperature data acquired at Prè de Bar station (2002-2024).....</i>	<i>70</i>
<i>Fig. 60 - Dataset complete and filled.....</i>	<i>70</i>
<i>Fig. 61 – Amplitude Spectrum and Phase Spectrum of the recorded temperature data.....</i>	<i>71</i>
<i>Fig. 62 - Temperature data (blue) with periodic component (red) and daily average temperature (black) .....</i>	<i>72</i>
<i>Fig. 63 - Data residuals obtained through the removal of the periodic component (red) and daily average temperature (black).....</i>	<i>72</i>
<i>Fig. 64 - Regression lines highlighted .....</i>	<i>73</i>
<i>Fig. 65 - Temperature data acquired at Ferrachet station (2002-2024) .....</i>	<i>77</i>
<i>Fig. 66 - Temperature data acquired at Mont de la Saxe station (2002-2024).....</i>	<i>78</i>
<i>Fig. 67 – Ferrachet station dataset complete and filled.....</i>	<i>78</i>
<i>Fig. 68 - Mont de la Saxe station dataset complete and filled.....</i>	<i>79</i>
<i>Fig. 69 - Ferrachet station Amplitude Spectrum and Phase Spectrum of the recorded temperature data.....</i>	<i>79</i>

Fig. 70 - Mont de la Saxe Amplitude Spectrum and Phase Spectrum of the recorded temperature data.....	80
Fig. 71 - Ferrachet station temperature data (blue) with periodic component (red) and daily average temperature (black).....	80
Fig. 72 - Mont de la Saxe station temperature data (blue) with periodic component (red) and daily average temperature (black).....	81
Fig. 73 - Ferrachet station data residuals obtained through the removal of the periodic component (red) and daily average temperature (black), with the regression line highlighted.....	81
Fig. 74 - Mont de la Saxe station data residuals obtained through the removal of the periodic component (red) and daily average temperature (black), with the regression line highlighted.....	82
Table 1 - Density, relative permittivity and velocity values referring to some materials present in nature.....	28
Table 2 - Maximum thickness and Maximum differences for Prè de Bar-Grapillon Glacier.....	56
Table 3 - Maximum thickness and Maximum differences for Planplencieux glacier and Whymperserac.....	58
Table 4 - Maximum thickness and Maximum differences for Toulou glacier and Col del Gigante glacier.....	60
Table 5 - Detailed summary of the three separate sites.....	68
Table 6 - Temperature trend obtained for the three different meteorological stations, with the tolerance and pValue.....	73

## 10 BIBLIOGRAPHY

- [1] Intergovernmental Panel On Climate Change (Ippc), *Climate Change 2021 – The Physical Science Basis: Working Group I Contribution to the Sixth Assessment Report of the Intergovernmental Panel on Climate Change*, 1<sup>a</sup> ed. Cambridge University Press, 2023. doi: 10.1017/9781009157896.
- [2] L. Langhammer, M. Grab, A. Bauder, e H. Maurer, «Glacier thickness estimations of alpine glaciers using data and modeling constraints», *The Cryosphere*, vol. 13, fasc. 8, pp. 2189–2202, ago. 2019, doi: 10.5194/tc-13-2189-2019.
- [3] R. Hock *et al.*, «GlacierMIP – A model intercomparison of global-scale glacier mass-balance models and projections», *Journal of Glaciology*, vol. 65, pp. 1–15, mag. 2019, doi: 10.1017/jog.2019.22.
- [4] M. Zemp *et al.*, «Global glacier mass changes and their contributions to sea-level rise from 1961 to 2016», *Nature*, vol. 568, fasc. 7752, pp. 382–386, apr. 2019, doi: 10.1038/s41586-019-1071-0.
- [5] C. Huggel, A. Kääb, W. Haeberli, P. Teysseire, e F. Paul, «Remote sensing based assessment of hazards from glacier lake outbursts: a case study in the Swiss Alps», *Can. Geotech. J.*, vol. 39, fasc. 2, pp. 316–330, apr. 2002, doi: 10.1139/t01-099.
- [6] H. Jiskoot, «Dynamics of Glaciers», 2011, pp. 245–256. doi: 10.1007/978-90-481-2642-2\_127.
- [7] M. Hambrey e N. Glasser, «Glaciers», *Encyclopedia of Geology*, vol. 4, pp. 663–678, gen. 2005.
- [8] A. Racoviteanu, F. Paul, B. Raup, S. J. Khalsa, e R. Armstrong, «Challenges and recommendations in mapping of glacier parameters from space: results of the 2008 Global Land

- Ice Measurements from Space (GLIMS) workshop, Boulder, Colorado, USA», *Annals of Glaciology - ANN GLACIOL*, vol. 50, pp. 53–69, feb. 2010, doi: 10.3189/172756410790595804.
- [9] S. H. Mernild *et al.*, «Mass loss and imbalance of glaciers along the Andes Cordillera to the sub-Antarctic islands», *Global and Planetary Change*, vol. 133, pp. 109–119, ott. 2015, doi: 10.1016/j.gloplacha.2015.08.009.
- [10] «W. S. B. Paterson 1994. The physics of glaciers. 3rd edition. Oxford, etc., Pergamon, 480 pp. ISBN 0-08037945 1. Hardback. £70; 0-08037944 3, Flexieover. £25. | Journal of Glaciology | Cambridge Core». Consultato: 25 novembre 2024. [Online]. Disponibile su: <https://www.cambridge.org/core/journals/journal-of-glaciology/article/w-s-b-paterson-1994-the-physics-of-glaciers-3rd-edition-oxford-etc-pergamon-480-pp-isbn-008037945-1-hardback-70-008037944-3-flexieover-25/FFF343EF62E4E3452C5D5BFC6F545442>
- [11] C. Schoof, «Ice sheet grounding line dynamics: Steady states, stability, and hysteresis», *Journal of Geophysical Research: Earth Surface*, vol. 112, fasc. F3, 2007, doi: 10.1029/2006JF000664.
- [12] K. Hutter, *Theoretical Glaciology: Material Science of Ice and the Mechanics of Glaciers and Ice Sheets*. Springer, 1983.
- [13] K. Cuffey e W. Paterson, «The Physics of Glaciers Fourth Edition», 2010. Consultato: 25 novembre 2024. [Online]. Disponibile su: <https://www.semanticscholar.org/paper/The-Physics-of-Glaciers-Fourth-Edition-Cuffey-Paterson/3d7902b452d6c5f5ee7011f64b075217beb48d11>
- [14] M. Huss, D. Farinotti, A. Bauder, e M. Funk, «Modelling runoff from highly glacierized alpine drainage basins in a changing climate», *Hydrological Processes*, vol. 22, pp. 3888–3902, set. 2008, doi: 10.1002/hyp.7055.
- [15] «Energy balance of ice streams - University of Texas at Austin». Consultato: 25 novembre 2024. [Online]. Disponibile su: <https://search.lib.utexas.edu>
- [16] D. B. Bahr, M. F. Meier, e S. D. Peckham, «The physical basis of glacier volume-area scaling», *Journal of Geophysical Research: Solid Earth*, vol. 102, fasc. B9, pp. 20355–20362, 1997, doi: 10.1029/97JB01696.
- [17] M. Morlighem, E. Rignot, H. Seroussi, E. Larour, H. Ben Dhia, e D. Aubry, «A mass conservation approach for mapping glacier ice thickness: BALANCE THICKNESS», *Geophys. Res. Lett.*, vol. 38, fasc. 19, p. n/a-n/a, ott. 2011, doi: 10.1029/2011GL048659.
- [18] D. Farinotti *et al.*, «How accurate are estimates of glacier ice thickness? Results from ITMIX, the Ice Thickness Models Intercomparison eXperiment», *The Cryosphere*, vol. 11, fasc. 2, pp. 949–970, apr. 2017, doi: 10.5194/tc-11-949-2017.
- [19] J. Oerlemans, *Minimal glacier models*, Second print (with some revisions). Utrecht: Igitur, 2011.
- [20] «ARPA RSA 2018\_completo.pdf». Consultato: 22 novembre 2024. [Online]. Disponibile su: [https://www.arpa.vda.it/images/stories/ARPA/RSA\\_web/rsa2018/XIII\\_RSA\\_definitiva\\_pdf/ARPA%20RSA%202018\\_completo.pdf](https://www.arpa.vda.it/images/stories/ARPA/RSA_web/rsa2018/XIII_RSA_definitiva_pdf/ARPA%20RSA%202018_completo.pdf)
- [21] G. E. Flowers, «Modelling water flow under glaciers and ice sheets», *Proceedings of the Royal Society A: Mathematical, Physical and Engineering Sciences*, vol. 471, fasc. 2176, p. 20140907, apr. 2015, doi: 10.1098/rspa.2014.0907.
- [22] «Modeling Ice-Sheet Flow | Science». Consultato: 29 novembre 2024. [Online]. Disponibile su: <https://www.science.org/doi/10.1126/science.1220530>
- [23] «Understanding jökulhlaups: From tale to theory | Journal of Glaciology | Cambridge Core». Consultato: 29 novembre 2024. [Online]. Disponibile su: <https://www.cambridge.org/core/journals/journal-of-glaciology/article/understanding-jokulhlaups-from-tale-to-theory/21FD9F138CE4F1F74856701D1BE0F51A>
- [24] D. Benn e D. J. A. Evans, *Glaciers and Glaciation, 2nd edition*, 2<sup>a</sup> ed. London: Routledge, 2010. doi: 10.4324/9780203785010.

- [25] S. Bate, «A RECONSTRUCTION OF EQUILIBRIUM LINE ALTITUDES OF THE LITTLE ICE AGE GLACIERS IN LINNÉDALEN, WESTERN SPITSBERGEN, SVALBARD AG-212», 2008. Consultato: 22 novembre 2024. [Online]. Disponibile su: <https://www.semanticscholar.org/paper/A-RECONSTRUCTION-OF-EQUILIBRIUM-LINE-ALTITUDES-OF-Bate/b4f7423d8a3c6c009afc47a357ad60279c2ff9b3>
- [26] «Glacier Stress and Strain», AntarcticGlaciers.org. Consultato: 22 novembre 2024. [Online]. Disponibile su: <https://www.antarcticglaciers.org/glacier-processes/glacier-flow-2/glacier-flow-ii-stress-and-strain/>
- [27] K. McArthur, F. S. McCormack, e C. F. Dow, «Basal conditions of Denman Glacier from glacier hydrology and ice dynamics modeling», *The Cryosphere*, vol. 17, fasc. 11, pp. 4705–4727, nov. 2023, doi: 10.5194/tc-17-4705-2023.
- [28] «Science of Glaciers», National Snow and Ice Data Center. Consultato: 22 novembre 2024. [Online]. Disponibile su: <https://nsidc.org/learn/parts-cryosphere/glaciers/science-glaciers>
- [29] «Taking a Measure of Sea Level Rise: Ice Height». Consultato: 22 novembre 2024. [Online]. Disponibile su: <https://earthobservatory.nasa.gov/images/147438/taking-a-measure-of-sea-level-rise-ice-height>
- [30] D. Farinotti, M. Huss, A. Bauder, M. Funk, e M. Truffer, «A method to estimate the ice volume and ice-thickness distribution of alpine glaciers», *J. Glaciol.*, vol. 55, fasc. 191, pp. 422–430, 2009, doi: 10.3189/002214309788816759.
- [31] M. Huss e D. Farinotti, «Distributed ice thickness and volume of all glaciers around the globe», *Journal of Geophysical Research: Earth Surface*, vol. 117, fasc. F4, 2012, doi: 10.1029/2012JF002523.
- [32] R. McNabb, C. Nuth, A. Käab, e L. Girod, «Sensitivity of glacier volume change estimation to DEM void interpolation», *The Cryosphere*, vol. 13, fasc. 3, pp. 895–910, mar. 2019, doi: 10.5194/tc-13-895-2019.
- [33] M. Zemp, «Glaciers and climate change: spatio-temporal analysis of glacier fluctuations in the European Alps after 1850», *Schriftenreihe Physische Geographie Glaziologie und Geomorphodynamik*, vol. 49, gen. 2006, doi: 10.5167/uzh-34258.
- [34] D. Egli e N. Mancktelow, «The structural history of the Mont Blanc massif with regard to models for its recent exhumation», *Swiss J Geosci*, vol. 106, fasc. 3, Art. fasc. 3, ott. 2013, doi: 10.1007/s00015-013-0153-5.
- [35] D. Viviroli *et al.*, «Climate change and mountain water resources: overview and recommendations for research, management and policy», *Hydrology and Earth System Sciences*, vol. 15, fasc. 2, pp. 471–504, feb. 2011, doi: 10.5194/hess-15-471-2011.
- [36] «4-valle-daosta».
- [37] M. Huss, G. Juvet, D. Farinotti, e A. Bauder, «Future high-mountain hydrology: a new parameterization of glacier retreat», *Hydrology and Earth System Sciences*, vol. 14, fasc. 5, pp. 815–829, mag. 2010, doi: 10.5194/hess-14-815-2010.
- [38] «cartella-stampa-ghiacciaio-planpincieux-e-whymper-2021-1».
- [39] M. Tiuri, A. Sihvola, E. Nyfors, e M. Hallikaiken, «The complex dielectric constant of snow at microwave frequencies», *IEEE Journal of Oceanic Engineering*, vol. 9, fasc. 5, pp. 377–382, dic. 1984, doi: 10.1109/JOE.1984.1145645.
- [40] H. M. Joll, *Ground penetrating radar theory and applications*. 2009. Consultato: 16 dicembre 2024. [Online]. Disponibile su: <https://www.marinespecies.org/imis.php?module=ref&refid=300414>
- [41] D. J. Daniels, A. c. di, *Ground Penetrating Radar*. Institution of Engineering and Technology, 2004. doi: 10.1049/PBRA015E.
- [42] L. Langhammer, M. Grab, A. Bauder, e H. Maurer, «Glacier thickness estimations of alpine glaciers using data and modeling constraints», *The Cryosphere*, vol. 13, fasc. 8, pp. 2189–2202, ago. 2019, doi: 10.5194/tc-13-2189-2019.

- [43] «Ice Volume and Subglacial Topography for Western Canadian Glaciers from Mass Balance Fields, Thinning Rates, and a Bed Stress Model in: Journal of Climate Volume 26 Issue 12 (2013)». Consultato: 10 gennaio 2025. [Online]. Disponibile su: <https://journals.ametsoc.org/view/journals/clim/26/12/jcli-d-12-00513.1.xml>
- [44] «Il ritiro dei ghiacciai accelerato a livello globale». Consultato: 3 febbraio 2025. [Online]. Disponibile su: <https://www.wsl.ch/it/news/il-ritiro-dei-ghiacciai-accelerato-a-livello-globale/>
- [45] L. Jorio, «Verso un mondo di ghiacciai neri», SWI swissinfo.ch. Consultato: 3 febbraio 2025. [Online]. Disponibile su: <https://www.swissinfo.ch/ita/economia/riscaldamento-climatico-ghiacciai-himalaya-perù-cile/46576940>